THE UNIVERSITY OF ALBERTA

AN INVESTIGATION OF THE ROLE OF VOIDS DURING TERTIARY CREEP OF COPPER

by

D. E. FRASER

A THESIS

SUBMITTED TO THE FACULTY OF GRADUATE STUDIES

IN PARTIAL FULFILMENT OF THE REQUIREMENTS FOR THE DEGREE

OF MASTER OF SCIENCE IN METALLURGICAL ENGINEERING

DEPARTMENT OF MINING AND METALLURGY

EDMONTON, ALBERTA

MARCH, 1968

UNIVERSITY OF ALBERTA

FACULTY OF GRADUATE STUDIES

The undersigned certify that they have read, and recommend to the Faculty of Graduate Studies for acceptance, a thesis entitled

AN INVESTIGATION OF THE ROLE OF VOIDS
DURING TERTIARY CREEP OF COPPER

submitted by D. E. FRASER

in partial fulfilment of the requirements for the degree of Master of Science in Metallurgical Engineering.

ABSTRACT

The effect of voids on the creep behavior of polycrystalline OFHC and tough pitch coppers was studied at constant stress, at one half of the absolute melting temperature, and in an argon atmosphere, by examining the trends in creep rate stress sensitivity, activation energy, and recovery rate as creep progressed to fracture.

The creep life was longer and the minimum creep rate lower for OFHC copper than for tough pitch copper, under similar testing conditions. Both the stress sensitivity and the activation energy decreased for OFHC copper upon the onset of tertiary creep; the opposite occurred with the tough pitch copper. For both coppers, an exponential relationship appeared to exist between the creep strain during tertiary creep and the recovery time; however no evidence suggested that creep and recovery occurred by the same mechanism. The relaxation time for OFHC copper was about three times that for the tough pitch copper. Tensile tests indicated that voids lower the strain hardening exponent, the strength coefficient, and the ductility.

Differences in creep behavior between the coppers were analysed from the standpoint of two different, simultaneously operative rate controlling mechanisms--one whose creep rate follows a power function, the other a linear function, of stress. Thus, tertiary creep was caused by a continuously increasing contribution of the linear mechanism. Also, total void volume was a linear function of this mechanism's contribution. The experimental data of this and other investigations suggest that tertiary creep of polycrystalline copper is most likely due to the combined and, at present, inseparable role of grain boundary deformation processes and cavity growth.

ACKNOWLEDGEMENTS

The author is indebted to Dr. F. H. Vitovec, who initiated the program and who guided it from its inception, for numerous helpful suggestions and worthwhile discussions which were so necessary to the experimental program and the interpretation of the results.

Thanks are due to Mr. F. Fitzgerald, whose machine-shop skills were responsible for the construction of a major part of the creep machine; to Mr. T. Foreman who, by his specialized knowledge of electronics, assembled much of the electrical equipment; and to Mr. R. Scott who, through his experience in metallography and photography, contributed to the physical examination of the creep specimens.

Appreciation is expressed to my wife, Helen, for her help with the typing and the proofreading of the manuscript.

The author is grateful to American Metal Climax, Inc., through whose courtesy the OFHC brand copper was obtained.

The National Research Council of Canada supported this project financially. For this, the author is indeed appreciative.

TABLE OF CONTENTS

TABLE OF CONTENTS (CONT'D)

LIST OF TABLES

LIST OF ILLUSTRATIONS

[illegible]

[illegible]

LIST OF ILLUSTRATIONS (CONT'D)

LIST OF ILLUSTRATIONS (CONT'D)

[illegible]

[illegible]

[illegible] [illegible]
[illegible]

[illegible] [illegible]

[illegible] [illegible]
[illegible]

[illegible] [illegible]
[illegible]

[illegible] [illegible]
[illegible]

INTRODUCTION

The phenomenon of time-dependent deformation under a constant load or stress, which has been observed in many materials, has been termed "creep". It is believed to be thermally activated and the result of a complex combination of elastic, plastic, and viscous deformations, which may involve other material variables, such as the physical and chemical states.

A "creep curve", which is a plot of creep strain, or creep deformation, versus time (Fig. 1), is frequently used to report creep test results. For convenience of investigation, the creep curve for polycrystalline materials has been arbitrarily divided into three stages: primary, secondary, and tertiary. Although much effort has been expended to examine each stage separately, care must be taken not to lose sight of the probability that these stages are not necessarily independent of one another. There may be little, or no, physical significance in these divisions.

As a glance through a review of creep literature[1] will indicate, much scientific effort has been spent on the study of primary and secondary creep, whereas a smaller volume of literature exists on the study of tertiary creep. This, however, has been growing steadily in recent years.

Associated with the onset and continuation of tertiary creep, investigators have observed the formation and growth of cavities and cracks along the grain boundaries of polycrystalline materials.[2,3,4] A range of cavity shapes has been found to exist, from sharp, wedge-shaped cracks to rounded or polyhedral voids. Cavity shape appears to be a function of experimental conditions.[2] The sharp cracks have been associated with relatively low temperatures and high stresses, while the rounded voids have corresponded to relatively high temperatures and low stresses. In both cases, the cavities tended to be on those planes which were at

right angles to the applied stress.

A body of experimental evidence exists which points to grain boundary sliding as an important factor in the initiation of voids and the propagation of intergranular fracture.[5,6]

Zener[7] suggested a mechanism by which the appearance of wedge-shaped cracks forming at grain triple points could be explained. He suggested that such cracks would open because of a high tensile stress concentration which could exist at such places. His mechanism has had wide acceptance, although recently Steigler et al[8] have illustrated that such triple point cracks could possibly open by the merging of several small voids near a triple point and subsequent sliding on an adjacent boundary. To explain the formation of rounded or elliptical voids, several mechanisms, such as: homogeneous vacancy condensation;[3] preexistent submicroscopic voids;[9] sliding along grain boundary ledges;[10] heterogeneous nucleation at the surfaces of second phase particles and non-metallic inclusions,[11] have been proposed. The mechanism of homogeneous vacancy condensation is considered to be unimportant, since it has been illustrated to be unlikely by thermodynamic arguments advanced first by Balluffi et al.[12] The other mechanisms have met with varying amounts of acceptance.

McLean has proposed that voids could grow, after nucleation, by continued grain boundary sliding.[13] The observation that cavity shape does not necessarily remain platelike, but frequently assumes an elliptical, spherical, or polyhedral shape, suggests that sliding alone is not responsible for growth; diffusion possibly plays a part, even if only to modify cavity shape. A more popular idea is that boundary cavities grow by absorption of vacancies from the surrounding grain boundary. Balluffi et al[14] outlined the thermodynamic conditions under which voids could grow by vacancy condensation under the influence of stress and

vacancy supersaturation. With this basis, Hull and Rimmer[15] developed a theory by which time to rupture could be estimated, assuming that fracture occurred when voids coalesced.

Much of the study which has been devoted to tertiary creep has been concerned directly with the voids themselves. For example, void geometry has been studied using both light and electron microscopy;[4,8,16] changes in sample density have been measured as creep progresses and voids develop;[17,18] changes in material ductility as a function of temperature plus correlation with cavitation have been studied.[3]

Fewer investigations have been conducted in which there have been attempts to study the changes in behavior of materials as creep progresses through second stage, through third stage, to fracture. For example, the strain rate dependency upon stress for secondary and primary stages has been studied.[1] Activation energies have been determined in an attempt to illuminate the rate controlling mechanisms for these stages. Modes of deformation have been investigated, as well.

Questions arise when one considers the lack of study of the problem of tertiary creep from this point of view. How does the presence of cavities change such qualities as stress sensitivity of a material, rate controlling creep mechanism, and deformation mode? Are voids a by-product of tertiary creep, or are they directly responsible for tertiary creep? How do voids contribute to tertiary creep if they are responsible for it?

It would seem that there is room for a general experimental program to investigate the trends in changing creep behavior as a material creeps through secondary and tertiary stages, and which would give a foundation for further investigation into the specific modes of creep deformation which are active contributors to third stage creep.

EXPERIMENTAL PROGRAM AND PROCEDURES

GENERAL PROGRAM

In an attempt to determine the role of voids during tertiary creep of a material, it was thought desirable to investigate the effect of stress upon tertiary creep rate and to compare this with the effect of stress upon secondary creep rate. Since activation energy has been considered to be representative of the mechanism of creep deformation,[19] it was thought that some activation energy data should be gathered and studied in the light of the results on stress sensitivity.

A natural outcome of the stress sensitivity tests (which would be conducted using the method of incremental stress changes[20]) would be recovery time data, hence this would be gathered, tabulated, and evaluated.

Because creep behavior is affected by the microstructure of a material and metallography can give clues to the deformation processes, some metallography would be included in this study.

In an attempt to reveal any striking differences in the behavior of the materials studied (e.g., strong differences in strain hardening rate or yield stress), a series of three tensile tests would be run at room temperature.

To carry out the experimental program, a material would be sought which would satisfy the following conditions:

(i) it should be readily available in a useable form;

(ii) it should exhibit a brittle type creep fracture (i.e., low macroscopic ductility) at low to intermediate stresses and at intermediate temperatures;

(iii) round-type voids should form along the grain boundaries, rather than wedge-shaped cracks;

(iv) the material should be relatively free from

impurities so that the observed behavior would be as close as possible to the true behavior without modification by impurities.

DESCRIPTION OF APPARATUS

The purpose of the experimental apparatus was to provide data on the phenomenon of creep at a constant stress, an elevated temperature, and in a controlled atmosphere. To achieve the constant stress, the apparatus changed the load on the sample in accordance with the changing cross-sectional area, by means of a specially contoured cam (see Appendix 1-A) whose motion was controlled by the sample elongation rate.

Fig. 2 and Fig. 3 serve to illustrate the experimental apparatus.

The creep sample was located by type 316 stainless steel extension arms inside a chamber of Mullite ceramic tubing which was surrounded by the exposed heating elements of an electric furnace. Each end of the Mullite chamber was sealed with a mild carbon steel end cap, through which passed a type 316 stainless steel extension arm and a short length of copper tubing. The copper tubing allowed the air to be flushed from the sample chamber and an inert atmosphere to be maintained. The lower stainless steel extension arm was attached at its upper end to the creep sample, while the lower end was held in place by a threaded crank which seated against a set of thrust bearings having curved surfaces. The purpose of the bearings was to reduce eccentricity of loading. The lower extension arm was prevented from rotating during adjustment of the crank by a key which fitted into a slot in the lower six inches of the extension arm. Therefore, during cranking, the extension arm motion was vertical only.

The upper extension arm was attached by its lower end

to the creep sample by a stainless steel collar. The upper end was attached to a cross-head by a 5/8-inch nut, which seated on a thrust bearing having a curved surface. The cross-head was secured to a 4-inch diameter brass hub by two 0.008 inch thick steel bands. The aluminum, constant stress cam was fastened to the brass hub by two triangular pieces of sheet steel. The weight of the cam was offset by a counterbalance on the appropriate diameter of the hub (see Appendix 1-B). A strip of steel strapping was attached to the upper end of the cam and followed the contoured surface of the cam down along its length. A weight pan was fixed to the free end of this piece of strapping. The whole assemblage was free to rotate on an axle which fitted through the brass hub and was supported by a pillow block on either end. The pillow blocks were bolted firmly to the frame of the machine.

The amount of creep extension which occurred during a test was measured by a linear variable differential transformer (LVDT) and recorded by a Heath Servo Recorder (model EUW-20A). The moveable core of the LVDT was attached to the hub axle by a fine wire, the upper end of which was secured to a 4-inch diameter brass wheel. The wheel was firmly secured to the axle. Thus, the motion of the axle during creep was used as a measure of the amount of sample extension. The LVDT and recorder system were calibrated with the help of a dial gauge which could be read to 5×10^{-4} in. From a series of calibrations, it was decided that for the set of conditions under which the servo-recorder and the LVDT were operating, 1/10 of the full scale deflection of the recorder represented a change in sample length of $(1.73 \pm 0.075)10^{-2}$ in. for 99 per cent confidence. (see Appendix 2-C) The recording chart could be read easily to at least 0.5×10^{-2} of the full scale. Both the recorder and the LVDT were connected to a constant voltage transformer.

The 15-inch, 750-watt furnace was mounted vertically about the Mullite sample chamber and was moveable, so that it could be positioned to give as low a temperature gradient as possible along the gauge length of the copper sample. With the heating elements of the furnace immediately next to the outer wall of the Mullite chamber, temperature increases within the chamber could be realized quickly. An initial calibration of the furnace showed that the thermal gradient along the gauge length of the sample could be kept within ± 3 C° at 400°C. Once the position of the furnace was found that would maintain these limits, the furnace was locked in position by four screws. This position was used throughout the experimental program without further adjustment. The weight of the furnace was counterbalanced by two 10-pound weights, so that the full weight of the furnace did not have to be carried by the locking screws. The furnace temperature was controlled by a Wheelco temperature controller which was able to keep the sample temperature within 1.5C° easily, once thermal equilibrium was established. The Wheelco controller monitored the furnace temperature by means of a Chromel-Alumel thermocouple which passed into the furnace and contacted the external surface of the Mullite chamber. The sample temperature was determined through the use of a Honeywell potentiometer connected to another Chromel-Alumel thermocouple which passed through a close fitting 3/16-inch diameter hole in the Mullite tubing and contacted the mid-point of the sample gauge length. To facilitate access to the Mullite chamber and to allow placement of the thermocouples, the two furnace halves were hinged together so that the front half could be swung to one side. When in operation, the two halves were clamped together.

To counteract the problem of sample oxidation during creep, an argon atmosphere was maintained within the Mullite chamber. Argon gas of laboratory purity was used. It was passed through a trap containing an activated alumina dessi-

cant before entry to the chamber. Upon exit from the chamber, it passed through a trap containing a heavy grade oil. This trap made possible the maintenance of a slight positive pressure within the sample chamber, thus preventing the entrance of air through small openings.

Upon sample fracture, all electrical equipment was shut off through the automatic tripping of a microswitch. The microswitch was activated by the dropping of the lower extension arm. The lower extension arm was prevented from dropping more than 1/4 in. by an adjustable collar which fitted around the extension arm, just above the guide through which it passed. Only the argon gas flow continued after fracture, so that oxidation of the sample could be kept to a minimum during cooling of the system.

Cooling to near room temperature took 6 to 7 hr. if the system was allowed to cool without interference. If the furnace was opened, and the argon flow increased, the cooling time was reduced to about 3-1/2 hr. When cool, the sample was removed and examined.

TEST MATERIALS AND SAMPLE PREPARATION

Tests were conducted using an OFHC brand copper (composition: Table 1) and a tough pitch copper. Tough pitch copper creep samples were machined to the dimensions shown in Fig. 4 from half-hard, 5/8-inch rod. OFHC brand copper samples were machined to the same dimensions, but from half-hard, 3/4-inch rod obtained through the courtesy of American Metal Climax, Inc.

The relatively long, 2-inch gauge length was chosen so that most of the measured deformation would be due to the material in the gauge length. Percentagewise, only small contributions would be made by fillets and threads.

The average cross-sectional area for each sample was calculated from an average sample diameter, determined as

follows: three measurements of the sample diameter were made at each end of the sample gauge length and halfway along the gauge length with a micrometer. Each set of three measurements was averaged to give an average diameter for each location. The average sample diameter was calculated using the averaged diameters of upper, central, and lower gauge length.

Prior to placement in the creep machine, each sample was cleaned in a solution of the following composition by volume:

55 per cent orthophosphoric acid,

25 per cent acetic acid,

20 per cent nitric acid.

The solution was heated to 65°C for cleaning. After removal of the copper sample from the cleaner it was immediately placed into a solution of Alconox to neutralize the reaction. The sample was then rinsed in clean water, flushed with alcohol, and dried. Upon completion of this operation, the specimen was placed in the creep machine.

Before the heating furnace was switched on, the air surrounding the creep specimen was displaced by argon gas. This was accomplished by flushing the system of hoses and sample chamber for about 20 min.

When flushing was completed, the argon gas flow was reduced so that a slight positive pressure of argon was maintained about the creep sample, and the furnace was switched on. The testing temperature was reached within 1/2 hr. The sample was maintained at this temperature for 2 hr. before application of the load, to allow for stabilization of grains.

Before the load was applied, the constant stress cam was re-positioned to the starting position (thermal expansion in the machine parts necessitated this) and the strain recorder positioned to zero. The load was applied gently through the use of a hydraulic jack. Immediately

after load application, the cam position was re-adjusted to zero to compensate for the elastic deflection in the creep machine, as measured by the LVDT and recorded by the servo-recorder. It was important that the cam be positioned properly at the beginning of each test, so that the test could be considered a constant stress test.

Upon the completion of the test, the sample was removed from the creep machine, given a brief examination, then stored in a dessicator until needed for metallographic examination.

Metallographic samples were cut from the creep samples by electrical discharge machining. Samples were then mounted in bakelite, ground lightly and polished on "kitten's ear" lap with Linde "B" alumina abrasive. Etching was done either with an alcoholic ferric chloride solution or a 30 per cent nitric acid solution. Creep samples were examined at different magnifications on a Reichert metallograph.

Creep curves from the Heath recorder were evaluated to obtain the pertinent data.

TEST RESULTS

EXPLORATORY TESTS

Copper was chosen as the test material because it was readily available and round type voids had been noticed to form during creep.[3] Greenwood et al reported that the ductility decreased with increasing temperature and with decreasing strain rate. The extent of cavitation increased with temperature. These authors reported that, at a temp= erature of 400°C and a strain rate of 1.2 per cent/hr., the elongation at fracture was less than 10 per cent. To test the creep machine, it was decided to run an exploratory test at a temperature near 400°C and a load of 282 lb. (equivalent to a nominal stress of 5590 psi.). This test was an ordinary creep test which lasted 12 hr. before failure of the sample; the test temperature was 676°K and the minimum creep rate was 0.4 per cent/hr. The elongation at fracture was 7.4 per cent (see Table 2). When the sample was studied metallographically, it was found that the voids were slightly more wedge-shaped than rounded. It was decided to reduce the nominal stress by about 1000 to 1500 psi. in an attempt to increase creep life and to move into the region where elliptical, or round-type, voids appear. After making some minor changes on the creep machine, to increase its efficiency, the experimental program was continued.

The next test, using the tough pitch copper with a reduced stress (4490 psi.) and a temperature of 681°K, yielded a secondary creep rate of 0.11 per cent/hr., an elongation at fracture of 8.4 per cent, and a creep life of 34.8 hr. Metallographic results from another test (Test 3) under similar conditions showed elliptical, or rounded, voids, suitable for this study.

The first creep test which was performed on OFHC brand copper (Test 6), was at 698°K and a stress of 4320 psi. A

[illegible]

[illegible]

[illegible]

[illegible]

[illegible]

secondary creep rate of 0.048 per cent/hr., an elongation at fracture of 6.4 per cent, and a creep life of 60.6 hr. resulted. Metallography showed the intergranular voids to be elliptical and suitable for this program.

Thus, it was decided that the tests could be conducted at temperatures around 673°K (400°C) and at stresses in the neighbourhood of 4000 psi with copper for the test material, to study the phenomenon of tertiary creep.

A typical creep curve is shown in Fig. 1. The shape of the curve was the same for both the tough pitch and the OFHC coppers, but the secondary creep rate lower and the creep life longer for the OFHC copper.

Fig. 5 shows a creep curve in which stress changes in the order of 10 per cent of the mean stress were made. Upon such a stress change a new creep rate was established and allowed to continue for 3 to 4 hr. before returning to the mean stress.

STRESS SENSITIVITY

According to Garofalo[21] the relationship between the minimum creep rate and the stress has been expressed by a number of different functions:

(i) the power function

$$\dot{\varepsilon} = A\sigma^{n}$$

(ii) the exponential function

$$\dot{\varepsilon} = A' \exp(\beta\sigma)$$

(iii) the hyperbolic sine function

$$\dot{\varepsilon} = A'' (\sinh \alpha\sigma)^{n}$$

For the power function, a plot of log $\dot{\varepsilon}$ versus log σ has been found to be linear with a slope n, over a range of low stresses for different materials,[21] whereas the exponential function has yielded a linear relationship when plotted semi-logarithmically for high stresses. The stress rela-

tionship which is applicable over the widest range is the hyperbolic sine function. When log $\dot{\varepsilon}$ is plotted versus log sinh$\alpha\sigma$, a linear relationship results which holds experimentally from low stresses through the intermediate range into high stresses. The hyperbolic sine function is cumbersome to evaluate from experimental results--data for both high and low stresses must be available. The hyperbolic sine function will degenerate to the exponential stress relationship at high stresses ($\alpha\sigma > 1.2$) and will degenerate to the power function at low stresses ($\alpha\sigma < 0.8$).

For creep at constant stress, A, n, A', and β are not dependent upon stress. A" and α remain constant for constant temperature.

The creep tests were carried out at relatively low stresses, so the power function was chosen to represent the relationship between secondary creep rate and stress. The data for OFHC copper is represented by Fig. 6. The power function appears to become stress sensitive above about 3000 psi.

Fig. 7 shows a similar plot for the tough pitch copper over a narrower range of stress. It appears linear over this range.

Some of the creep data used in the plotting of Fig. 6 and Fig. 7 was obtained from ordinary creep tests but most of the points were determined from a few creep tests in which a number of differential stress changes was made. The minimum creep rate was determined from the minimum slope of the creep curve while the sample was undergoing secondary creep at the mean stress; another minimum creep rate was determined after a differential stress change (usually a decrease) when the new steady state creep rate was established. After steady state creep progressed for 3 to 4 hr. at the new stress, the stress was returned to the mean stress and the test allowed to continue.

The power,n, in the relationship:

$$\dot{\varepsilon} = A\sigma^n \tag{1}$$

where $\dot{\varepsilon}$ is the creep rate,

A is a constant,

σ is the stress,

is a measure of the response of a material to stress. If n is high, the creep rate is sensitive to a change in stress. For many pure metals n is around 5, but copper tends to show lower values.[21] For OFHC copper (test number 11, which explored the linear range of the power function) an average value for n was calculated to be 3.59 for a temperature of 698°K. This value was calculated using:

$$n = \frac{\log \dot{\varepsilon}_1/\dot{\varepsilon}_2}{\log \sigma_1/\sigma_2} \tag{2}$$

where $\dot{\varepsilon}_1$ and $\dot{\varepsilon}_2$ are steady state creep rates under the action of stresses σ_1 and σ_2 respectively.

The average n of five stress changes was taken.

This is in close agreement with those values of n determined by Feltham and Meakin[22] of 3.57 and 3.36 at temperatures of 673°K and 723°K, respectively, for OFHC copper.

Inherent in this method of stress sensitivity evaluation are several assumptions which, if they can be accepted, will allow n to be determined using several incremental changes in stress on one sample. They are:

(i) no change in structure occurs before, during, or immediately after the change in stress;

(ii) the only condition which changes is that of load (all other variables remain constant);

(iii) the response of the sample to the new stress is due entirely to the behavior of the sample (there are no machine effects);

(iv) the effect of sample creep history is small.

The advantage to this method is that any statistical

differences which often exist among a given set of samples are eliminated as a set of data is determined from only one specimen.

When the stress sensitivity, n, is plotted as a function of creep strain, an interesting trend is observed. As Fig. 8 shows, there is a definite change in the magnitude of n as tertiary creep is entered--for both OFHC and tough pitch coppers. The second stage points for 5 tests are plotted versus the creep strain and are marked by the numeral "2". Also, the corresponding tertiary points are plotted but they are distinguished by the numeral "3".

An important difference in the behaviors of n between OFHC and tough pitch coppers is that as tertiary creep is entered for OFHC copper, the magnitude of n decreases, whereas the magnitude of n increases for tough pitch copper. Even though there is scatter in the points, this does not mask the change which seems to occur.

Notice that the secondary creep value of n for OFHC copper is about 12. This is far from the value 3.59 reported above, but referral to Fig. 6 will verify that these tests were conducted outside the linear range of the power function--in the region of increasing slope, or n. Thus, tests done under similar conditions should only be compared.

ACTIVATION ENERGY

The activation energy for creep was determined by using:[23]

$$\Delta H = \frac{R \ln \dot{\varepsilon}_1/\dot{\varepsilon}_2}{(1/T_2 - 1/T_1)} \tag{3}$$

where R is the gas constant (1.98717 Cal./$^{\circ}$K mole),
$\dot{\varepsilon}_1, \dot{\varepsilon}_2$ are creep rates,
T_1, T_2 are the temperatures at which the creep rates were observed.

[illegible]

[illegible]

[illegible]

[illegible]

[illegible]

A small increase or decrease in the temperature ($10^{\circ}K$ to $20^{\circ}K$) was made and a new creep rate established within 15 min. The data gathered in this way was then used to calculate activation energies.

The validity of this method of activation energy determination hinges upon the assumptions that:

(i) the activation energy is independent of stress over small ranges;

(ii) the new creep rate is due mainly to the change in temperature (there is little effect of the temperature change upon the frequency factor for constant stress and creep strain);

(iii) the structure does not change appreciably.

Fig. 9, a plot of activation energy versus creep strain, shows a trend similar to that illustrated in Fig. 8. In both the case of the OFHC copper and the tough pitch copper, there seems to be a pronounced change in the magnitude of the activation energy upon transition to tertiary creep. However, for the OFHC copper there is a decrease in activation energy upon transition from secondary to tertiary creep, whereas the tough pitch copper exhibits an activation energy increase.

The average activation energy for the steady-state points of OFHC copper is about 80 kcal./mole. This is much higher than other reported values of 28 to 32 kcal./mole for a temperature range of $673^{\circ}K$ to $723^{\circ}K$.[22] This difference will be considered more thoroughly later in this report.

For the tough pitch copper, the average activation energy for secondary creep is 26 kcal./mole. This is closer to Feltham's and Meakin's value.

The activation energy for tertiary creep of OFHC copper dropped to the neighbourhood of 35 kcal./mole; the tertiary creep activation energy for the tough pitch copper increased to the range of 40 to 55 kcal/ mole.

INDUCTION TIME

To estimate the recovery characteristics of the coppers, a method based on a technique proposed by Cottrell and Aytekin[24] and used in an investigation reported recently by Davies and Dutton[25] was employed. Upon an incremental decrease in stress, an induction period ensued before the new characteristic creep rate was established. The length of this period was taken to be a measure of the recovery time. Because of the practical problems associated with measuring the small changes in slope of the creep curve, a method similar to that used by Davies and Dutton was employed to decide upon the length of the induction period following a small change in stress. The induction period was defined to be the length of time from the stress change to the point of intersection of the horizontal tangent and the new steady-state creep rate. The recovery times found in this way are plotted versus creep strain in Fig. 10. There may be considerable error in some of the secondary creep recovery values (some may be reported too low) because of the difficulty of reading extremely small slope changes in the creep curve. One thing is certain, however, the induction times decrease as creep progresses through third stage, for all cases examined, both for tough pitch and for OFHC coppers. The error involved in measuring tertiary induction times was much less than that made in measuring secondary induction times as slope changes were more definite. There appears not to be a linear relationship between recovery time and strain for third stage creep.

METALLOGRAPHY AND GRAIN SHAPE DATA

A series of photographs is included showing the structure during different phases of the testing (Figs. 11 to 25). As Fig. 13 shows, fracture occurred in a brittle manner (i.e.

low macroscopic ductility); Fig. 14 illustrates the typical void shape. Figs. 17 and 20 suggest that grain boundary motion took place. These photomicrographs were taken of Sample 11 which was tested at 698°K under a stress of 2642 psi.

Grain size determinations were made on Samples 6, 10, and 11 for both the gauge lengths and the threaded grip sections. Samples 6 and 10 were tested to failure, whereas Sample 11 was tested under a lower stress to 1.32 per cent strain. The grain size measurements on Sample 6 were done in two ways:

(i) by ignoring the voids and considering the centre of the void to be the dividing line between two grains;

(ii) by not ignoring the voids, but rather considering the grain to terminate at the void edge.

The data from the second count yielded an average void dimension as well as an average grain dimension. It was assumed that more deformation and change occurred in the gauge section than in the threaded grips, so that the grain shape in the grips represented more closely the equilibrium shape. Thus, the gauge length grain shape was referred to the grip grain shape to see if a significant change in grain shape had occurred during creep. In both Samples 6 and 10 the final grain shape was close to equiaxial. In these two samples, the grain dimensions were determined by counting the number of grains which lay on a line of known length and dividing the line length by the number of grains. This method gives an average grain size but will not indicate whether there are a number of different grain sizes present, which might be the case if recrystallization and grain growth occurred. To investigate this possibility, a more extensive grain count was performed on Sample 11. Figs. 26 and 27 show curves for cumulative frequency versus grain dimension as well as their derivatives. These plots show

[illegible]

that in both the gauge section and the threaded grip, there are a number of different grain sizes. By considering the area under each peak of the derivative curve and the mean grain size for the peak, weighted average grain dimensions for the gauge section and for the threaded grip were determined. Using this approach, the average longitudinal and transverse dimensions for the gauge section were found to be 0.79×10^{-2} cm. and 0.58×10^{-2} cm. respectively (Table 3). For the threaded grip section, the weighted average longitudinal and transverse dimensions were 0.76×10^{-2} cm. and 0.68×10^{-2} cm. respectively. The weighted averages for the threaded grip section of Sample 11 compare favourably with the corresponding grain dimensions determined from Sample 6, where the average longitudinal dimension of 0.71×10^{-2} cm. and the average transverse dimension of 0.64×10^{-2} cm. were estimated using the first mentioned method of grain size determination. The gauge sections will not be compared because Sample 11 did not enter tertiary creep, whereas Sample 6 did. The average grain size for Sample 10 (longitudinal: 0.56×10^{-2} cm.; transverse: 0.55×10^{-2} cm.) appears to be a little smaller than that of Samples 6 and 11.

GRAIN DISTORTION AND GRAIN BOUNDARY SLIDING

A method was proposed by Rachinger[26] for estimating the amounts of grain deformation and grain boundary sliding from measurements of the change in grain shape. He showed that the strain due to deformation within the grain could be calculated from:

$$\varepsilon_g = W^{2/3} - 1 \tag{4}$$

where $W = a/b$,

a is the average length of grains parallel to the stress axis,

[illegible]

b is the average grain dimension in the transverse direction.

He assumed that the grains were equiaxed before straining. The amount of strain due to grain boundary sliding could be found from:

$$\varepsilon_{gb} = \varepsilon_t - \varepsilon_g \tag{5}$$

where ε_{gb} is the strain due to grain boundary sliding,

ε_t is the total strain,

ε_g is the strain due to grain deformation.

To check this method of grain strain determination, a grain shape evaluation was performed on a piece of "as received", OFHC copper (half-hard) and the grain strain found to be 56 per cent. This is about right for the half-hard material.

To apply Equation 4 to this investigation, a slight modification to the foregoing was made. Apparently, grains were not equiaxed before straining, hence, the final dimensions should be referred to the initial dimensions. Equation 4 was modified to:

$$\varepsilon_g = \left(W_{gl}/W_{thd}\right)^{2/3} - 1 \tag{6}$$

where W_{gl} is the ratio of longitudinal grain dimensions to transverse grain dimensions for the gauge length,

W_{thd} is the corresponding ratio for the threaded grip section.

Grain shape data (Table 3) from Tests 6 and 10, both of which were tested to fracture, was used to estimate the strain due to grain deformation in each of these tests. For Test 6, W_{gl}/W_{thd} was 0.87 and for Test 10, W_{gl}/W_{thd} was 0.93. Theoretically the ratio should not be less than 1.0 for

[illegible]

tension. The values of these ratios are close to 1.0. This suggests that strain due to grain deformation is nearly zero and most of the measured strain is due to grain boundary sliding. On the other hand, if recrystallization and grain growth occurred, the effects which must be measured, to use Equation 6, may have been masked. Fig. 20 suggests that boundary migration did occur.

Grain measurements of Sample 11 were applied to Equation 6, too. This sample did not enter tertiary creep. A strain due to grain deformation of 14 per cent was calculated. This is about a factor of 10 too large, for the total measured creep strain was only 1.3 per cent. This result would indicate that most deformation occurred by intragranular deformation. Again, if recrystallization and grain growth were active, the grain size data may not reflect a true picture when applied to Equation 6.

TENSILE TESTS

Three tensile tests were performed: one on OFHC copper (uncrept), one on tough pitch copper (uncrept), and one on Sample 12 which was crept to 5.04 per cent strain--well into tertiary creep. The results of these tests are presented in Fig. 28. Both the uncrept copper samples were annealed at 698°K for 2 hr. and cooled to room temperature before tensile testing. This was to produce a structure similar to that produced in creep samples before creep testing. Fig. 12 and Fig. 23 show these structures for OFHC and tough pitch coppers respectively. It appears as if recrystallization has occurred and that grain growth was in progress, as several different grain sizes seem apparent.

As can be seen from Fig. 28, both OFHC and tough pitch coppers yielded near the same stress (2000 psi). The tough pitch copper seems to have had a higher ultimate strength than the OFHC copper, but the difference in ductility is not

significant. Sample 12, which received a relatively large amount of creep damage, yielded at a much higher stress (6000 psi) than the others. Note, too, that the ductility of Sample 12 was about 1/3 that of the uncrept OFHC and tough pitch coppers.

Tensile test data has been evaluated using a power function of the form:[27]

$$\sigma = K \varepsilon^{m} \tag{7}$$

where σ is the true stress,
ε is the true strain,
K is the strength coefficient,
m is the strain hardening exponent.

This expression allows the strain hardening behaviors of different materials to be compared.

In Fig. 29, the tensile test data from this investigation was plotted logarithmically to show the strain hardening behavior. Both the uncrept OFHC and tough pitch coppers have the same strain hardening exponent of 0.46, whereas the exponent for Sample 12 (the crept copper) was 0.3. The strength coefficient, as determined for a strain of 100 per cent, was 62,000 psi for the uncrept samples, but only 40,000 psi for Sample 12.

DISCUSSION AND ANALYSIS

One of the most striking differences which must be accounted for between the behaviors of OFHC and tough pitch coppers is the apparently contradictory trends upon the onset of tertiary creep, illustrated by Fig. 8. A similar trend is followed in Fig. 9 with the activation energy data. With the appearance of tertiary creep, an apparent change in both the stress sensitivity and the activation energy occurred. It should be recalled that these two sets of data were obtained independently of each other, from two different types of test. The fact that similar trends were obtained from the two independent test types suggests that the changes occurring upon the onset of tertiary creep were not the result of the test method, but were attributable to the behavior of the samples.

SOME PRELIMINARY QUESTIONS

Initially, two fundamental questions had to be answered before a complete evaluation of the creep data could be performed. They were:

(i) could the constant stress cam be used to maintain a constant stress during tertiary creep?

(ii) Could the observed change in stress sensitivity, n, which appears during tertiary creep be due to a reduction of the cross-sectional area (hence, an increase in stress), caused by the presence of voids, but unaccounted for by the assumption that the stress remained constant throughout the test?

The first question was answered by comparing the creep strain as measured by the recorder with that calculated from the change in the nominal cross-sectional area which occurred as a result of creep well into tertiary creep (Sample

12). The recorder indicated that the sample had strained 5.04 per cent. The strain determined from:

$$\varepsilon = \ln (A_o/A) \tag{8}$$

where ε is the strain,
A_o is the initial cross-sectional area,
A is the final cross-sectional area,

was found to be 4.88 per cent. This was within the experimental error of the strain determined from the recorder. (The experimental error was 0.2 per cent strain). Therefore, use of the constant stress cam into tertiary creep seemed justified. This suggested, as well, that creep did not stop in the homogeneous material within the sample when the voids formed. If this were not the case, there would be a larger disagreement between these two methods of strain determination.

A solution to the second problem was found by developing an expression which described the change in n with the change in the ratio σ_1/σ_2, where σ_1 is the stress before a stress change and σ_2 is the stress after a stress change. Experimentally determined values were substituted into the expression.

The reasoning was as follows: assuming that the function

$$\dot{\varepsilon} = A\,\sigma^n \tag{9}$$

describes the behavior of the sample adequately, then the stress sensitivity, n, is given by:

$$n = \log(\dot{\varepsilon}_1/\dot{\varepsilon}_2) \Big/ \log(\sigma_1/\sigma_2) \tag{10}$$

Upon differentiation with respect to the ratio σ_1/σ_2, the desired expression results:

$$\frac{\partial n}{\partial(\sigma_1/\sigma_2)} = -\log\left(\frac{\dot{\varepsilon}_1}{\dot{\varepsilon}_2}\right)\left\{\left[\log\left(\frac{\sigma_1}{\sigma_2}\right)\right]^2\left(\frac{\sigma_1}{\sigma_2}\right)\right\}^{-1} \tag{11}$$

Data from Test 3 was substituted into this equation to see whether the change in n could be due to the use of the wrong ratio .

An approximation to Equation 11 results when $\partial n/\partial(\sigma_1/\sigma_2)$ is replaced by $\Delta n/\Delta(\sigma_1/\sigma_2)$. From the first tertiary creep stress change (ε = 0.035) in Test 3, values of n = 8.6 and $\dot{\varepsilon}_1/\dot{\varepsilon}_2$ = 0.461 were found. A ratio of σ_1/σ_2 = 0.914 was assumed. If the value n = 8.6 was caused by an error in σ_1/σ_2 and not the result of tertiary creep, then the second stage creep value of n should result if the correct ratio is used. Hence, it was assumed, for the purpose of the calculation, that the real value of n was 5, not 8.6, and the ratio of σ_1/σ_2 which should have been used was calculated. From this, the new cross-sectional area was estimated. It was found to be 13 per cent smaller than the original area. This seemed unreasonably high, bearing in mind that this change occurred over a period of about 2 hr., for only one stress change and that n did not continue to change by a similar magnitude throughout the remainder of the creep test. The total change in area for the completed test would have to be greater than this. The check which was performed to provide an answer to question (i) would suggest that the change in area for this case should be near the value for the linear creep strain which was 3 to 4 per cent. From this exercise it was concluded that the magnitude of the change in n which occurred upon transition to tertiary creep could not be accounted for solely by an error in assuming that stress remained constant throughout the creep test.

The possibility that an error was introduced into n by the definition of strain rate was considered briefly. The measured deformation was referred to the sample gauge length, even though the deformation may have occurred locally within the sample. This method, while an accepted one, could yield rates of strain which were lower than those actually occur-

[illegible]

ring in the region of deformation. Microscopic examination of fractured samples revealed a fairly uniform distribution of voids along the sample gauge length. This was taken as evidence for close to uniform straining along the gauge length, even though it is not conclusive. This aspect was not investigated further.

With no satisfactory explanation apparent, from these foregoing considerations, for the observed trends, it was decided to turn to some of the existing creep theories to try to explain this behavior.

CREEP THEORIES

Most theories which have been advanced to explain creep may be placed, generally, in one of four categories:

(i) viscous creep theories,
(ii) dislocation creep theories,
(iii) grain-boundary sliding theories,
(iv) macroanalytical theories.

Table 4 summarizes some of these theories as well as the respective rate equations.

Many of the expressions proposed to explain primary and secondary creep are founded upon one of the earliest theories --reaction rate theory. Kauzman in 1941 proposed a creep theory in which he coupled the concept of activated complexes with statistical mechanics. He viewed the solid state as composed of elementary "units of flow" which, upon overcoming an energy barrier and sliding past one another, completed a "unit of shear". The energy barrier was surmounted by activated flow units. An applied stress tended to lower the activation energy for flow in the direction of the applied stress. Net flow would be zero under zero stress. A disadvantage of this general approach was that activation energy could not be estimated until a particular deformation mechanism was specified. Thus, Table 4 contains a number of

creep expressions similar in appearance to that for the reaction rate theory, except that the "flow units" have been specified to be dislocation processes of some kind.

Under certain testing conditions, creep is believed to be diffusion controlled. For high temperatures (above 0.8 of the melting temperature) and low stresses, the Nabarro-Herring equation, or a modification of it, which describes a form of intragranular diffusional creep, has been found to be satisfied by some materials.[28,29,30] A modification of the Nabarro-Herring approach has been used to explain a linear stress dependency of creep rate due to grain boundary sliding. This equation is shown in Table 4 as well. It has been reported that copper, among other materials, showed a linear relationship between the amount of grain boundary sliding and stress.[31]

A slightly different approach to creep than either of the previous ones has been developed within the last ten years, or so. It is based upon the change in mobile dislocation density with time. A number of expressions which have been developed utilizing the concept of mobile dislocation density behavior begin with an expression of the form:

$$\dot{\varepsilon} = \bar{v} b \rho \tag{12}$$

where $\dot{\varepsilon}$ is the creep rate,
$\bar{v}$ is the mean dislocation velocity,
b is the Burger's vector,
ρ is the mobile dislocation density.[32]

Functions which define $\bar{v}$ and ρ in terms of the creep variables are substituted into Equation 12. The resulting creep rate equations depend, at least in part, for their stress dependency upon the stress dependency of the mobile dislocation density.

Barrett[33] has shown that a range of stress dependencies is available depending upon the value of the friction stress,

σ_o , in the equation:

$$\sigma = \sigma_o + \alpha G b \sqrt{\rho} \tag{13}$$

where σ is the applied stress,
α is a constant ≈ 1,
G is the shear modulus,
b is the Burger's vector,
ρ is the dislocation density.

Equation 13 represents the general form to which much of the dislocation density data, gathered for high temperature, steady-state creep, can be fitted.[34,35,36] Barrett represented the stress dependency of the dislocation density as:

$$\rho \propto \sigma^d \tag{14}$$

Then Equation 13 can be written:

$$\frac{\partial \ln \rho}{\partial \ln \sigma} = \frac{2\sigma}{\sigma - \sigma_o} = d \tag{15}$$

where σ cannot be less than or equal to σ_o. But for $\sigma > \sigma_o$, the power, d, can have a wide range of values. Barrett discussed how the magnitude of d changed with variations in σ_o and, hence, how the stress dependency of steady-state creep rate could be expected to change with the stress dependency of the dislocation density. His expectations were borne out by an investigation into the behavior of a polycrystalline Fe-3.1 Si alloy.

Notice, from Table 4, that creep rate stress dependencies are expressed either as power, exponential, hyperbolic sine, or linear functions. Recall that, over small ranges of stress, the exponential and hyperbolic sine functions can be represented by power functions with the right choice of power. Hence, at constant temperature, the use of a power function to express the stress dependency of the creep rate

over a small stress range seemed justified.

MULTIPLE MECHANISMS

Because creep is a complex phenomenon and the creep behavior of materials is strongly dependent upon specific testing conditions, it should not seem unreasonable that more than one deformation mechanism operates at any given time. The observed creep behavior may be the result of several mechanisms with, perhaps, one which is rate controlling. For example, mechanisms such as: dislocation intersection (which can form jogs), jog motion, and vacancy diffusion, may operate under a given set of experimental conditions. Each makes a contribution to the observed strain rate and each mechanism has a specific relationship between $\dot{\varepsilon}$ and σ. How they are related will depend whether the mechanisms operate in series, parallel, or a combination of both.

It was thought that this idea of simultaneously operative mechanisms could be used to explain the apparently contradictory behavior of the OFHC and tough pitch coppers. As mentioned earlier, the stress dependency of the creep rate may be represented by a power function. From Table 4, notice too, that some theories predict a linear relationship between creep rate and stress. To a first approximation, let the observed creep rate be a linear combination of the creep rate, $\dot{\varepsilon}_p$, due to mechanisms which are expressed by the power function:

$$\dot{\varepsilon}_p = C\sigma^m \tag{16}$$

and the creep rate, $\dot{\varepsilon}_L$, due to mechanisms which are expressed by the linear function:

$$\dot{\varepsilon}_L = B\sigma \tag{17}$$

Mathematically, this is written as:

$$\dot{\varepsilon}_t = \dot{\varepsilon}_p + \dot{\varepsilon}_L \tag{18}$$

or

$$\dot{\varepsilon}_t = C\sigma^m + B\sigma \tag{19}$$

Implicit in Equations 18 and 19 is the assumption that the non-linear and linear contributions are independent of one another (i.e., they operate in series).

Equation 16 would represent the combined effect of several deformation mechanisms whose rate controlling one was non-linear. Similarly, Equation 17 would represent the combined effect of several deformation mechanisms whose rate controlling one was linear.

Equation 19 cannot be evaluated absolutely for either of the coppers studied because there is no way of separating the linear and non-linear mechanisms. However, if some assumptions are made about the behavior of the OFHC copper, the terms may be separated relative to the behavior of the OFHC copper. It was assumed that this copper (with 50 ppm. impurities) behaved more closely to pure copper than the tough pitch copper (with about 0.08 per cent impurities). Thus, it was decided that secondary creep of OFHC copper should be taken as the datum against which all other behavior would be judged. The high value of the power (n = 12) for secondary creep of OFHC copper, under a constant stress in the region of 4200 lb./in.^{2}, suggested that the contribution of linear deformation mechanisms was small and would be neglected.

Thus for secondary creep of OFHC copper, the relationship:

$$\dot{\varepsilon}_t = \dot{\varepsilon}_p$$

$$\dot{\varepsilon}_t = C\sigma^m = A\sigma^n$$

was assumed to express the behavior. The behavior observed while OFHC samples were in tertiary creep and the behavior of tough pitch samples undergoing secondary or tertiary

[illegible]

[illegible]

[illegible]

creep was investigated using:

$$\dot{\varepsilon}_t = A\sigma^n + B\sigma \tag{20}$$

Once having decided upon the approach to adopt, the problem of evaluating A and B arose. It was found that for small stress changes (in the order of 10 per cent) the magnitude of the constant in the power function did not change much for secondary creep in the non-linear range of the logarithmic plot of $\dot{\varepsilon}_s$ versus σ. For example, upon a stress change from 4298 psi. to 3892 psi., the constant A changed from $8.4 \times 10^{-48}(\text{in./lb.})^n$ to $8.7 \times 10^{-48}(\text{in./lb.})^n$ which is within the experimental error. It appears then, that A and B can be estimated by using the data obtained from the incremental stress changes if the assumption that, for small stress changes, A and B are almost constant is applied.

For a given stress, σ_1,

$$\dot{\varepsilon}_{t_1} = A'\sigma_1^{\,n} + B'\sigma_1 \tag{21}$$

describes the behavior of the sample. After a small change in stress (less than 10 per cent), a new creep rate is established, and is described by:

$$\dot{\varepsilon}_{t_2} = A'\sigma_2^{\,n} + B'\sigma_2 \tag{22}$$

where σ_2 is the new stress.

Upon rearrangement and rationalization of Equation 21, an expression for A' can be found:

$$A' = \frac{(\sigma_1/\sigma_2)\,\dot{\varepsilon}_{t_2} - \dot{\varepsilon}_{t_1}}{(\sigma_1/\sigma_2)\,\sigma_2^{\,n} - \sigma_1^{\,n}} \tag{23}$$

Also, B' is found from Equation 21 to be:

$$B' = \frac{\dot{\varepsilon}_{t_1} - A\sigma_1^{\,n}}{\sigma_1} \tag{24}$$

Thus, A' and B' are approximations to the values of A and B of Equation 20 and the contribution of a linear deformation mechanism relative to secondary creep of OFHC copper can be estimated.

To summarize the picture presented thus far, it can be said that homogeneous OFHC copper is assumed to behave as pure copper following a power function of the form of Equation 16; that OFHC copper with voids and tough pitch copper with or without voids behave as two phase materials, one phase of which follows a function similar to Equation 16, while the other phase follows a linear stress function of the form of Equation 17.

Table 5 summarizes the data used to calculate A' and B', the calculated values of A' and B', as well as the percentage contributions of each term of Equation 21 to the observed total creep rate, $\dot{\varepsilon}_t$. The power, n, to which stress was raised was taken to be the power determined from data of secondary creep at constant stress of OFHC copper.

Fig. 30 shows a plot of percentage contribution made by the linear term to the total creep rate versus creep strain. Secondary creep points are marked by the numeral "2", while the numeral "3" marks tertiary creep points.

Notice that the tertiary creep points for both OFHC copper and tough pitch copper appear to lie on straight lines and that there seems to be an increase in the contribution of the linear term, $\dot{\varepsilon}_L = B\sigma$, as creep progresses through the third stage. In other words, it looks as if the linear deformation process becomes more important in tertiary creep. The figure would suggest, too, that for tough pitch copper undergoing secondary creep there is a strong contribution from some linear mechanism, the role of which decreases as tertiary creep is approached and then increases through tertiary creep. There is no reason to believe that the linear term represents the same mechanism for both.

INDUCTION TIMES

Further light may be shed on what happens during tertiary creep by considering the induction time data shown in Fig. 10. Induction time data was evaluated first by using the method followed by Davies and Dutton[25] in which the rate of recovery was determined to be:

$$r = \partial\sigma/\partial t \approx \Delta\sigma/\Delta t \qquad (25)$$

where r is the rate of recovery of flow stress,
$\Delta\sigma$ is the change in stress which was made,
Δt is the induction time.

Fig. 31 shows a plot of recovery rate versus logarithmic strain in which the recovery rate was determined using Equation 25. Even though a scatter exists in the data, a trend towards increasing recovery rate with strain is apparent. Induction times for similar tertiary creep points, but different samples, were not significantly longer for samples which had undergone larger stress changes. Induction times for secondary creep appear not to increase proportionally with increased magnitude of the stress change. This is responsible for the separation of the data into three curves as shown in Fig. 31. If induction times were proportional to the stress change magnitudes, then one would expect that when plotted in the form shown, all data would lie on one curve.

An expression was desired which would show the relationship between the induction time and the creep rate, to help understand what was occurring. It was thought that recovery might depend on a power relationship between recovery rate and stress. Nadai gives an expression for the recovery strain in terms of the stress and the time which is based on a similar power function[37] which, when differentiated with respect to time and rearranged so that Nadai's power function is in terms of the power function used in

this report, gives the recovery rate, $\dot{\varepsilon}''$, at time t as:

$$\dot{\varepsilon}'' = -\varepsilon''_o \left[1 + \left(\frac{n-1}{n}\right)\left(\frac{nE}{\Delta\sigma}\right) A\cdot\Delta\sigma^{n}\cdot t\right]^{-\left(\frac{2+n}{n-1}\right)} \left(\frac{E}{\Delta\sigma}\right) A\cdot\Delta\sigma^{n} \qquad (26)$$

where $\dot{\varepsilon}''$ is the recovery rate,

ε''_o is the creep strain at the time t = 0 when the decrease in stress, $\Delta\sigma$, was made,

n is the power in the power function and A the constant,

E is Young's modulus.

The observed strain rate was taken to be the sum of the recovery rate and the creep rate under the action of the stress to which the decrease was made, i.e.:

$$\dot{\varepsilon}_t = \dot{\varepsilon}'' + \dot{\varepsilon}_2 \qquad (27)$$

The induction time, according to the method used in the experiment would be the time for which $\dot{\varepsilon}_t$ = 0 (i.e., zero slope). Hence, upon setting $\dot{\varepsilon}_t$ = 0, substituting Equation 26 into Equation 27 and rearranging to find the induction time, an expression results, such as:

$$t_r = \left\{\left[\left(\frac{\dot{\varepsilon}_2}{\varepsilon''_o}\right)(EA)^{-1}(\Delta\sigma)^{n-1}\right]^{\frac{1-n}{2+n}} - 1\right\} \Big/ \left[(n-1)(EA)(\Delta\sigma)^{n-1}\right] \qquad (28)$$

where t_r is the induction time (a measure of the recovery time).

When this expression was checked using secondary creep data, it gave induction times which were orders of magnitude too small (e.g., 10^{-4} or 10^{-5} hr.). It was concluded that the recovery process did not follow the same function as creep, especially for the small changes in stress involved.

An attempt was made to linearize the dependency of induction time on creep rate as follows. At first appearances, the tertiary creep points of Fig. 10 were reminiscent of the function (as Fig. 32 illustrates):

$$y = e^{-x} \qquad (29)$$

[illegible]

One will recall the strain response to stress for the Kelvin model of a solid follows a similar function (a "Kelvin solid" is one whose response to stress is analogous to that behavior of a linear spring and a linear dashpot in parallel). The applied stress for this model can be considered to be carried by two inseparable components: (i) an elastic component, and (ii) a viscous component. The strain response to stress of such a model is described by:[38]

upon loading: $$\varepsilon = \frac{\sigma}{E}\left(1 - e^{-t/\tau}\right) \tag{30}$$

upon unloading: $$\varepsilon = \frac{\sigma}{E}\left(e^{-t/\tau}\right) \tag{31}$$

where ε is the strain at time, t,
σ is the applied stress,
E is Young's modulus,
τ is a constant known as the relaxation time.

Differentiation of Equations 30 or 31 gives the strain rate dependence upon time,

$$\dot{\varepsilon} = \frac{\sigma}{E\tau} e^{-t/\tau} \tag{32}$$

the logarithm of which is:

$$\log \frac{\dot{\varepsilon}}{\sigma} = \frac{-t}{2.3\tau} + \log \frac{1}{E\tau} \tag{33}$$

One would expect that a plot of log $\dot{\varepsilon}/\sigma$ versus t should be linear with a slope of $-1/2.3\tau$, and that all the data should lie on a straight line, if this relationship correctly describes the behavior of the material. The ordinate, at t = 0, should be a constant whose value is log $1/E\tau$.

Upon a negative stress change, the creep rate decreased to zero, or nearly so, then increased gradually to the new creep rate. To apply the experimental results to Equation 32, the creep curve immediately after a stress change has to

be viewed as a recovery curve. To understand how this was done, consider the following discussion along with Fig. 33.

As shown by Fig. 33(a), the intersection of the horizontal tangent and the new creep rate defined the induction period. If Fig. 33(a) is rotated through an angle defined by the new creep rate, to give Fig. 33(b), a curve similar to a strain recovery curve defined by Equation 31 results, the slope of which at t = 0 is the same as $-\dot{\varepsilon}_2$ (i.e., $\dot{\varepsilon}_2$ is the new steady state creep rate). Because of the small changes in strain rate involved, only a small error will be made in the induction time by assuming that the slope, $\dot{\varepsilon}_r$, remains constant during the time t_i and by letting the slope change suddenly to the new value, $\dot{\varepsilon}_2$, after the time t_i. With this in mind, then, from Fig. 33(a):

$$\dot{\varepsilon}_t = \dot{\varepsilon}_2 + \dot{\varepsilon}_r \tag{34}$$

where $\dot{\varepsilon}_t$ is the total slope during the induction time t_i,

$\dot{\varepsilon}_2$ is the new steady state creep rate,

$\dot{\varepsilon}_r$ is the recovery rate until the time t_i.

Upon substitution for $\dot{\varepsilon}_r$:

$$\dot{\varepsilon}_2 = -\frac{\Delta\sigma}{E\tau} e^{-t_i/\tau} \tag{35}$$

This is the version of Equation 32 which was used to treat the experimental results. Fig. 34 shows the induction time data plotted according to the equation:

$$\log \frac{\dot{\varepsilon}_2}{\Delta\sigma} = -\frac{t_i}{2.3\tau} + \log \frac{1}{E\tau} \tag{36}$$

where $\dot{\varepsilon}_2$ is the steady state creep rate after a negative stress change,

$\Delta\sigma$ is the magnitude of the stress change,

t_i is the induction time and the other symbols are as defined for Equation 31.

[illegible]

Tests 9, 10, and 12 were run specifically to estimate induction times at different stress change magnitudes. To reduce the effect of sample history, the time at reduced stress was kept to a minimum by returning to the test reference stress soon after the creep curve deviated from the horizontal tangent. Thus, not enough time was spent at some of the new steady-state creep rates to give accurate measurements. For this reason, $\dot{\varepsilon}_2$ was calculated using:

$$\dot{\varepsilon}_2 = \dot{\varepsilon}_1 (\sigma_2/\sigma_1)^n \tag{37}$$

where $\dot{\varepsilon}_1$ is the creep rate before the stress change,

σ_1 and σ_2 are the stresses before and after the change,

n is the stress sensitivity.

A power, n, of 12 was used for secondary creep points and a power of 6 was used for tertiary points on the creep curves. (Table 6)

Notice that the tertiary points for Test 9 ($\Delta\sigma = 4.7$ per cent) lie on a straight line and that, even though the other data is more scattered, a similar trend is followed by the tertiary points of Tests 7 ($\Delta\sigma = 9.45$ per cent) and 12 ($\Delta\sigma = 14.2$ per cent).

A relaxation time of 23 min. was calculated for the data shown. A spread in the apparent values of E exists because the curves intercept the ordinate at different points. Values of E were found to be 2.6×10^5 psi. for $\Delta\sigma = 4.7$ per cent; 1.21×10^6 psi. for $\Delta\sigma = 10$ per cent; 1.5×10^6 psi. for $\Delta\sigma = 14.2$ per cent. These numbers should not be given much emphasis because all points do not lie on one curve as would be expected if Equation 36 correctly described the behavior of the OFHC copper.

The results suggest that the recovery rate for OFHC copper decreased with the logarithm of the creep strain. Apparently Equation 36 does not describe the stress depen-

dency of the recovery rate. The split in the data suggests that either:

(i) the recovery rate stress dependency is described by a non-linear function, such as a power function with a power less than 1, or

(ii) the recovery rate is a function of the applied stress, or

(iii) the observed stress dependency is a machine effect which, for the case of small stress changes, is strong enough to mask the true stress dependency of induction time.

The problem could, possibly, be resolved by a more intensive investigation into the phenomenon of creep strain recovery upon small decreases in stress.

There were fewer data available for the tough pitch copper, but all the induction times which could be obtained for the stress changes in the neighbourhood of 9 per cent were plotted on Fig. 34. Not enough data were available to determine curves for stress changes near 5 per cent and 15 per cent, so that the effect of stress change magnitude upon induction time could be seen. But, for the tough pitch copper data which was plotted, a relaxation time of 8 min. and an E of 3.2×10^5 psi. were calculated.

The relaxation time for the tough pitch copper was about 1/3 that for the OFHC copper, during tertiary creep. The results for the tough pitch copper suggested, too, that the recovery rate increased with the logarithm of the creep strain. Further experimentation would be necessary to discern the effect of stress upon induction time.

ANALYSIS OF THE LINEAR TERM CONSTANT

The trends observed in the variation of the induction time with creep strain supported the trends observed in the contribution of the term:

$$\dot{\varepsilon}_L = B\,\sigma \qquad (38)$$

As tertiary creep progressed, there seemed to be an increase in the contribution of some linear, or near-linear, mechanism which tended to accelerate the rate of recovery of the creep sample. This suggested that recovery was controlled by the linear term. An attempt was made to correlate the experimentally determined magnitudes of B with the term:

$$B = e^{-t/\tau}/E\tau \qquad (39)$$

but this exercise met with no success. The experimental values of B were 2 or 3 orders of magnitude lower than those predicted by Equation 39. This was understood to mean that, possibly, creep and recovery occurred by different mechanisms.

It should be noted, also, that the induction time data was evaluated using an equation which expressed the behavior of a specific model for recovery. The model does not express the behavior of copper exactly, but only approximates it. Total agreement, therefore, of experimental and predicted results should not be expected.

Attempts were also made to correlate B with the constants of the Nabarro-Herring and the Gifkins equations for creep rate, but to no avail. These constants, as can be seen from Table 4, are:

$$c\,b^3 D/L^2 kT \qquad \text{Nabarro-Herring}$$

$$\kappa \delta N \Omega D_{gb}/\ell kT \qquad \text{Gifkins}$$

To calculate B, the following values of terms were used:

b^3 is (Burger's vector)^3 = 16.5 x 10^{-24}cm.^{3},

D is the diffusion coefficient,

(i) for lattice diffusion: 3.42 x 10^{-16}cm.^{2}/sec.,

(ii) for surface diffusion: 8 x 10^{-12} cm.^{2}/sec.,

(iii) for grain boundary diffusion:

$$2 \times 10^{-9} \text{ cm.}^2/\text{sec.},$$

L is the grain diameter=5.5×10^{-3} cm.,

T is the absolute temperature=698°K,

N is the number of boundaries per cm.=180,

Ω is the atomic volume=1.17×10^{-23} cm.^{3}/at.,

ℓ is the length of the longest grain boundary ledge which controls diffusion path = 100 atoms,

$\kappa\delta$ is a constant $\approx$ 2.

The calculated values for B were at least 6 orders of magnitude too small. One can only conclude that neither of these equations satisfactorily expresses the behavior of the copper undergoing tertiary creep.

A SIMPLE APPROACH TO TERTIARY STRAIN

It was recalled that some investigators have sought to explain tertiary creep as being caused by the growth of voids alone.[15,39] To investigate the question as to whether the tertiary creep strain, as measured by the creep recorder, could be caused by the growth of voids in the longitudinal direction, void size measurements obtained from the mensuration of grains of Samples 6 and 10 were treated, using strain to be defined as:

$$\varepsilon_v = \ln[(l_v + n_g l_g / n_g l_g)] \qquad (40)$$

where ε_v is the creep strain due to voids,

l_v is the average length of a void in the longitudinal direction,

n_g is the average number of grains between voids,

l_g is the average grain dimension in the

longitudinal direction.

For Sample 6, values of l_v, n_g, and l_g were found to be 0.09×10^{-2} cm., 3.3 grains, and 0.61×10^{-2} cm. respectively. When substituted, they yielded a strain due to voids of about 4.3 per cent.

Similarly, for Sample 10, values of $l_v = 0.1 \times 10^{-2}$cm., $n_g = 3.0$ grains, and $l_g = 0.54 \times 10^{-2}$ cm. were substituted to yield a strain due to voids of about 6 per cent.

Assuming that all tertiary creep strain was due to voids alone, the strains due to voids as determined from the creep curve was about 3 per cent for both Samples 6 and 10, at fracture. As it turned out, this was lower than those calculated from the grain measurement data. It is worth noting that implicit in this method of strain estimation is the assumption that the void shape is rectangular. In reality, this is not true. Thus, the overestimation of the strain which this method produces may be the result of the simplification of void shape. This factor does not rule out the possibility that the growth of voids makes a significant contribution to the tertiary creep strain.

Some other questions are raised by the overestimation as well, which, for the moment, have no satisfactory answers. Could the voids be enlarged sufficiently by the etchant to account for the discrepancy? Oliver and Girifalco[40] found that an etchant increased the mean creep cavity size linearly with the etching time. Do those grains which have an extra degree of freedom on a boundary strain more readily, under the action of local forces, than the overall creep sample? Could surface diffusion modify the cavity shape enough to account for the difference?

DISCUSSION OF POSSIBLE DEFORMATION MECHANISMS

From the foregoing consideration of the data, it becomes apparent that three major trends must be explained

concurrently by a particular proposal, if it is to be considered a suitable candidate for further investigation. These three trends are:

(i) the increase in the contribution of the linear term to the total creep rate as creep progresses;

(ii) the increase in the amount of grain boundary sliding as creep progresses;

(iii) the increase in the amount of cavitation as creep progresses.

A fourth observation which must be explained, but not necessarily concurrently with the aforementioned, is the observation that the recovery time decreases as the creep strain increases.

An idea which suggests itself from the evaluation of the data is that grain boundaries play an important role during creep of the copper samples. Several observations, coupled with some findings of other investigators, point in this direction. It has been found that the amount of grain boundary sliding varies linearly with the stress for a number of materials, copper included.[31] Also, it has been noticed that the ratio:

$$\varepsilon_b/\varepsilon_t = \text{constant} \qquad (41)$$

where ε_b is the strain due to grain boundary sliding,

ε_t is the total strain,

for a wide range of strains in several materials including copper.[41] These two findings are similar to trend (i). This suggests that some deformation process associated with the grain boundaries is important.

Even though the grain boundary sliding calculations, based upon the grain dimension data, must be interpreted with caution, because of the possible effects of boundary migration, it is worth noting that they follow a trend

similar to the other observations. That is, the amount of sliding based on grain dimension data gathered from the sample which underwent secondary creep only was zero, while the amount of sliding based on grain dimension data gathered from samples which underwent tertiary creep was found to be 100 per cent or more. This observation leaves the impression that, sometime between secondary creep and fracture, some deformation process becomes important which is associated with the grain boundary.

The offsets of a line of etch pits in Fig. 19 suggests that some sliding may have occurred. Also, some of the voids in Fig. 25 seem to have linked as a result of a shearing process.

The reason for considering grain boundaries is that they open the door to a possible explanation for trends (i), (ii), and (iii)--an explanation which could account for all three of these trends simultaneously.

There is no reason to believe that intragranular creep processes, such as dislocation motion, and grain boundary sliding would not operate concurrently. There is evidence which indicates that grain boundary sliding is dependent upon intragranular deformation processes so that sliding may continue.[42] Grain boundaries can be sources for dislocations either because of the presence of ledges[43,44] or impurity particles. The dislocations could move through the crystal, thus contributing to creep, and undergo such reactions as: pile-up, intersection, climb, locking, and jogging.

The high activation energy determined for OFHC copper (ΔH = 80 kcal./mole) undergoing secondary creep could be indicative of a rate controlling mechanism, such as: cross-slip (calculated ΔH = 230 kcal./mole), or dislocation intersection (calculated ΔH = 60 kcal./mole). It may be that the role of the grain boundaries under these conditions is, primarily, the production and annihilation of mobile dislocations.

Certain experimental evidence indicates that, as creep progresses through second stage, grain boundary voids are nucleated.[17,18] Gittins[18] found that the number of voids nucleated varied with the square root of time, and that the amount of grain boundary sliding varied in the same way. He concluded, therefore, that void nucleation was dependent upon grain boundary sliding. The rate of void nucleation is apparently dependent upon the existence of stress raisers, within the boundary, as well as boundary sliding, according to Boettner and Robertson.[17] It could be that the longer creep life and the lower secondary creep rate for the OFHC copper was attributable to a smaller contribution from grain boundary sliding during the early part of the test and a fewer number of void nucleation sites (i.e., fewer impurity particles). Voids, once nucleated and reaching a stable size, could contribute to the creep processes by:

(i) reducing the boundary area across which a force can act, thereby causing an increased shear stress on the boundaries;

(ii) removal of obstacles to the creep mechanism;

(iii) causing an increase in the number of mobile dislocations.

With an increased shear stress on the boundaries, sliding on any given boundary would be more frequent; the contribution to the total creep rate would increase with strain. Impurities and ledges within the boundaries act as obstacles to creep mechanisms by causing pile-up of dislocations, inhibiting of boundary sliding, and slowing of diffusion. If a void opens up at such a stress raiser, then dislocations could egress the crystal at that point where they were held back before. With the removal of obstacles to dislocation motion, more dislocations would become mobile, thus accelerating the creep mechanism.

Consider briefly the behavior of the tough pitch copper. It is not known what mechanism the activation energy

for secondary creep of tough pitch copper represents (ΔH = 26 kcal./mole), but, as stated earlier, it agrees with that found by Feltham and Meakin.[22] The mechanism whose activation energy is closest to this is viscous grain boundary sliding. If this is one of the deformation mechanisms which plays a leading role during the secondary creep on this material, then, this, coupled with the higher number of impurities, could be responsible for the higher creep rates and the shorter creep lives than those of the OFHC copper. For example, if there is a greater contribution to the total creep rate earlier in the test by grain boundary sliding, voids would be nucleated sooner and at a higher rate. With the voids present sooner, the accelerated creep rate would become apparent sooner.

The activation energy for tertiary creep of OFHC copper (ΔH = 35 kcal./mole) falls within the range for viscous grain boundary sliding. This may be indicative that the rate controlling mechanism is sliding, during tertiary creep.

It is not clear how much emphasis should be placed upon the difference between the activation energy for tertiary creep of tough pitch copper and OFHC copper. Further investigation into this should be done to learn whether this difference is real and whether it is indicative of the rate controlling mechanism. If the activation energy for the tertiary creep of tough pitch copper is representative of the rate controlling process, it indicates that self-diffusion is rate controlling (ΔH = 45.1 to 56 kcal./mole). One way of looking at this might be to consider the grain boundary to be similar in structure to the island model proposed by Gifkins.[45] He took the view that the grain boundary was composed of regions of good and poor fit. Between the "islands" of good fit were channels or areas of irregular atomic structure. If the channels contained many of the impurity particles, atoms or vacancies would be

forced to diffuse through the regions of good fit to reach the growing voids. Again, as before, as a void grows within a particular boundary, it causes an increase in the shear stress acting on that boundary; as this stress reaches a critical value, an increment of sliding could occur. Continued reduction of the area by void growth would cause the process to be repeated many times until the linking of voids resulted.

To summarize thus far, the observed behavior of the coppers--as outlined in trends (i), (ii), and (iii)--can be explained by considering the grain boundaries to play an important role in the creep process.

A body of experimental evidence exists which points to the idea that growth of cavities is controlled by vacancy diffusion from the grain boundary.[8,14,15,18]

The first mathematical treatment of the effect of voids upon the time to rupture was presented by Hull and Rimmer.[15] Their expressions for the rate of change of void radius and time to fracture are included in Table 4. One shortcoming of their theory was that all void nuclei were assumed to begin growing at the first application of the load. Allowance for cavity nucleation during creep was not made.[46] The formula for void growth predicted vanishingly small growth rates for large void spacings--an idea which was not borne out by experiment. Speight and Harris[39] have developed an expression for void growth which overcame this difficulty (see Table 4).

Both the Hull-Rimmer and the Speight-Harris equations for void growth predict the time dependency of void radius, r. From the integration of dr/dt with respect to time, one obtains, for each case:

$$\text{Hull-Rimmer:} \qquad r \propto t^{1/2} \tag{42}$$

$$\text{Speight-Harris:} \qquad r \propto t^{1/3} \tag{43}$$

The volume of a single void, v, depends upon the

cube of the radius,

$$\text{i.e.,} \qquad v \propto r^3 \tag{44}$$

Hence, by Hull's and Rimmer's theory:

$$v \propto (t^{1/2})^3 = t^{3/2} \tag{45}$$

And by Speight's and Harris's theory:

$$v \propto (t^{1/3})^3 = t \tag{46}$$

which, it should be added, was observed experimentally by Gittins for copper crept to tertiary creep.[18]

The total cavity volume, V, is a function of the number of cavities, N, and the average void volume, v.

$$V = Nv \tag{47}$$

According to the Hull-Rimmer theory, where the number of cavities is constant with time, the total void volume should increase according to:

$$V \propto (t^0)(t^{3/2}) = t^{3/2} \tag{48}$$

Now, as was mentioned earlier, Gittins found for high-purity copper crept to third stage, at 400°C, that:

$$N \propto t^{1/2} \tag{49}$$

This, when substituted into the Speight-Harris theory for large void spacings, shows the total void volume to change with time as:

$$V \propto (t^{1/2})(t) = t^{3/2} \tag{50}$$

It should be emphasized that the Hull-Rimmer theory would be applicable for small ratios of a/r--where a is the void spacing and r the void radius--and that the Speight-Harris expression should be applied to large a/r. Both predict that total void volume changes in the same way. The important difference between them is that one considers the number of cavities to be constant, while the other considers void number to change with time.

Lay aside this theoretical consideration for the

moment and consider that from the data gathered in this experimental program, it should be possible, indirectly, to estimate the time dependency of the term $(B\sigma/\dot{\varepsilon}_t)$. Notice, from Fig. 30, that:

$$B\sigma/\dot{\varepsilon}_t \propto \varepsilon_{t_3} \tag{51}$$

for tertiary creep. A logarithmic plot of total creep strain, ε_{t_3}, for tertiary points, versus time, t, should be a straight line, if voids are the prime contributor to the changing tertiary creep strain.

Such a graph for OFHC and tough pitch coppers, in Fig. 35, yields straight lines with slopes of about 1.5--within experimental error. Therefore,

$$\varepsilon_{t_3} \propto t^{1.5} \tag{52}$$

and also, therefore,

$$B\sigma/\dot{\varepsilon}_{t_3} \propto t^{1.5} \tag{53}$$

Thus, barring fortuitous agreement, it appears that the percentage contribution of the linear term to the total creep rate is a function of total void volume:

$$B\sigma/\dot{\varepsilon}_{t_3} \propto V \tag{54}$$

This is seen from the similarity of Functions 53, 48, and 50. It is difficult to be more explicit than this because a question arises as to which of Functions 48 or 50 to use. Late in tertiary creep, the ratio a/r should be lower than it is during late secondary or early tertiary creep, but would it be low enough for the Hull-Rimmer expression to be more valid than the Speight-Harris function?

Contributions to total void volume, V, by N and v cannot be discerned as no data is available which shows how N and v changed with time during tertiary creep of samples in this program.

Grain boundary sliding and void nucleation by sliding

cannot be excluded as possible contributors to tertiary creep, until the roles played by each during the third stage have been established. If both of these contribute significantly to tertiary creep, this might offer an explanation for the inability to correlate B with any single mechanism.

Finally, consideration should be given to the observation that the recovery time decreases as creep progresses through third stage for both coppers. The recovery process could occur within the grain boundary or it could be an intragranular mechanism. Consider the OFHC copper first. The metallography revealed that some boundary migration may have occurred during creep. While this may not have been the major recovery mechanism, especially for tertiary creep, it cannot be discounted as a non-contributor to recovery. If it were the rate controlling mechanism, one would expect that the activation energy for the OFHC copper would be closer to that for self-diffusion. The recovery mechanism should be one which tends to lower the internal stress of the sample. This could be done by the motion of dislocations to the voids. The surfaces of the voids may present free surfaces to the dislocations at which to egress the crystals, thus reducing the internal stress. Or, perhaps, grain boundary sliding could be the recovery mechanism. An increased stress on a boundary could be relieved by local sliding.

Similar mechanisms could be pictured for the tough pitch copper. Strictly speaking, the recovery process should be investigated further with the hope of illuminating the mechanism by which recovery occurs.

During this investigation into the phenomenon of creep in copper, several trends have become apparent. It has been suggested that these are caused by the role of grain boundaries and the growth of voids. At the same time, a number of questions have appeared:

(i) how is grain boundary sliding related to the intragranular creep processes?

(ii) Is there a significant difference between the tertiary creep activation energies for tough pitch and OFHC coppers?

(iii) If grain boundary sliding is an important deformation mechanism for the coppers, is it controlled by the same process in both?

(iv) How is recovery associated with sliding?

(v) How does recovery depend upon stress?

(vi) By what processes do voids actually contribute to the recovery mechanism?

To supply answers to these and other questions with respect to the phenomenon of tertiary creep, there remains much work yet to be done in future experimental programs.

CONCLUSIONS

From this experimental program certain trends in the behaviors of OFHC and tough pitch coppers undergoing tertiary creep at constant stress, near 4000 psi., at constant temperature, near 700°K, and in an argon atmosphere, were studied. The following conclusions apply to the particular conditions of this experimental program:

(i) during tertiary creep, the sample nominal cross-sectional area changed in much the same way as it did during secondary creep. Therefore, use of the constant stress cam for tertiary creep was justified.

(ii) OFHC and tough pitch coppers failed in a brittle way (i.e., low macroscopic ductility); round-type grain boundary voids were prevalent.

(iii) OFHC copper had a lower minimum creep rate and a longer creep life than tough pitch copper, under similar test conditions.

(iv) For small ranges of stress, the minimum creep rate and stress can be related by a power function.

(v) Below about 3000 psi., the OFHC copper exhibited a constant power of 3.59. As stresses were increased above about 3000 psi., the power function became stress sensitive so that the power was near 12 when the stress was near 4300 psi.

(vi) The power for tough pitch copper was constant at about 5 for a range of stress from 4000 psi. to 5500 psi.

(vii) The activation energy for OFHC copper during secondary creep was near 80 kcal./mole. For tough pitch copper, it was 26 kcal./mole. Tertiary creep values were: ΔH = 35 kcal./mole for OFHC copper and ΔH = 40 to 55 kcal./mole for tough pitch copper. These values should be investigated further.

(viii) An analysis of grain dimension data for OFHC copper showed that the grain size was not uniform.

[illegible]

This suggested that grain growth and recrystallization may have occurred during creep.

(ix) The results of the application of Rachinger's method of grain boundary sliding measurement suggested that more sliding occurred during tertiary creep of OFHC copper than during secondary creep.

(x) The tensile tests indicated that voids lower the strain hardening exponent, the strength coefficient, and the ductility of copper. For OFHC and tough pitch coppers, the strain hardening exponent was 0.46; for a cavitated sample (OFHC), it was 0.3.

(xi) An apparent change in the stress sensitivity occurred upon transition to tertiary creep. The stress sensitivity decreased for OFHC copper; it increased for tough pitch copper.

(xii) The stress sensitivity change could not be accounted for by a change in sample net cross-sectional area.

(xiii) Stress sensitivity measurement is a sensitive way to reveal changes in deformation mechanism and structure of a material.

(xiv) The concept of two simultaneously operative creep rate controlling mechanisms was able to resolve the apparently contradictory behavior of the two coppers. The total creep rate was considered to be the sum of a creep rate whose stress dependency was a power function and a creep rate whose stress dependency was linear.

(xv) The tertiary creep of OFHC and tough pitch coppers was parallelled by an increase in the contribution of the linear mechanism to the total creep rate.

(xvi) Creep and recovery seem to occur by different mechanisms.

(xvii) The total creep strain during tertiary creep seems to be exponentially related to the recovery time

for both coppers.

(xviii) The relaxation time for tertiary creep of OFHC copper is about three times that for tough pitch copper.

(xix) The grain boundaries play an important role during the creep of copper. Exactly how they contribute to creep is not explicitly apparent, however trends in the data suggest that grain boundary sliding is important.

(xx) The total tertiary creep strain varied as the test time raised to the power 3/2.

(xxi) From (xx), it was inferred that the total cavity volume varied linearly as the total creep strain for tertiary creep.

(xxii) The contribution of the linear creep mechanism to the total creep rate seems to be linearly related to the total void volume.

(xxiii) The tertiary creep of copper, under the conditions of this investigation, is likely the result of an interplay of grain boundary sliding, void nucleation by sliding, and cavity growth. These areas should prove worthwhile to investigate further.

BIBLIOGRAPHY

1. Garofalo, F., Fundamentals of Creep and Creep-Rupture in Metals, The Macmillan Company, New York, 1965.
2. Nemy, A. S., Rhines, F. N., Trans. AIME, 215 (1959), p. 992.
3. Greenwood, J. N., Miller, D. R., Suiter, J. W., Acta Met., 2 (1954), p. 250.
4. Taplin, M. R., Barker, L. J., Acta Met., 14 (1966), p. 1527.
5. Chang, H. C., Grant, N. J., Trans. AIME, 206 (1956), p. 1241.
6. Davies, P. W., Finniear, T. C., Wilshire, B., J. Inst. Met., 90 (1961-62), p. 368.
7. Garofalo, F., op. cit., p. 234.
8. Steigler, J. O., Farrell, K., Loh, B. T. M., McCoy, H.E., ASM Trans. Quart., 60 (1967), p. 494.
9. McLean, D., Grain Boundaries in Metals, Oxford University Press, Oxford, 1957.
10. Gifkins, R. C., Acta Met., 4 (1956), p. 98.
11. Cottrell, A. H., Structural Processes in Creep, Iron and Steel Inst., London, 1961, p. 1.
12. Balluffi, R. W., Seigle, L. L., Acta Met., 3 (1955), p. 170.
13. McLean, D., J. Australian Inst. Met., 8 (1963), p. 45.
14. Balluffi, R. W., Seigle, L. L., Acta Met., 5 (1957), p. 449.
15. Hull, D., Rimmer, D. E., Phil. Mag., 4 (1959), p. 673.
16. Nelson, R. S., Mazey, D. J., Barnes, R. S., Phil. Mag., 11 (1965), p. 91.
17. Boettner, R. C., Robertson, W. D., Trans. AIME, 221 (1961), p. 613.
18. Gittins, A., Metals Sci. J., 1 (1967), p. 214.
19. Garofalo, F., op. cit., p. 67.
20. Conrad, H., Experimental Evaluation of Creep and

Stress Rupture in Mechanical Behavior of Materials at Elevated Temperatures, Dorn, J. E., McGraw-Hill Book Company, Inc., New York, 1961, p. 169.

21. Garofalo, F., op. cit., p. 50.
22. Feltham, P., Meakin, J. D., Acta Met., 7 (1959), p. 614.
23. Garofalo, F., op. cit., p. 68.
24. Cottrell, A. H., Aytekin, V., J. Inst. Metals, 77 (1950), p. 389.
25. Davies, P. W., Dutton, R., Acta Met., 15 (1967), p.1365.
26. Rachinger, W. A., J. Inst. Metals, 81 (1952-53), p.33.
27. McGregor Tegart, W. J., Elements of Mechanical Metallurgy, The Macmillan Company, New York, 1966, p. 17.
28. Prantis, A. L., Pound, G. M., Trans. AIME, 203 (1955), p. 664.
29. Greenough, A. P., Phil. Mag., 43 (1952), p. 1075.
30. Price, A. T., Hall, H. A., Greenough, A. P., Acta Met., 12 (1964), p. 49.
31. Garofalo, F., op. cit., p. 141.
32. Cottrell, A. H., Dislocations and Plastic Flow in Crystals, Oxford University Press, Oxford, 1953, p. 18.
33. Barrett, C. R., Trans. AIME, 239 (1967), p. 1726.
34. Barrett, C. R., Nix, W. D., Acta Met., 13 (1965), p. 1247.
35. McLean, D., Reports on Progress in Physics, 29 (1966), p. 1.
36. Ishida, Y., McLean, D., J. I. S. I., 205 (1967), p. 88.
37. Nadai, A., Theory of Flow and Fracture of Solids, Vol. 2, McGraw-Hill Book Company, Inc., New York, 1963, p. 546.
38. Nadai, A., op. cit., p. 164.
39. Speight, M. V., Harris, J. E., Met. Sci. J., 1 (1967), p. 83.
40. Oliver, P. R., Girifalco, L. A., Acta Met., 10 (1962),

[illegible]

p. 765.

41. McLean, D., Farmer, M. H., J. Inst. Metals, 85 (1956-57), p. 41.

42. Garofalo, F., op. cit., p. 145.

43. Strutt, P. R., Lewis, A. M., Gifkins, R. C., J. Inst. Metals, 93 (1964), p. 71.

44. Li, J. C. M., J. Appl. Physics, 32 (1961), p. 525.

45. Gifkins, R. C., Mat. Sci. Eng., 2 (1967), p.181.

46. Greenwood, G. W., Phil. Mag., 8 (1963), p. 707.

[illegible]

TABLES

TABLE 1

SPECTROGRAPHIC ANALYSES OF OFHC COPPER

Element	Concentration (ppm.) Specimen 1	Specimen 2
O_2	3	<3
Ag	10	10
Fe	1	1
S	9	12
As	<3	<3
Pb	7	6
P	<1	<1
Sb	4	4
Bi	0.2	0.2
Te	<2	<2
Sn	2	1
Zn	<0.5	<0.5
Ni	3	3
Hg	<1	<1
Cd	<0.1	<0.1
Mn	<0.1	<0.1
Conductivity (% IACS)	101.7	101.6
Bends *	12-11	12-11

* Represents number of 90° reverse bends before breaking of 0.080 in. dia. wire heated for 30 min. in hydrogen at $850^{\circ}C$ and quenched.

TABLE 2

A SUMMARY OF THE CREEP TESTS

TEST NO.	TYPE OF COPPER	TEST TEMP. (^{o}K)	STRESS (psi.)	STEADY STATE CREEP RATE (%/hr.)	APPROX. START OF TERTIARY CREEP STRAIN (%)	FRACTURE STRAIN (%)	DURATION OF TEST (hr.)	REMARKS
1	Tough Pitch	676	5588	0.4	~1.4	7.4	12	Ordinary creep test.
2	Tough Pitch	681	4688 4486 4082	0.145 0.107 0.077	~2.6	8.4	34.8	Stress sensitivity & activation energy determinations.
3	Tough Pitch	687	4198 4594 3802	0.097 0.15 0.068	~2.9	7.05	34.1	Stress sensitivity determination.
4	Tough Pitch	708	4266	0.193	~2.2	7.8	22.9	Activation energy determination.
5	Tough Pitch	703	4317 3910	0.208 0.115	?	6.18	22.0	Stress sensitivity determination.
6	OFHC	698	4317	0.048	~2.4	6.4	60.6	Ordinary creep test.
7	OFHC	699	4298 3892	0.077 0.024	~3.2	6.2	65.3	Stress sensitivity determination.
8	OFHC	700	4291	0.046	~1.8	9.3(?)	57.5	Activation energy determination.*

[illegible]

TABLE 2 (CONT'D)

TEST NO.	TYPE OF COPPER	TEST TEMP. (^{o}K)	STRESS (psi.)	STEADY STATE CREEP RATE (%/hr.)	APPROX. START OF TERTIARY CREEP. STRAIN (%)	FRACTURE STRAIN (%)	DURATION OF TEST (hr.)	REMARKS
9	OFHC	698	4288 4086	0.057 0.0087(?)	~2.1	5.3	61.5	Induction times measured.
10	OFHC	698	4307	0.069	~1.8	5.55	56.05	Induction times measured.
11	OFHC	698	2642 2442 3042 1641	0.0088 0.0076 0.0173 0.0019	---	---	126.6	The stress sensitivity of the lower stress range was investigated.
12	OFHC	698	3890 3485	0.0374 0.018	~1.4	---	83.8	Stress sensitivity determination. Total sample strain = 5.04% when removed from creep machine & tensile tested at room temperature.

* Some technical difficulties arose with the recorder near the end of the test.

TABLE 3

A SUMMARY TABLE OF GRAIN MEASUREMENTS

SAMPLE	DIRECTION	AVG. VOID DIMENSION (cm.)	AVG. GRAIN DIMENSION (cm.)	TOTAL STRAIN (%)	GRAIN STRAIN (%)	GRAIN BOUNDARY SLIDING STRAIN (%)
As received	Long.* Trans.**	--	0.64×10^{-2} 0.33×10^{-2}	--	56	0
Annealed for 55hr. at 425°C	Long. Trans.	--	0.63×10^{-2} 0.58×10^{-2}	--	--	--
Sample 6 lower grip	Long. Trans.	--	0.71×10^{-2} 0.64×10^{-2}	--	--	--
Sample 6 gauge length	Long. Trans.	0.09×10^{-2} 0.13×10^{-2}	0.61×10^{-2} 0.63×10^{-2}	6.41	~0	~100
	Long. Trans.	Ignored voids.	0.67×10^{-2} 0.74×10^{-2}	--	--	--
Sample 10 thread end	Long. Trans.	--	0.56×10^{-2} 0.55×10^{-2}	--	--	--
Sample 10 gauge length	Long. Trans.	0.1×10^{-2} 0.29×10^{-2}	0.54×10^{-2} 0.55×10^{-2}	5.55	~0	~100

TABLE 3 (CONT'D)

SAMPLE	DIRECTION	AVG. VOID DIMENSION (cm.)	AVG. GRAIN DIMENSION (cm.)	TOTAL STRAIN (%)	GRAIN STRAIN (%)	GRAIN BOUNDARY SLIDING STRAIN (%)
Sample 11 thread end	Long. Trans.	--	0.76×10^{-2} 0.68×10^{-2}	--	--	--
Sample 11 gauge length	Long. Trans.	--	0.79×10^{-2} 0.58×10^{-2}	1.3	~ 14	~ 0

* "Long." means "longitudinal".

** "Trans." means "transverse".

TABLE 4

A SUMMARY OF SOME CREEP THEORIES

THEORY	RATE EQUATION
A. Reaction Rate	$\dot{\varepsilon} = \frac{2 x k T}{d h} \exp\left(\frac{\Delta S}{R}\right) \exp\left(\frac{-\Delta H_i}{RT}\right) \sinh\left(\frac{A l \sigma}{RT}\right)$ $x \equiv$ distance between flow units, $Al \equiv$ activation volume, $d \equiv$ avg. distance between flow unit layers.
B. Lattice Friction	$\dot{\varepsilon} = C \exp[B(\sigma - \sigma_G)] \exp - \left[\frac{\Delta H_k (1 + 1/4 \log(16\sigma_p/\pi\sigma))}{kT}\right]$ $\Delta H_k \equiv$ kink energy, $\sigma_p \equiv$ Peierl's stress, $\sigma_G \equiv$ internal stress.
C. Dislocation Intersection	$\dot{\varepsilon} = C \exp\left[\frac{-\Delta H_i - V(\sigma - \sigma_i)}{RT}\right]$ $V \equiv$ activation vol. = bXl (X = distance over which activation occurs; l = avg. dislocation spacing in forest), $\Delta H_i \equiv$ activation energy at zero σ, $\sigma_i \equiv$ avg. local internal stress caused by dislocations on parallel glide planes.
D. Cross Slip	$\dot{\varepsilon} = C \exp - \left[\frac{\Delta H_0 - a \log(\sigma/\sigma_0)}{kT}\right]$
Schoeck & Seeger	$\sigma_0 \equiv$ critical resolved shear stress, $\Delta H_0 \equiv$ activation energy for cross slip.
Jaffe & Dorn	$\dot{\varepsilon} = \frac{\alpha L A \nu_0 n^2 \sigma}{4\pi G} \exp\left(\frac{2 U_c}{kT}\right)$ $L \equiv$ total length of screw dislocation per unit vol.

[illegible]

TABLE 4 (CONT'D)

THEORY	RATE EQUATION
E. Average Behavior of Large Numbers of Dislocations	$\dot{\varepsilon} = b(V_0 - k\rho)\rho$ where: $\rho = \dfrac{\alpha_1 - \alpha_2\theta\exp(-\phi t)}{[1 + \theta\exp(-\phi t)]}$ $\alpha_1, \alpha_2, \beta \equiv$ constants, $\theta = \dfrac{\alpha_1 - \rho_0}{\alpha_2 + \rho_0}$ $V_0 = V^* \exp(-P/\sigma)$ $\phi = \beta(\alpha_1 + \alpha_2)$ $k = \dfrac{V^* Q \exp(-P/\sigma)}{\sigma}$
F. Dislocation Climb	$\dot{\varepsilon} = C\sigma^n \exp\left(\dfrac{-\Delta H_{SD}}{kT}\right)\sinh\left(\dfrac{B\sigma^m}{kT}\right)$ $\Delta H_{SD} \equiv$ self-diffusion activation energy, $n \approx m \approx 2$.
G. Dislocation-jog	$\dot{\varepsilon} = C\exp\left(\dfrac{-\Delta H_{SD}}{kT}\right)\sinh\left(\dfrac{l_j b \sigma^2}{kT}\right)$
Weertman	$l_j \equiv$ distance between jogs.
Barrett & Nix	$\dot{\varepsilon} = 2\pi\rho_s D\alpha\left(\dfrac{b}{a_0}\right)^3 \sinh\left(\dfrac{b^2\sigma\lambda}{2kT}\right)$
H. Dislocation Nodes	$\dot{\varepsilon} = \dfrac{2^n N k T b^2}{h}\sin\phi\exp\left(-\dfrac{G_v + n\Delta F_s^*}{kT}\right)\left(\dfrac{\sinh\sigma b^2 l \sin\phi}{nkT}\right)^n$ $n \equiv$ no. atoms at node, $G_v \equiv$ free energy vacancy formation, $\Delta F_s^* \equiv$ free energy of activation for slip & climb rate controlling process, $\phi \equiv$ angle between two sets of dislocations, $l \equiv$ length between nodes.
I. Dislocation Kink	$\dot{\varepsilon} = \dfrac{12\sigma^{2.5}\nu a}{G^{2.5}b^{2.5}N^{1/2}}\exp\left(\dfrac{-\Delta H_c}{RT}\right)\exp\left(\dfrac{\pi\sigma\Delta H_c}{2\sigma_p RT}\right)$

TABLE 4 (CONT'D)

THEORY	RATE EQUATION
J. Viscous Dislocation Motion (solute atmospheres dragged)	$\dot{\varepsilon} = C\sigma \exp\left(\frac{-\Delta H_{so}}{kT}\right)$
Cottrell	
Weertman	$\dot{\varepsilon} = C\sigma^3 \exp\left(\frac{-\Delta H_{so}}{kT}\right)$
K. Intragranular Diffusion Creep (Nabarro-Herring)	$\dot{\varepsilon} = \frac{c b^3 D \sigma}{L^2 kT}$ $D \equiv$ diffusion coefficient, $L \equiv$ grain dia.
L. Grain Boundary Sliding (Gifkins)	$\dot{\varepsilon}_{gb} = \frac{\delta K N \Omega D_{gb} \sigma}{l kT}$ $K \equiv$ conversion factor, $N \equiv$ no. grain boundaries per unit length, $\delta \equiv$ constant, $\Omega \equiv$ atomic vol., $l \equiv$ length of longest grain boundary ledge which controls diffusion path.
M. Quantum Mechanical Tunnelling	Same as I, except that $\exp\left(\frac{-\Delta H}{RT}\right)$ is replaced by the tunnelling probability: $\exp\left\{-\int 2\hbar^{-1}\left[2m(V-W)\right]^{1/2}dx\right\}$ $m \equiv$ jog mass, $V(x) \equiv$ Peierl's potential energy at point x, $W \equiv$ kinetic energy of a jog.

TABLE 4 (CONT'D)

THEORY	RATE EQUATION
N. Hull and Rimmer Void Growth	$\frac{dr}{dt} \approx \frac{D_g \, \delta z \, (\sigma - P)\Omega}{2kTar}$; $t_r \approx \frac{kTa^3}{4(D_g \, \delta z)(\sigma - P)\Omega}$ $r \equiv$ void radius, $a \equiv$ void spacing, $\Omega \equiv$ atomic vol., $\delta z \equiv$ grain boundary thickness, $t_r \equiv$ time to rupture.
O. Speight and Harris Void Growth (for large void spacing)	$\frac{dr}{dt} = \frac{D_g \, \Omega \, \delta z \, (\sigma - 2\gamma/r)}{2kTr^2\left[\ln(a/2r) - 1/2\right]}$ $a/r > 26$.

BIBLIOGRAPHY FOR TABLE 4

A. Kauzman, W., Trans. AIME, 143 (1941), p. 57.

B. Conrad, H., Acta Met., 6 (1958), p. 339.
Weertman, J., J. Appl. Phys., 29 (1958), p. 1685.

C. Seeger, A., Dislocations and Mechanical Properties of Crystals, John Wiley and Sons, Inc., New York, 1957, p. 243.
Seeger, A., Phil. Mag., 45 (1954), p. 771.
Seeger, A., Phil. Mag., 1 (1956), p. 651.
Friedel, J., Les Dislocations, Gauthier-Villas, Paris, 1956.

D. Schoeck, G., Seeger, A., Defects in Crystalline Solids, Phys. Soc. of London, 1955, p. 340.
Jaffe, N., Dorn, J. E., Trans. AIME, 224 (1962), p.1167.

E. Webster, G. A., Phil. Mag., 14 (1966), p. 775.

F. Weertman, J., J. Appl. Phys., 26 (1955), p. 1213.
Weertman, J., J. Appl. Phys., 28 (1957), p. 362.

G. Mott, N. F., NPL Creep and Fracture of Metals, Philosophical Library, Inc., New York, 1957, p. 21.
Raymond, L., Dorn, J., Trans. AIME, 230 (1964), p. 560.
Barrett, C., Nix, W. D., Acta Met., 13 (1965), p. 1247.

H. Li, J. C. M., Trans. AIME, 227 (1963), p. 1474.

I. Weertman, J., J. Appl. Phys., 28 (1957), p. 1185.

J. Cottrell, A. H., Dislocations and Plastic Flow in Crystals, Oxford Press, London, 1953, p. 136.
Weertman, J., J. Appl. Phys., 28 (1957), p. 1185.

K. Nabarro, F., Proceedings of the Conf. of Strength of Solids, Phys. Soc., London, 1948, p. 75.
Herring, C., J. Appl. Phys., 21 (1950), p. 437.
Williams, R. O., Acta Met., 5 (1957), p. 55.

L. Gifkins, R. C., Snowden, K. U., Trans. AIME, 239 (1967), p. 910.
Gifkins, R. C., Snowden, K. U., Nature, 212 (1966), p. 916.

BIBLIOGRAPHY FOR TABLE 4 (CONT'D)

M. Glen, J. W., Phil. Mag., 1 (1956), p. 400.

N. Hull, D., Rimmer, D. E., Phil. Mag., 4 (1959), p. 673.

O. Speight, M. V., Harris, J. E., Met. Sci. Jour., 1 (1967), p. 83.

TABLE 5

A SUMMARY OF THE DATA FOR THE RELATIVE CONTRIBUTIONS OF THE NON-LINEAR AND THE LINEAR CREEP MECHANISMS

TEST NO.	TYPE OF COPPER	CREEP STRAIN (%)	POWER, n, FOR NON-LINEAR TERM	STRESS, σ_1 (psi.)	TOTAL CREEP RATE x 10^4 (in./-in.hr.)	A' $\left(\frac{in.^2}{lb.}\right)^n$	$B' \times 10^8$ (in./-lb.)	CONTRIBUTION TO TOTAL CREEP RATE OF: NON-LINEAR TERM (%)	LINEAR TERM (%)
12	OFHC	1.8	10.8	3890	5.19	6.26×10^{-43}	3.83	71.3	28.7
		3.1		3890	6.35	7.02×10^{-43}	5.66	65.3	34.7
		3.9		3890	10.38	1.22×10^{-42}	8.15	69.5	30.5
		4.7		3485	6.49	2.13×10^{-42}	7.6	59.2	40.8
7	OFHC	3.31	12.1	4298	7.8	4.95×10^{-48}	7.56	58.3	41.7
		3.63		3892	4.5	7.86×10^{-48}	5.98	48.2	51.8
		4.25		4298	11.8	4.03×10^{-48}	18.9	31.4	68.6
		4.45		3892	10.7	8.93×10^{-48}	21.2	23.0	77.0
3	Tough Pitch	1.15	12.1	4198	10.0	3.46×10^{-48}	18.2	23.9	76.0
		1.54		4198	10.0	3.47×10^{-48}	18.1	24.2	75.9
		1.68		4198	10.0	5.7×10^{-48}	14.5	39.3	60.7
		2.76		4000	11.6	2.82×10^{-47}	18.3	93.7	6.3
		3.41		4198	20.3	1.93×10^{-47}	16.7	65.6	34.5
		4.34		4198	32.8	2.82×10^{-47}	31.8	59.3	40.7
		6.4		3802	55.0	1.18×10^{-46}	79.7	44.9	55.1

[illegible]

[illegible]	[illegible]

TABLE 5 (CONT'D)

TEST NO.	TYPE OF COPPER	CREEP STRAIN (%)	POWER, n, FOR NON-LINEAR TERM	STRESS, σ_1 (psi.)	TOTAL CREEP RATE x 10^4 (in./-in.hr.)	A' $\left(\frac{in.^2}{lb.}\right)^n$	$B' \times 10^8$ (in./-lb.)	CONTRIBUTION TO TOTAL CREEP RATE OF: NON-LINEAR TERM (%)	LINEAR TERM (%)
5	Tough Pitch	1.1	12.1	4317	20.8	1.25×10^{-47}	20.2	58.2	41.8
		3.8		4317	53.4	3.5×10^{-47}	45.2	63.4	36.6
		4.8		3910	41.8	7.86×10^{-47}	48.2	54.9	45.1
2	Tough Pitch	2.2	12.1	4486	10.7	3.3×10^{-48}	12.4	47.9	52.1
		2.5		4688	14.5	3.46×10^{-48}	11.6	62.5	37.5

TABLE 6

TOTAL CREEP STRAIN AND CORRESPONDING CREEP TIMES; INDUCTION TIMES

TEST NO.	TYPE OF COPPER	TOTAL CREEP STRAIN (%)	TOTAL CREEP TIME (hr.)	STRESS CHANGE MAGNITUDE, $\Delta\sigma$ (psi.)	CREEP STAGE	STRESS SENSITIVITY, n, TO ESTIMATE $\dot{\varepsilon}_2$	CREEP RATE: BEFORE $\Delta\sigma$. $\dot{\varepsilon}_1$ $\left(\frac{in.}{in.hr.}\right)x10^4$	CREEP RATE: AFTER $\Delta\sigma$. $\dot{\varepsilon}_2$ $\left(\frac{in.}{in.hr.}\right)x10^4$	INDUCTION TIME (min.)	REMARKS
9	OFHC	1.42	19.3	202	2		6.06	3.4	36	$\dot{\varepsilon}_2$ was calculated.
		1.68	24.8		2	12	5.19	2.9	40	
		1.80	31.5		2		6.06	3.4	36	
		2.58	39.8		3		8.22	6.2	28	
		3.34	48.7		3	6	11.25	8.4	20	
		4.25	56.3		3		16.44	12.3	12	
7	OFHC	1.11	7.8	406	2		7.2	2.3	40	$\dot{\varepsilon}_2$ was determined from the creep curve.
		1.78	19.8		2	--	5.19	3.1	40	
		2.46	30.6		2-3		8.08	2.2	26	
		3.31	44.0		3	--	7.85	4.5	20	
		4.25	54.0		3		11.8	8.6	17	
12	OFHC	1.38	24.0	405	2	12	3.79	1.2	40	$\dot{\varepsilon}_2$ was calculated.
		1.80	41.4		3		5.19	2.5	30	
		3.10	66.0		3	6	6.35	3.3	15	
		3.90	77.0		3		10.38	5.0	12	

TABLE 6 (CONT'D)

TEST NO.	TYPE OF COPPER	TOTAL CREEP STRAIN (%)	TOTAL CREEP TIME (hr.)	STRESS CHANGE MAGNITUDE, $\Delta\sigma$ (psi.)	CREEP STAGE	STRESS SENSITIVITY, n, TO ESTIMATE $\dot{\varepsilon}_2$	CREEP RATE: BEFORE $\Delta\sigma$, $\dot{\varepsilon}_1$ $(\frac{in.}{in.hr.})x10^4$	CREEP RATE: AFTER $\Delta\sigma$, $\dot{\varepsilon}_2$ $(\frac{in.}{in.hr.})x10^4$	INDUCTION TIME (min.)	REMARKS
10	OFHC	0.84	7.7	612	1-2	12	6.92	1.1	30	$\dot{\varepsilon}_2$ was calculated.
		1.39	17.2		2		6.49	1.03	50	
		1.93	26.0		2-3	6	8.22	3.3	26	
		3.12	43.8		3		10.81	4.3	20	
		4.36	51.2		3		26.82	10.7	8	
3	Tough Pitch	1.53	--	396	2	--	15.4	10.0	17	$\dot{\varepsilon}_2$ was determined from the creep curve.
		1.68	--		2		10.0	6.7	20	
		4.34	29.7		3	--	72.4	32.8	10	
		6.4	33.7		3		115.0	55.0	5	
5	Tough Pitch	3.83	18.2	407	3	--	53.4	27.9	12	$\dot{\varepsilon}_2$ was determined from the creep curve.
2	Tough Pitch	3.51	20	--	--	--	--	--	--	--
		4.4	26							
		5.4	30							
		7.2	34							

[illegible]

ILLUSTRATIONS

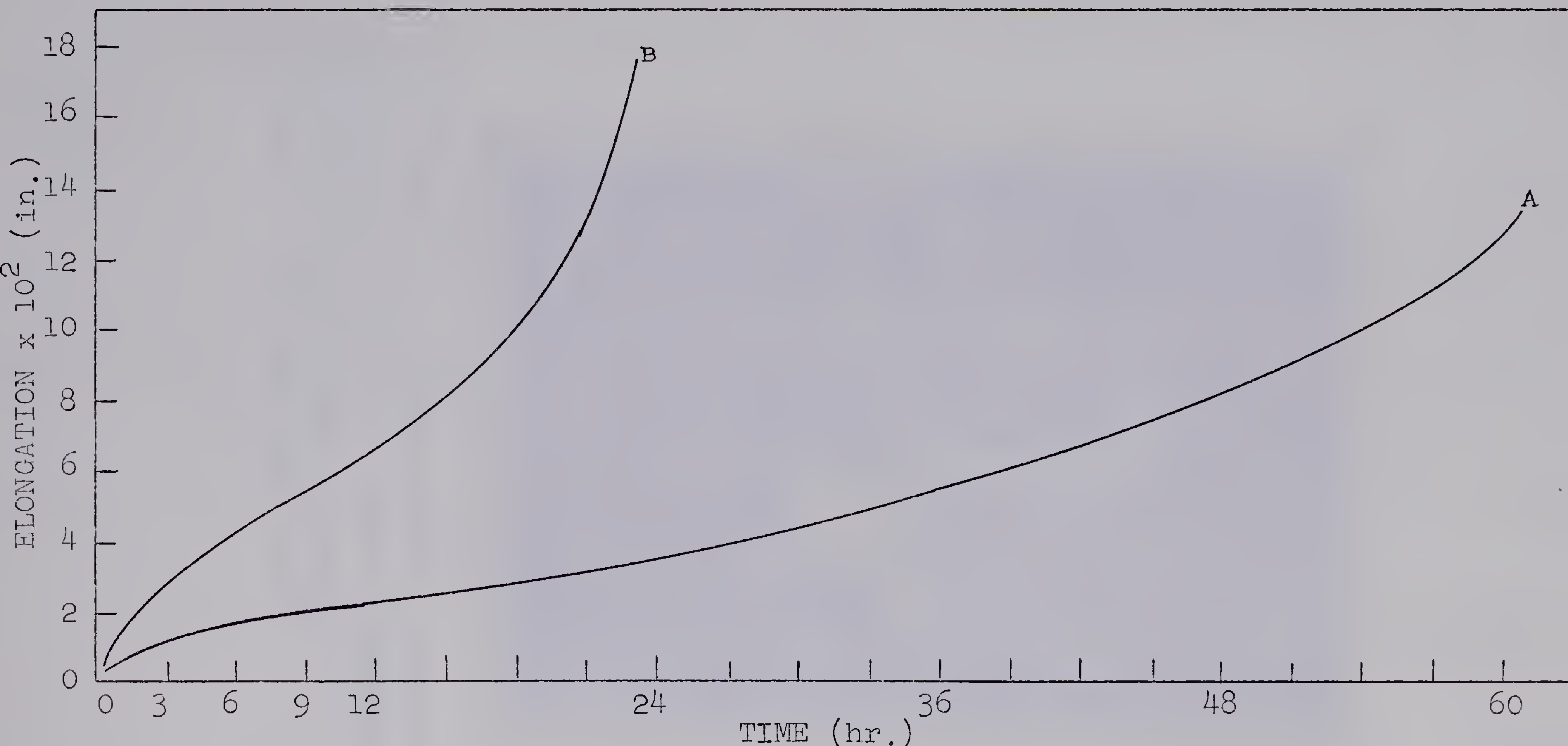

FIG. 1. TYPICAL CREEP CURVES. (A) OFHC COPPER CREPT AT 698°K AND 4317 psi. STRESS; (B) TOUGH PITCH COPPER CREPT AT 708°K AND 4266 psi. STRESS.

FIG. 2. A PHOTOGRAPH OF THE EXPERIMENTAL APPARATUS SHOWING, FROM LEFT TO RIGHT: THE FURNACE CONTROLLER AND POTENTIOMETER, THE CREEP MACHINE, THE STRAIN RECORDER, AND THE ARGON GAS CYLINDER.

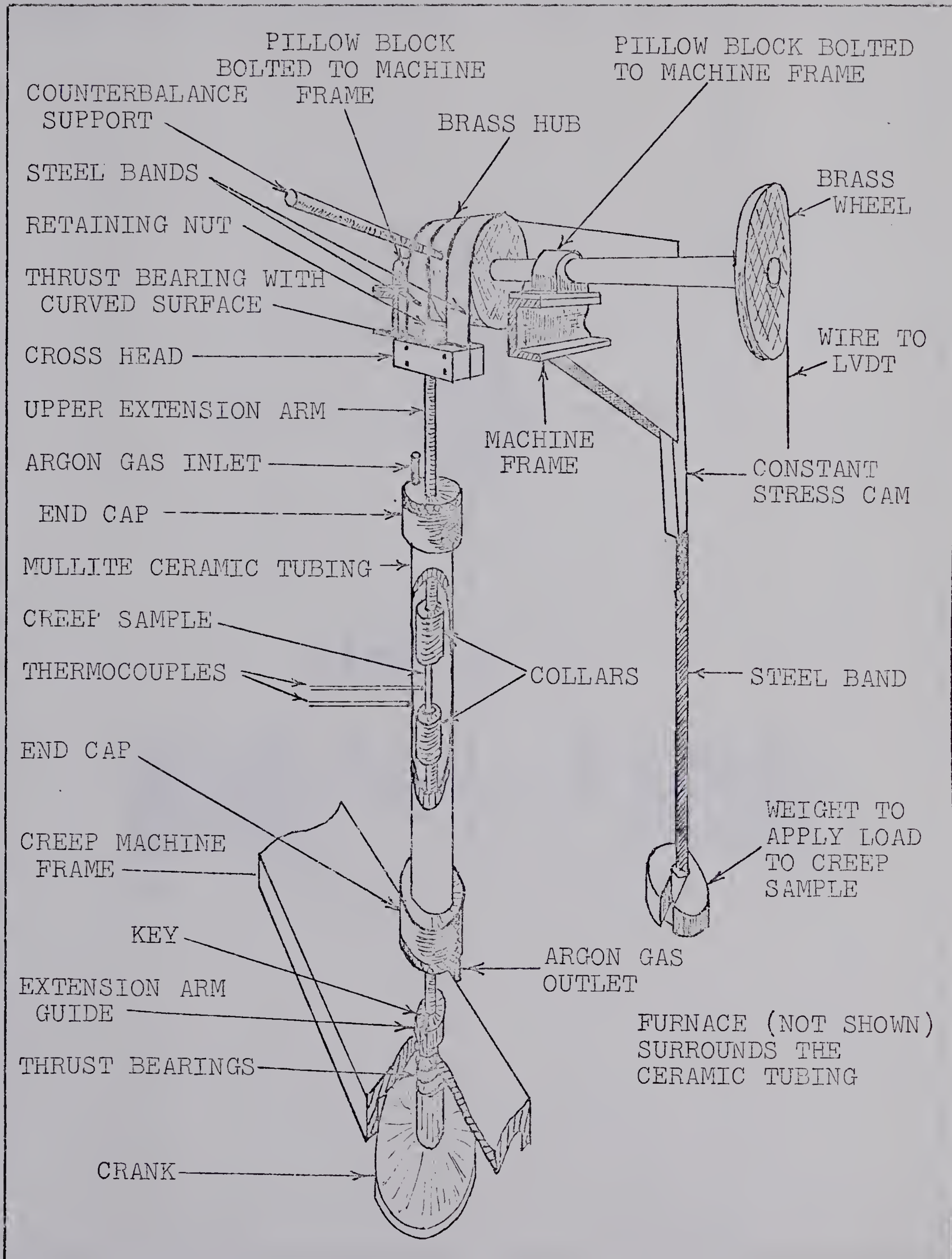

FIG. 3. AN ILLUSTRATION SHOWING THE RELATIVE LOCATIONS OF THE MAJOR CREEP MACHINE COMPONENTS.

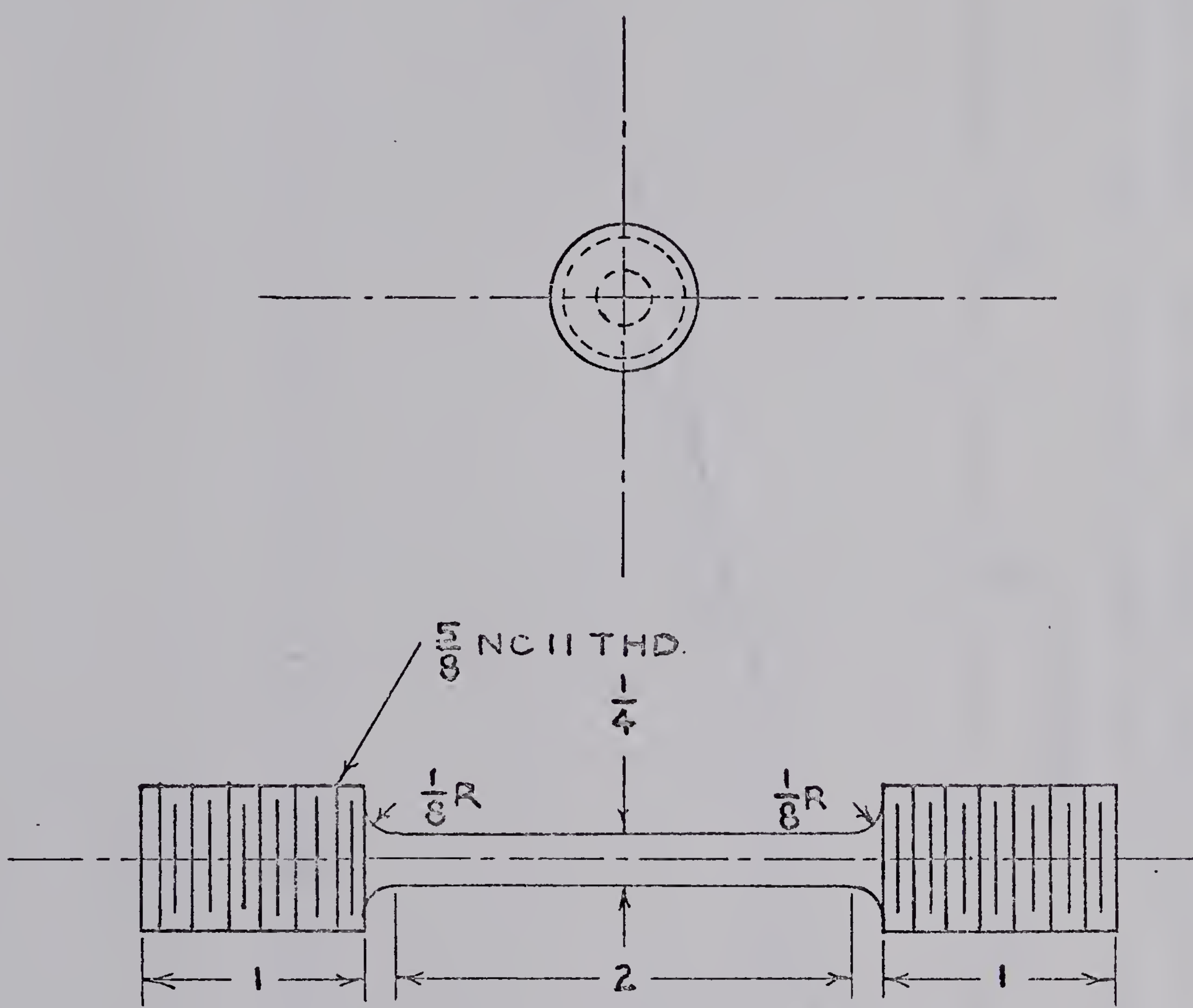

FIG. 4. THE CREEP SAMPLE DIMENSIONS. (SCALE: 1 in.= 1 in.)

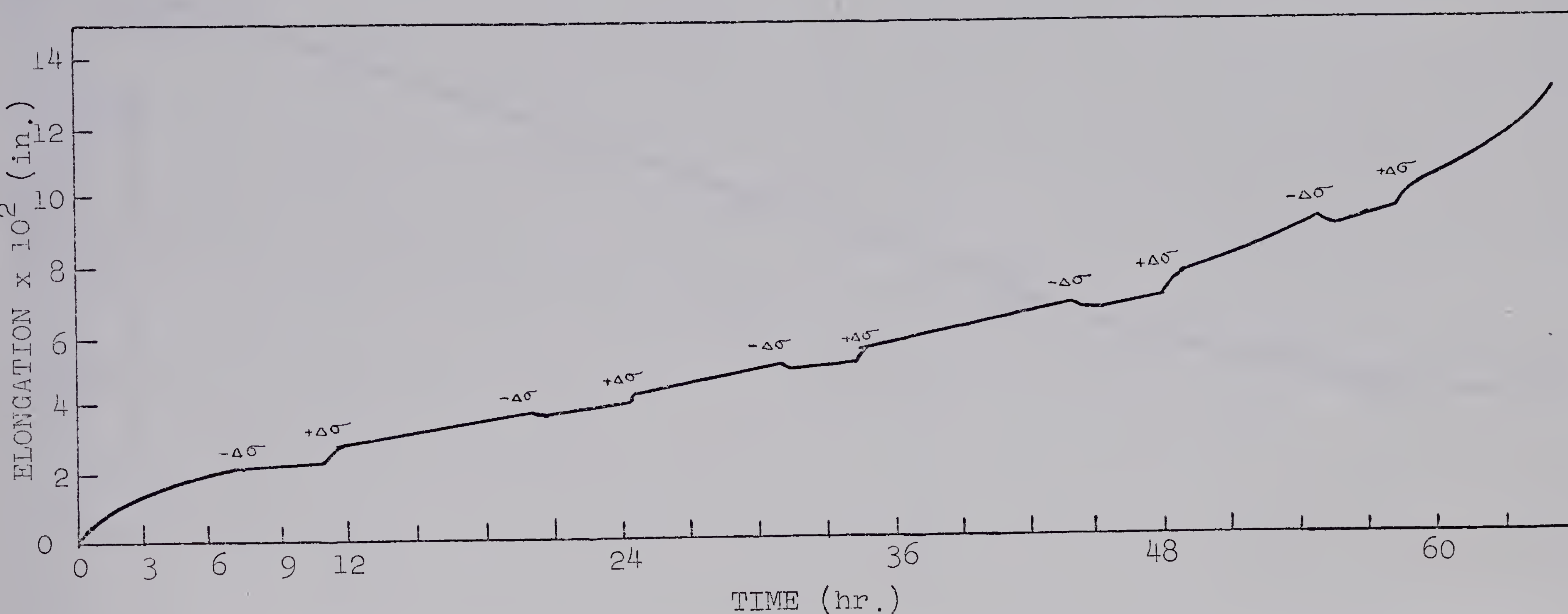

FIG. 5. A TYPICAL CREEP CURVE WITH STRESS CHANGES FOR OFHC COPPER. TEMPERATURE = 699°K; CREEP STRESS = 4298 psi ; STRESS CHANGE = 406 psi.

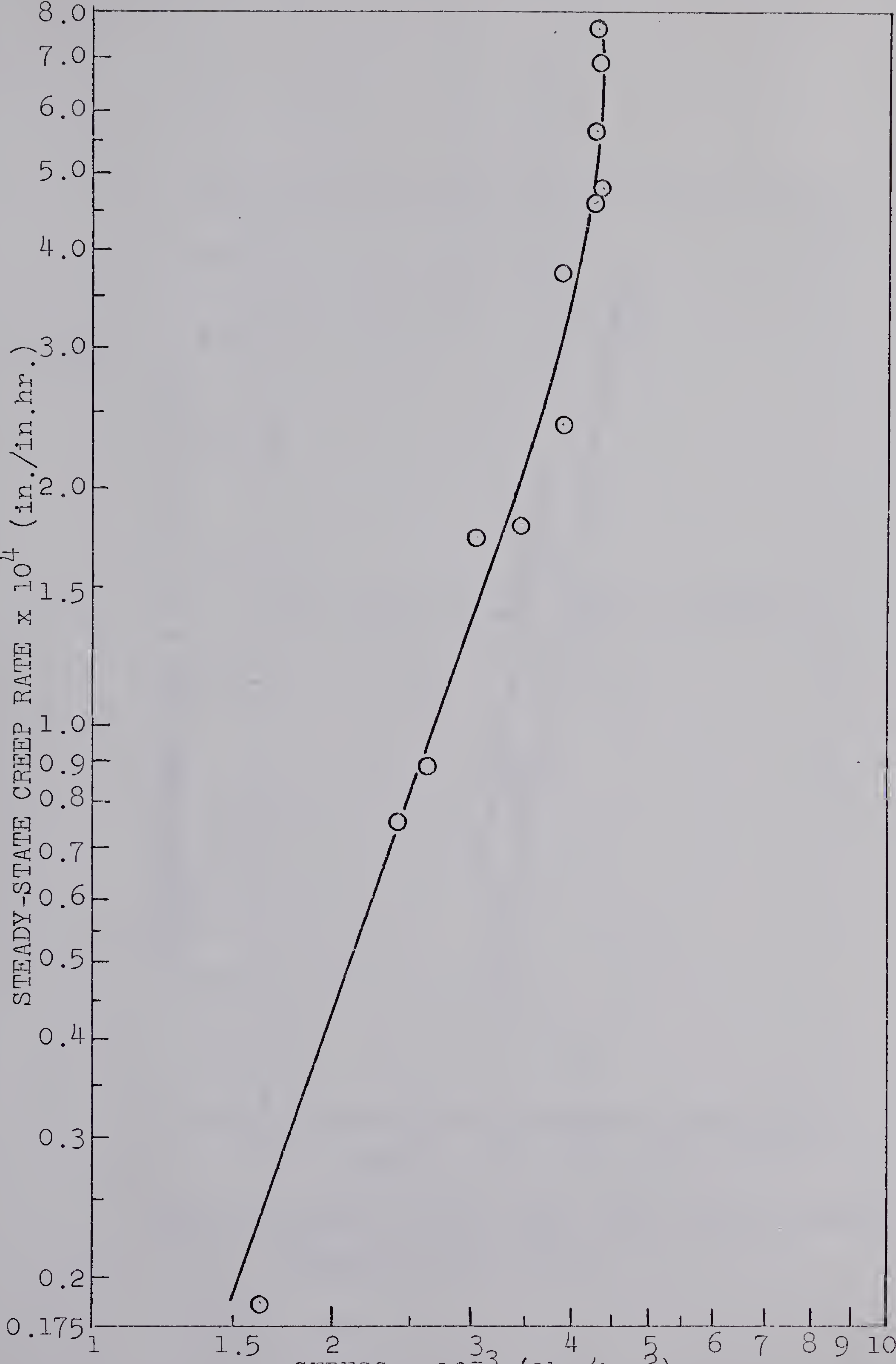

FIG. 6. STEADY-STATE CREEP RATE VERSUS STRESS (OFHC COPPER)
THE AVERAGE TEST TEMPERATURE FOR ALL DATA WAS 698.5°K.

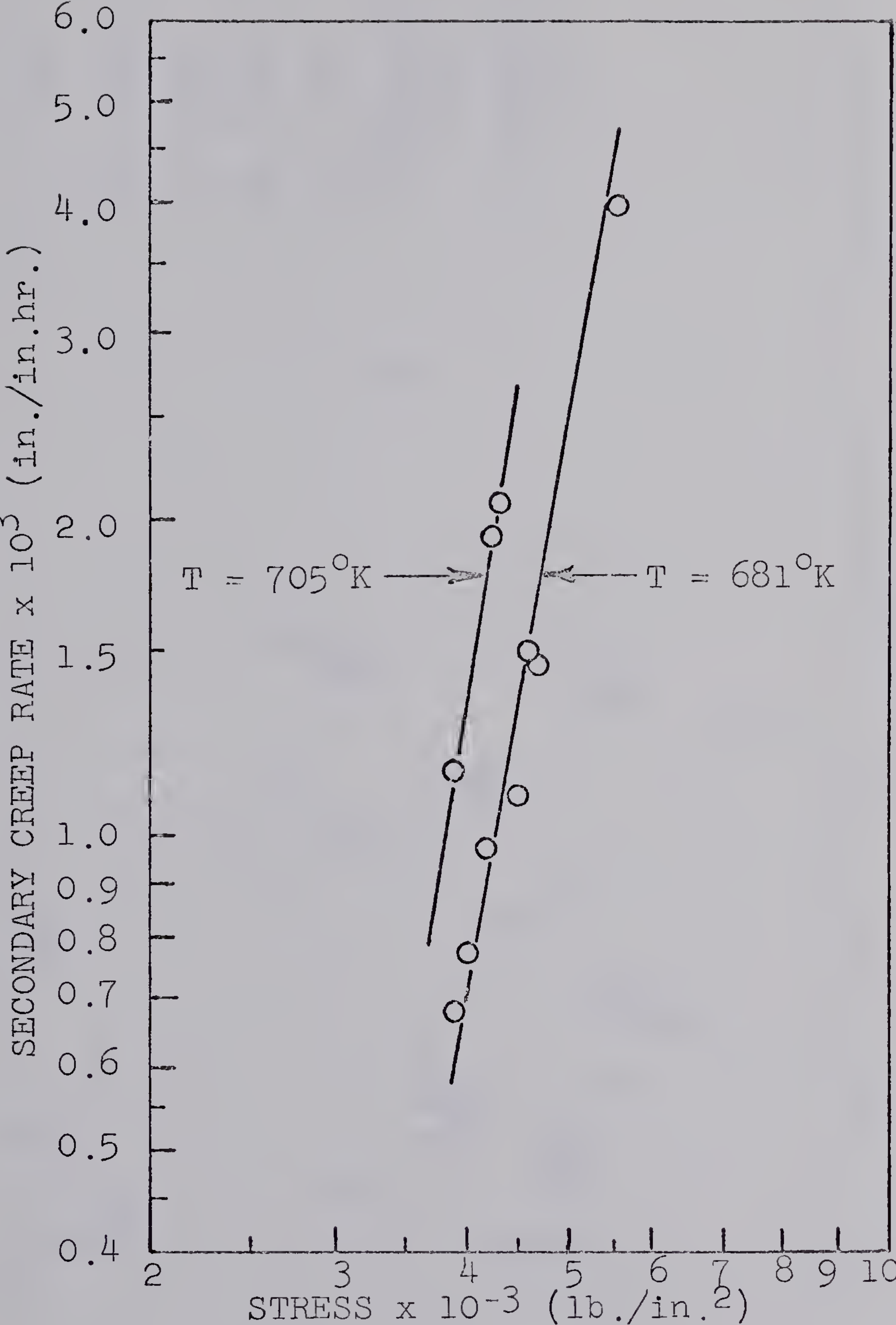

FIG. 7. STEADY-STATE CREEP RATE VERSUS STRESS
(TOUGH PITCH COPPER)

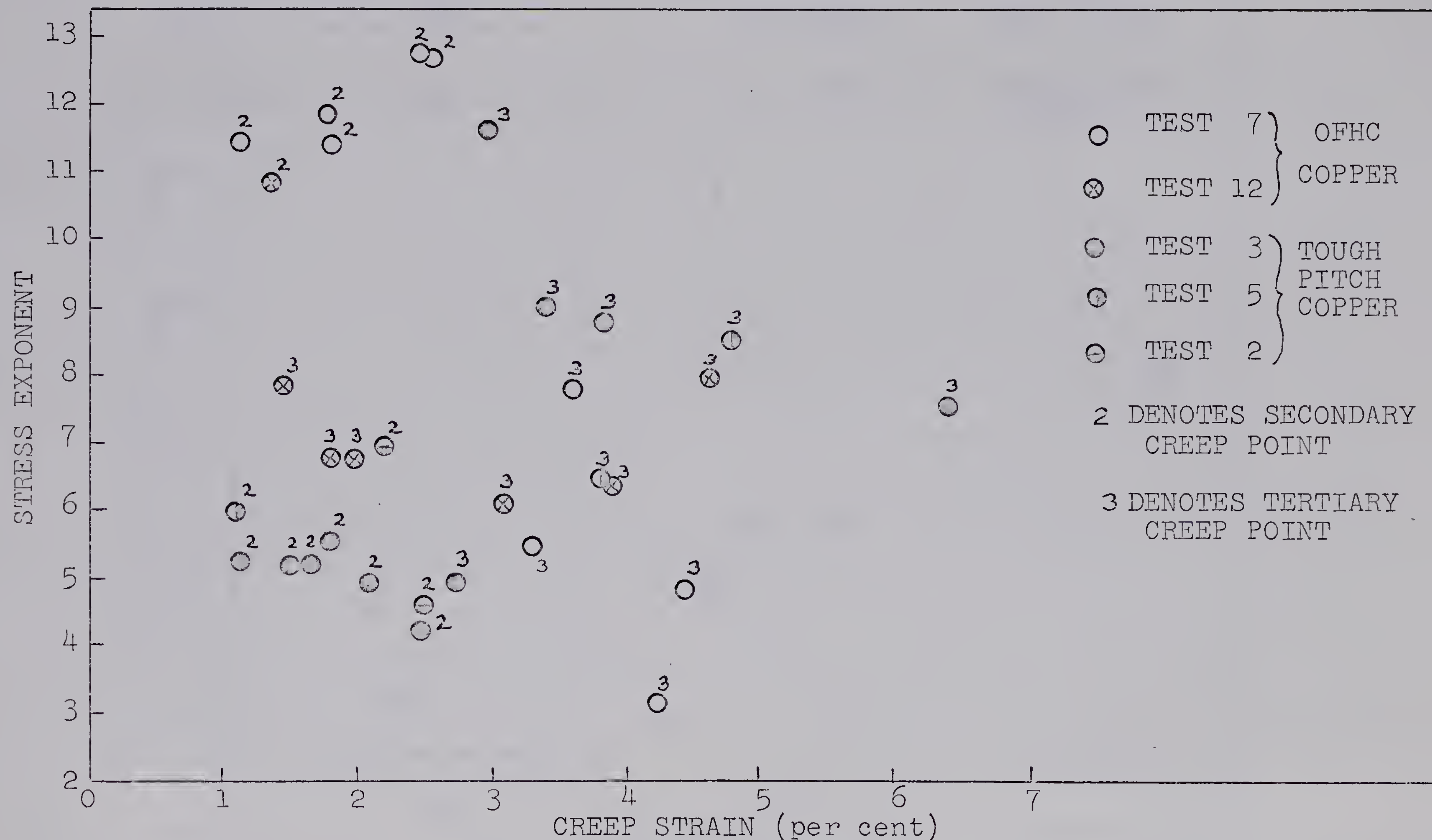

FIG. 8. STRESS EXPONENT VERSUS CREEP STRAIN

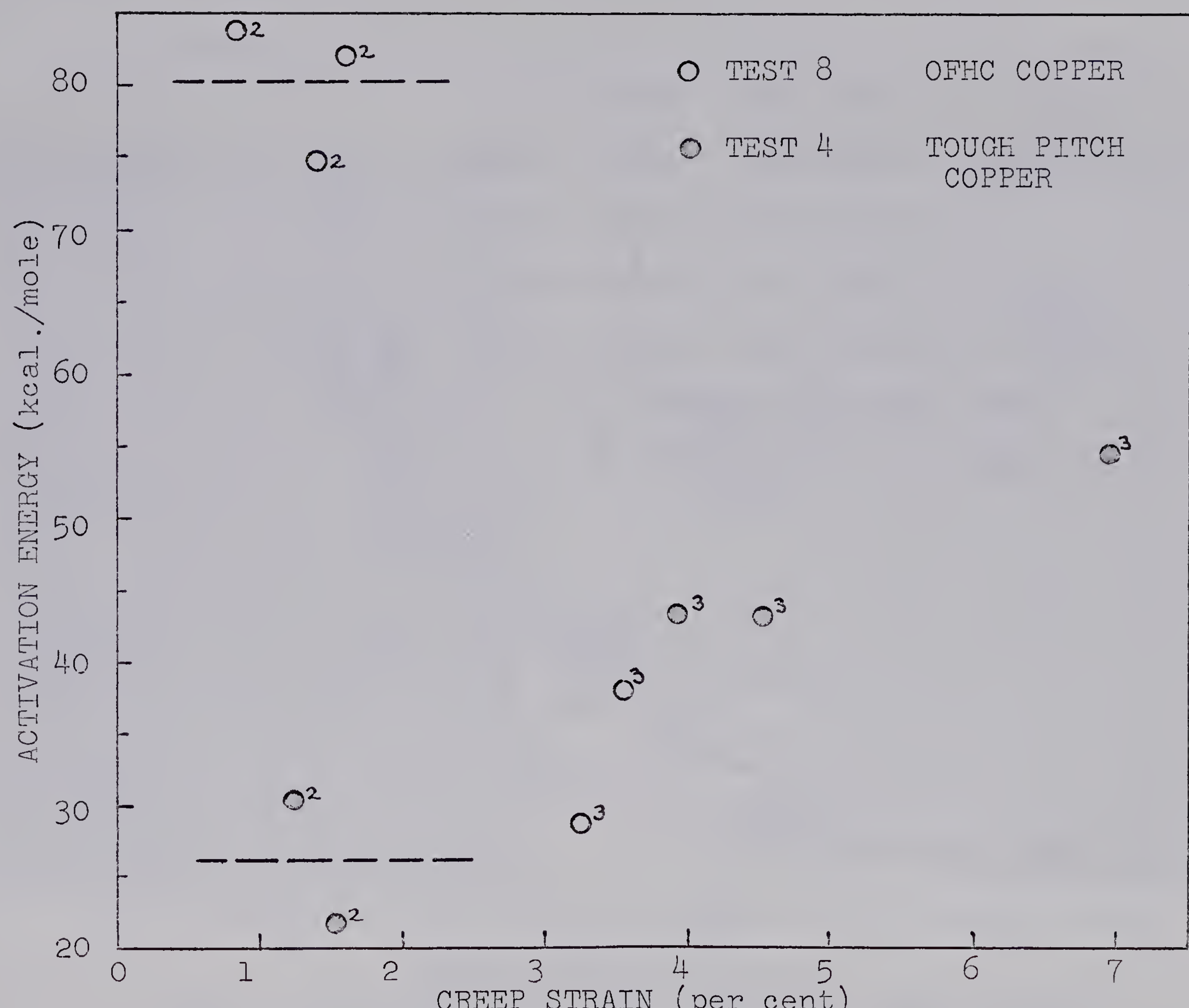

FIG. 9. ACTIVATION ENERGY FOR CREEP VERSUS CREEP STRAIN

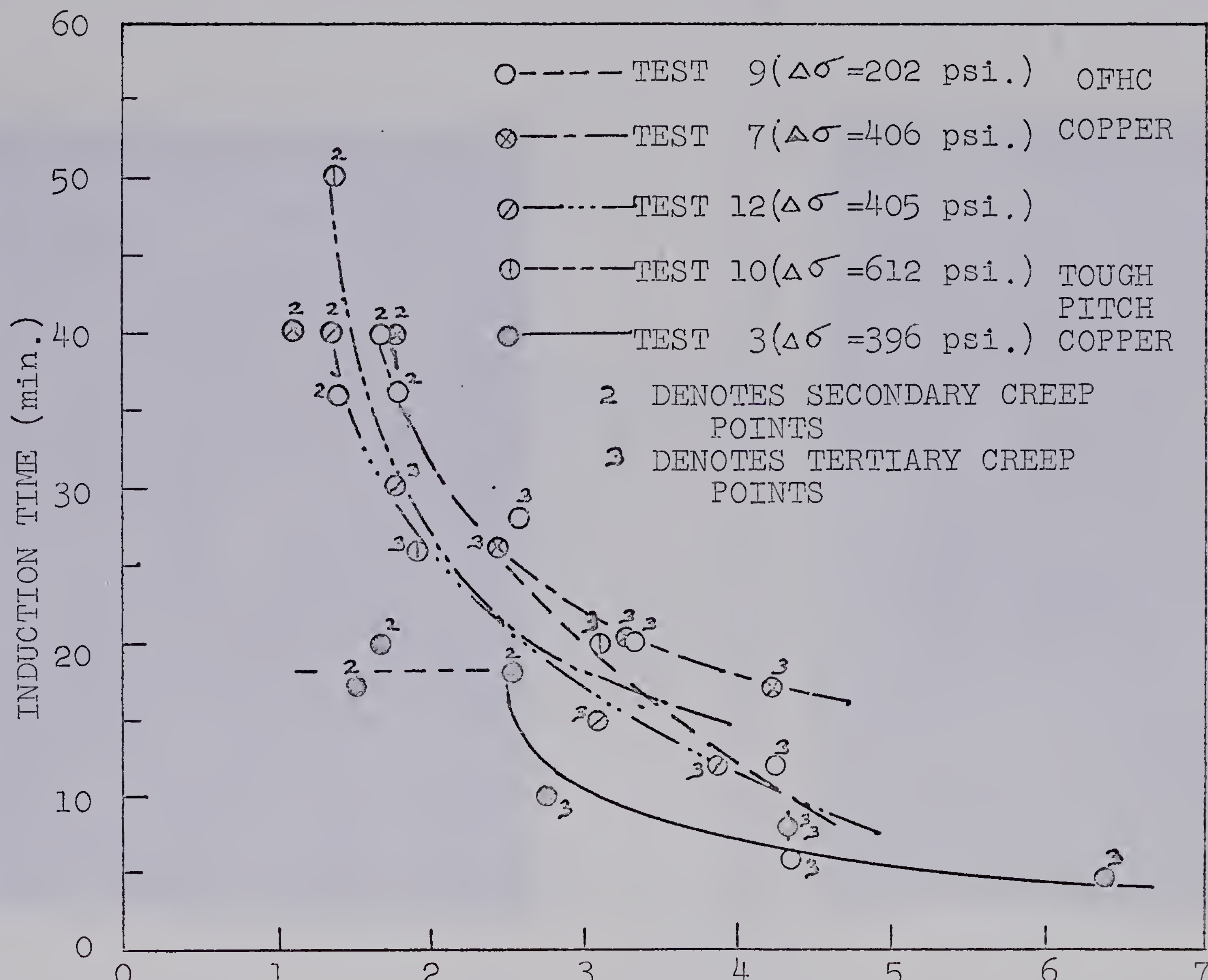

FIG. 10. THE INDUCTION TIME VERSUS THE CREEP STRAIN

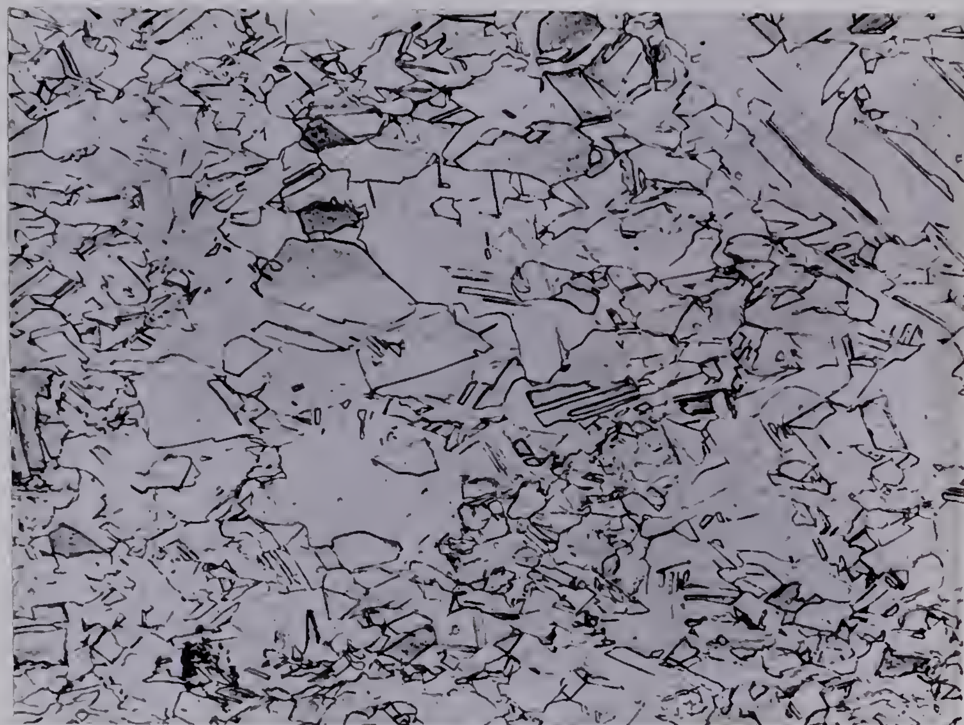

FIG. 11. OFHC COPPER IN THE "AS RECEIVED" CONDITION. x100

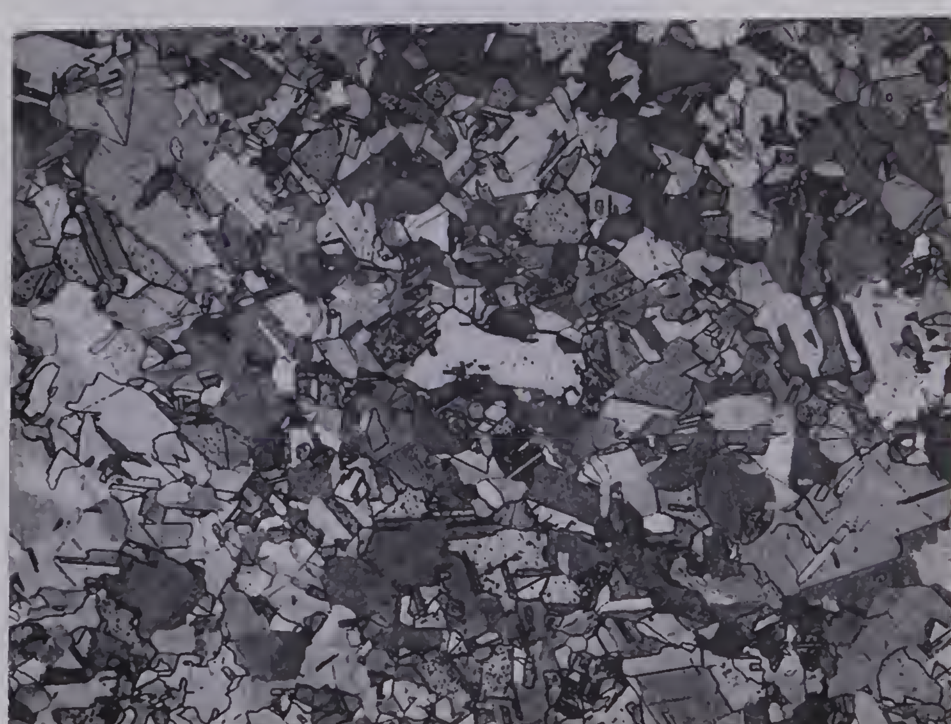

FIG. 12. OFHC COPPER AFTER 2 hr. AT THE TESTING TEMPERATURE, BUT BEFORE THE LOAD APPLICATION. x100

FIG. 13. A TYPICAL FRACTURED OFHC COPPER SAMPLE. x6.5

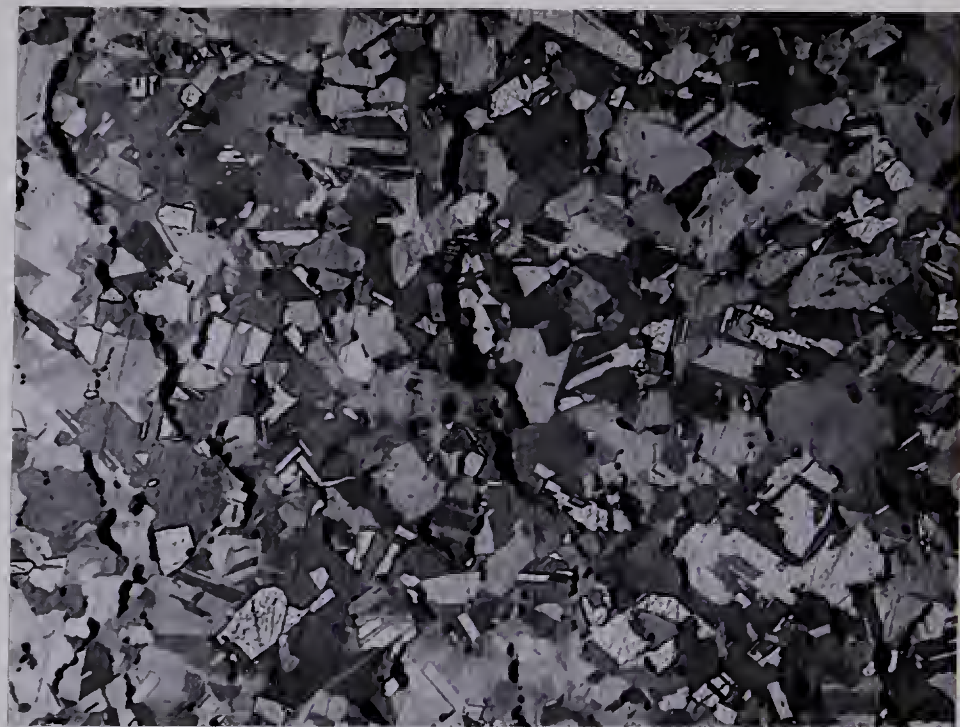

FIG. 14. VOIDS IN THE GAUGE LENGTH OF SAMPLE 10. x100

FIG. 15. A SECTION FROM THE THREADED END OF SAMPLE 10 FOR COMPARISON. THE SAMPLE WAS CREPT TO FRACTURE. x100

FIG. 16. VOIDS IN OFHC COPPER SHOWING THE TYPICAL ROUNDED, OR ELLIPTICAL, SHAPE. x700

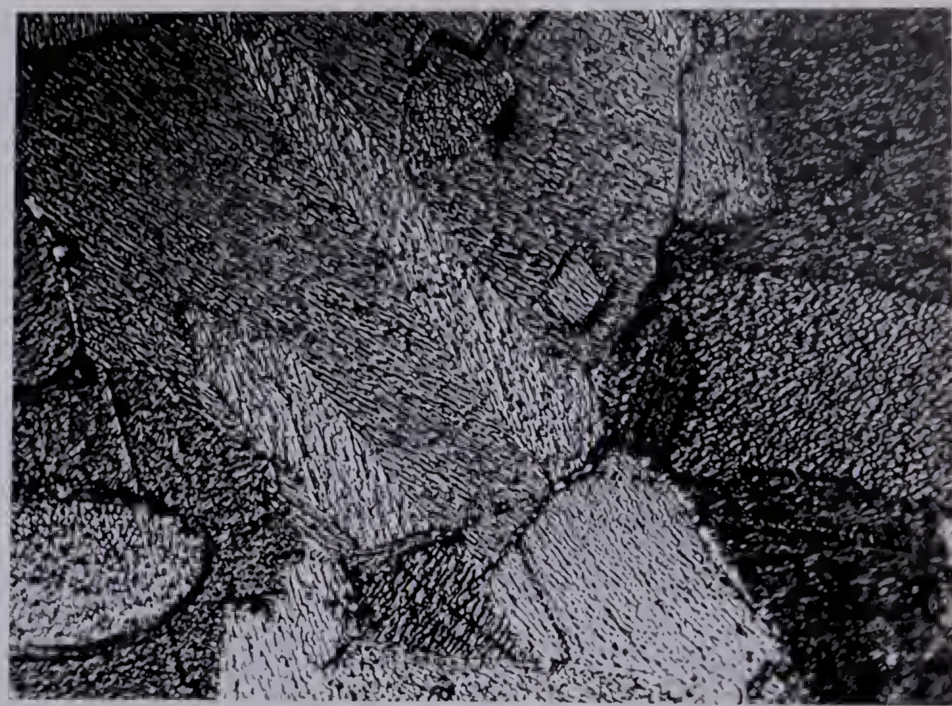

FIG. 17. PHOTOMICROGRAPH OF OFHC COPPER. IT APPEARS THAT BOUNDARY MOTION HAS OCCURRED AROUND THE TWINS IN THE LARGE, CENTRAL GRAIN. x600

FIG. 18. PHOTOMICROGRAPH OF OFHC COPPER. POSSIBLE GHOST BOUNDARIES OUTLINING TWINS IN THE LIGHT-COLOURED, CENTRAL GRAIN AND THE LOWER RIGHT GRAIN. x600

FIG. 19. PHOTOMICROGRAPH OF OFHC COPPER. NOTE THE DISPLACEMENT OF THE LINE OF ETCH PITS, ON THE LEFT, AS THE BOUNDARIES ARE CROSSED. x600

FIG. 20. PHOTOMICROGRAPH OF OFHC COPPER. THE LOWERMOST BOUNDARY APPEARS TO HAVE MIGRATED. x600

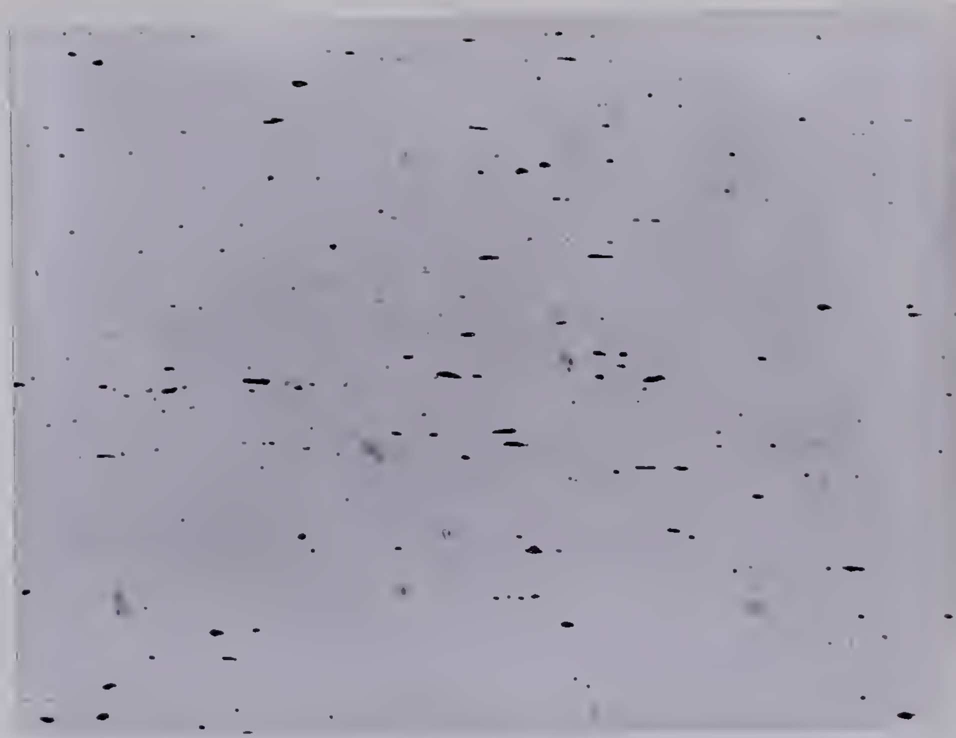

FIG. 21. SOME INCLUSIONS IN THE UNCREPT TOUGH PITCH COPPER. x75

FIG. 22. SOME INCLUSIONS IN TOUGH PITCH COPPER, AT HIGHER MAGNIFICATION, BEFORE CREEP. NOTICE THAT THEY APPEAR TO HAVE FRACTURED DURING THE FABRICATION PROCESS. x600

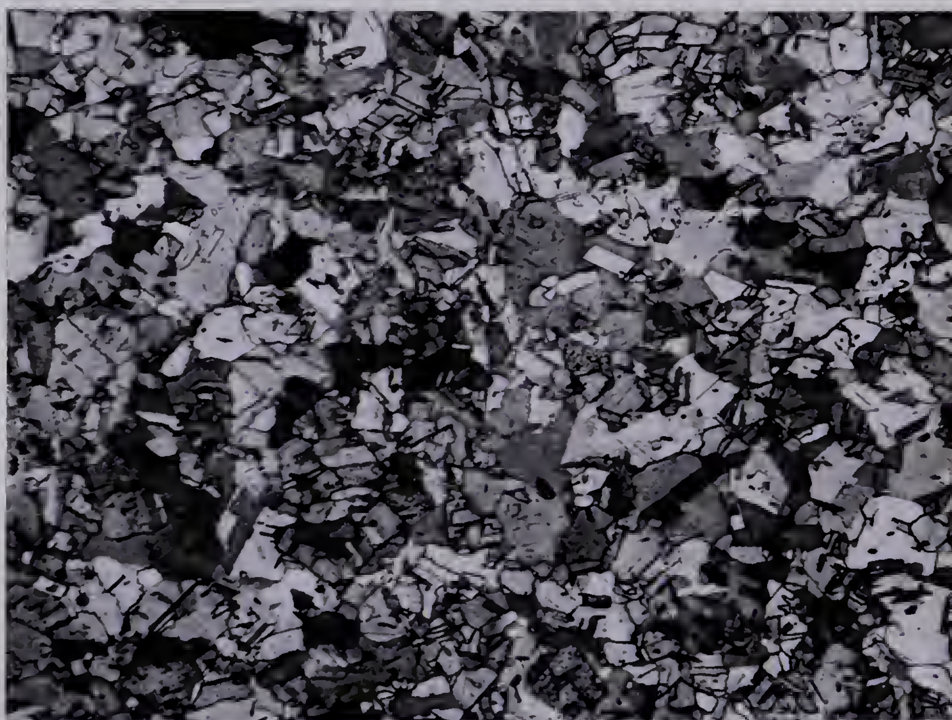

FIG. 23. TOUGH PITCH COPPER AFTER 2 hr. AT THE TEST TEMPERATURE, BUT BEFORE THE LOAD APPLICATION. x100

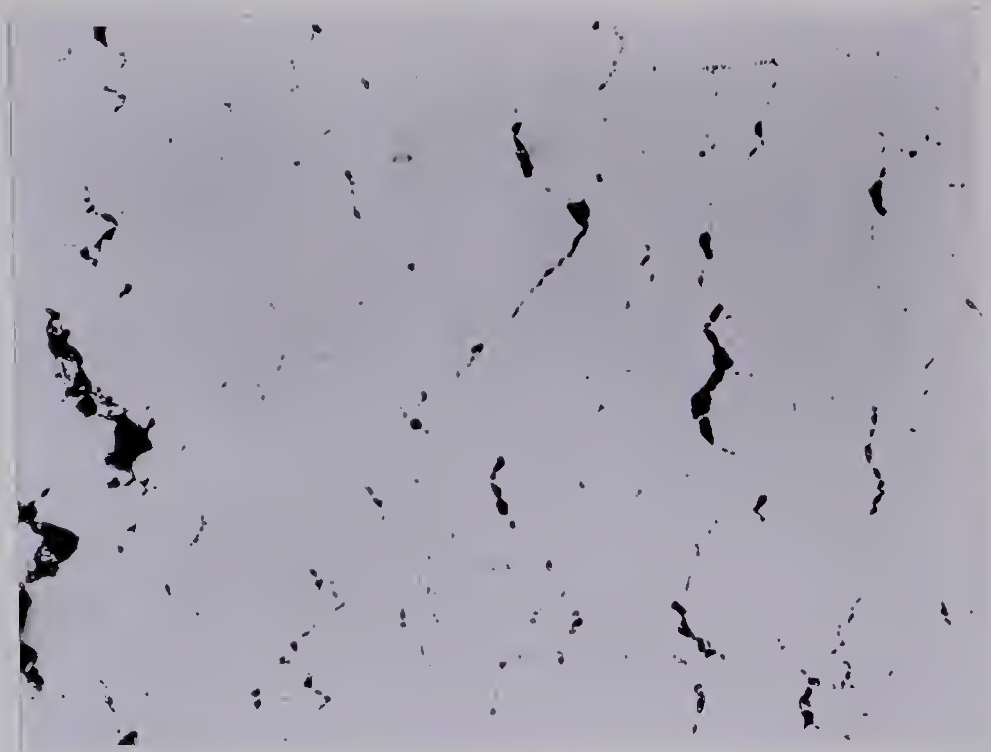

FIG. 24. TYPICAL VOIDS IN TOUGH PITCH COPPER. x125

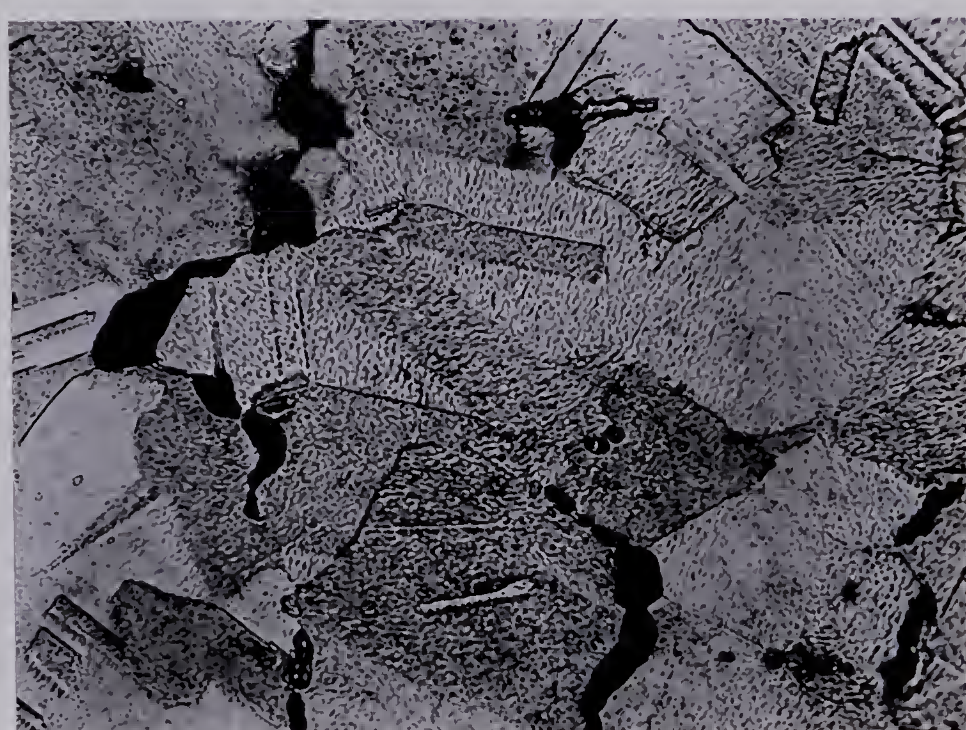

FIG. 25. TOUGH PITCH COPPER VOIDS. NOTICE THAT SOME VOIDS APPEAR TO HAVE OPENED BY A SHEAR PROCESS. x710

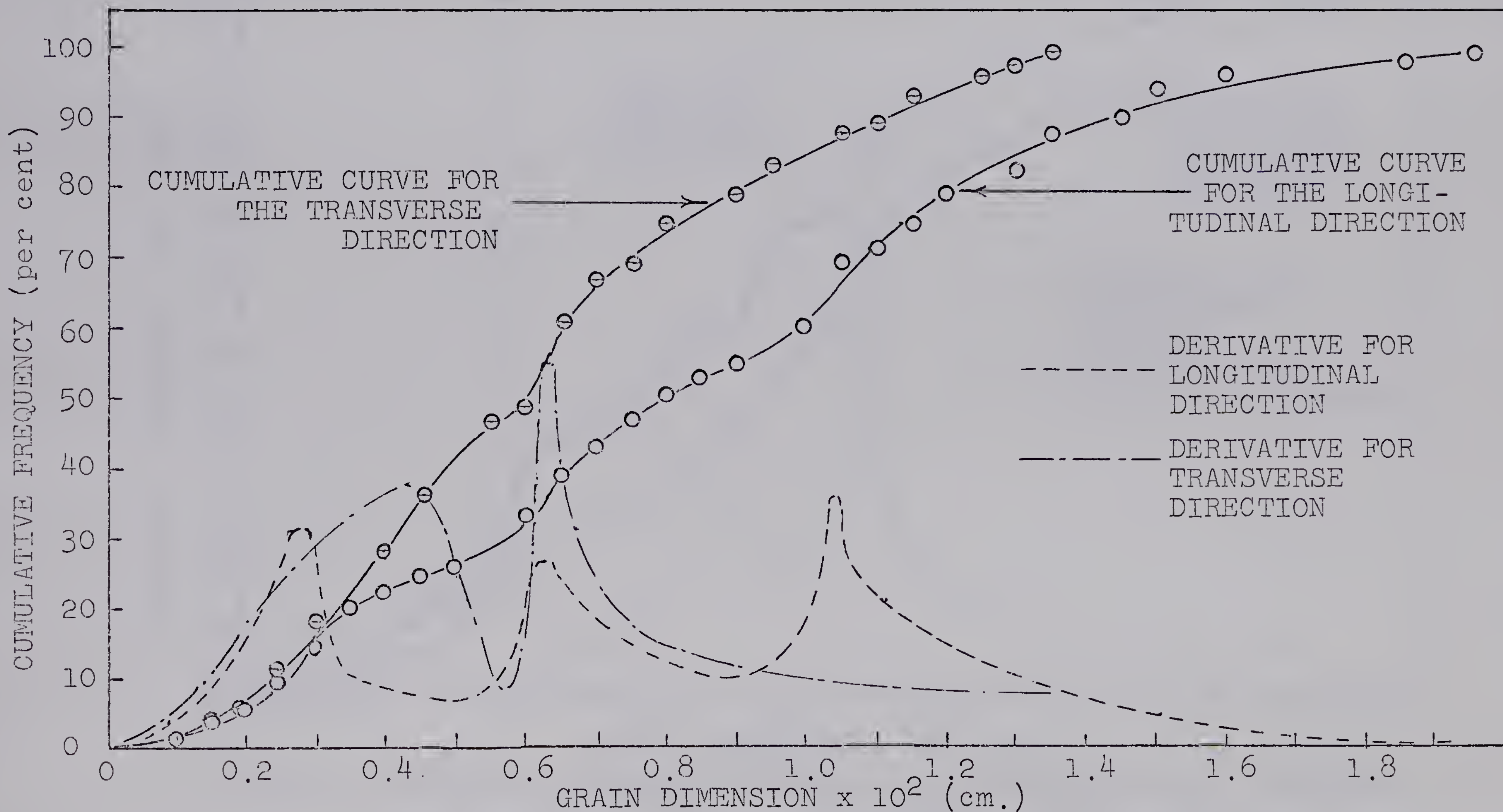

FIG. 26. CUMULATIVE FREQUENCY VERSUS GRAIN DIMENSION FOR A GAUGE LENGTH SECTION OF SAMPLE 11. CURVES FOR TRANSVERSE AND LONGITUDINAL GRAIN DIMENSIONS ARE SHOWN ALONG WITH THEIR RESPECTIVE GRAPHICAL DERIVATIVES.

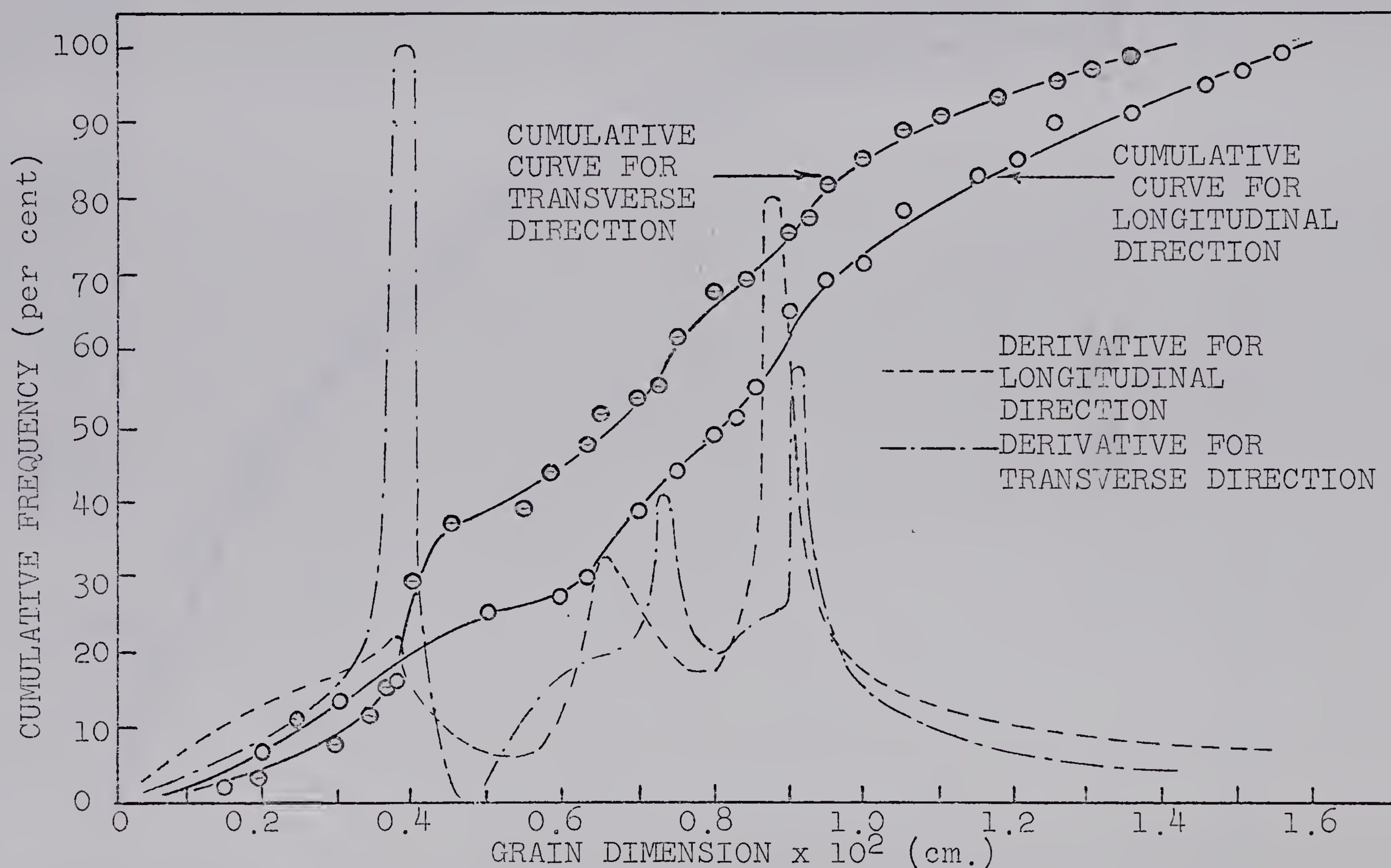

FIG. 27. CUMULATIVE FREQUENCY VERSUS GRAIN DIMENSION FOR A THREADED GRIP SECTION. CURVES FOR TRANSVERSE AND LONGITUDINAL DIMENSIONS ARE SHOWN ALONG WITH THEIR RESPECTIVE GRAPHICAL DERIVATIVES. (SAMPLE 11)

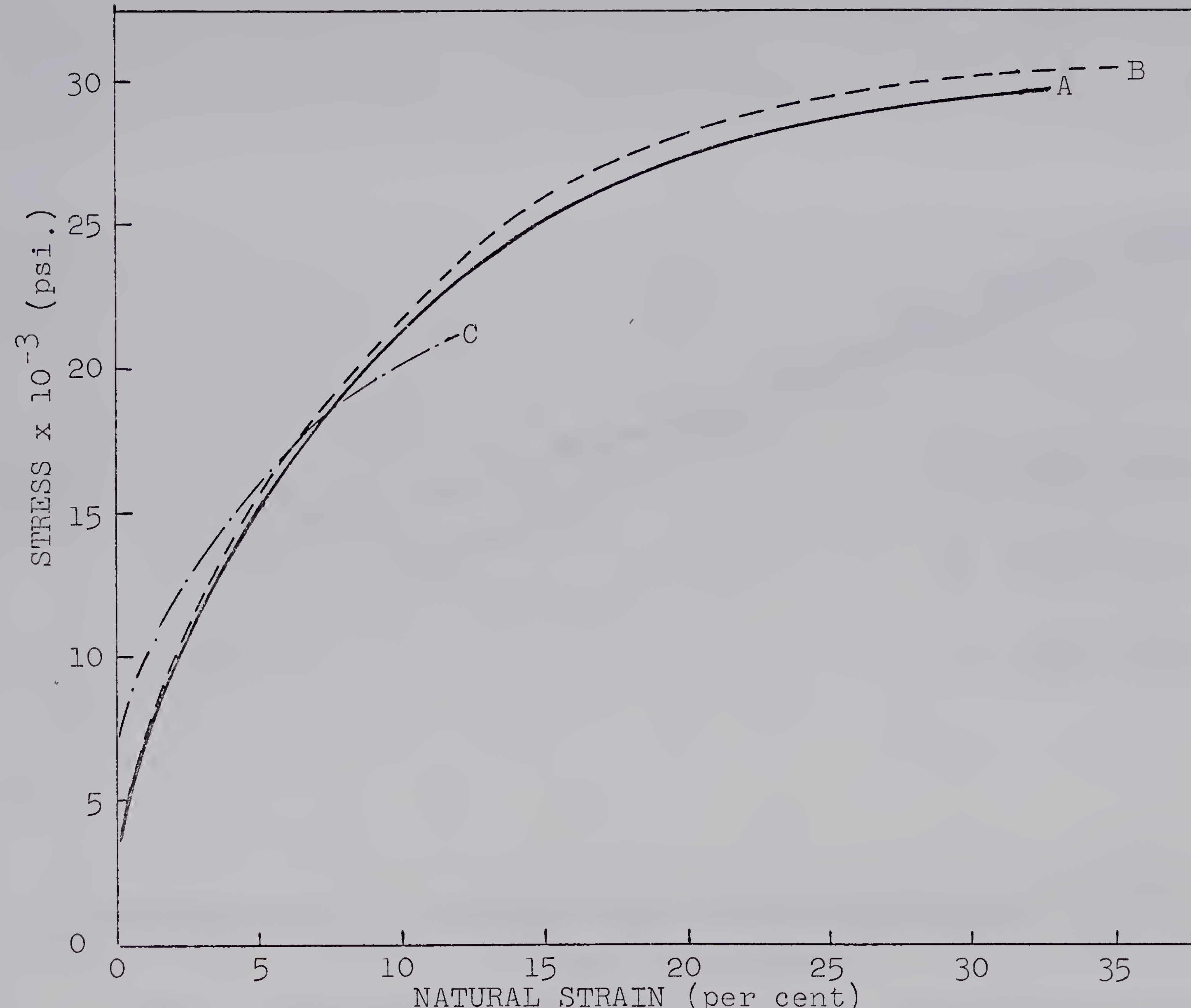

FIG. 28. STRESS-STRAIN CURVES FOR (A) OFHC COPPER, (B) TOUGH PITCH COPPER, (C) OFHC COPPER WITH CREEP CAVITATION. THE TESTS WERE DISCONTINUED AFTER THE SAMPLES BEGAN TO NECK.

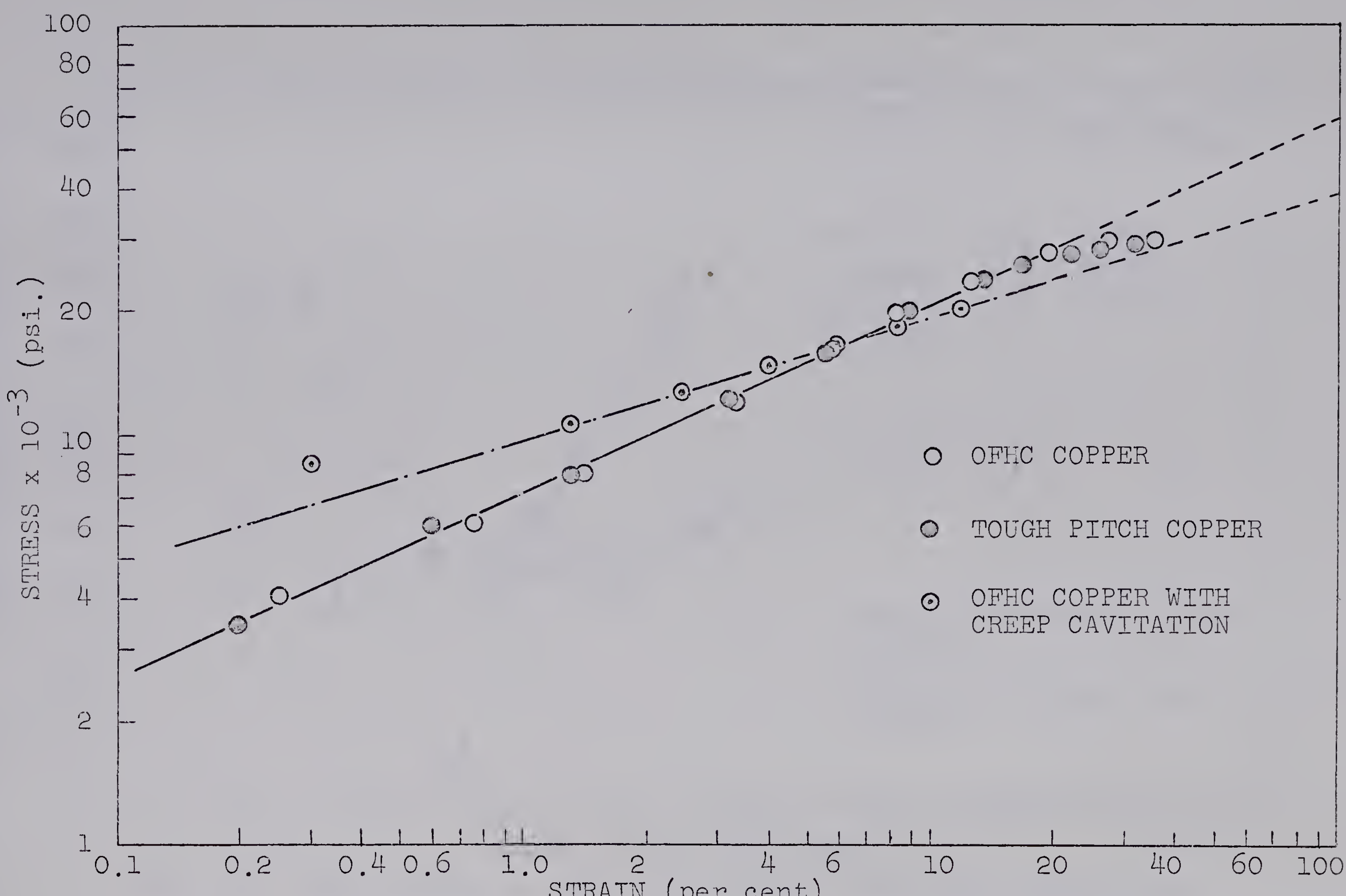

FIG. 29. THE TENSILE TEST RESULTS PLOTTED LOGARITHMICALLY TO REVEAL THE STRAIN HARDENING BEHAVIOR

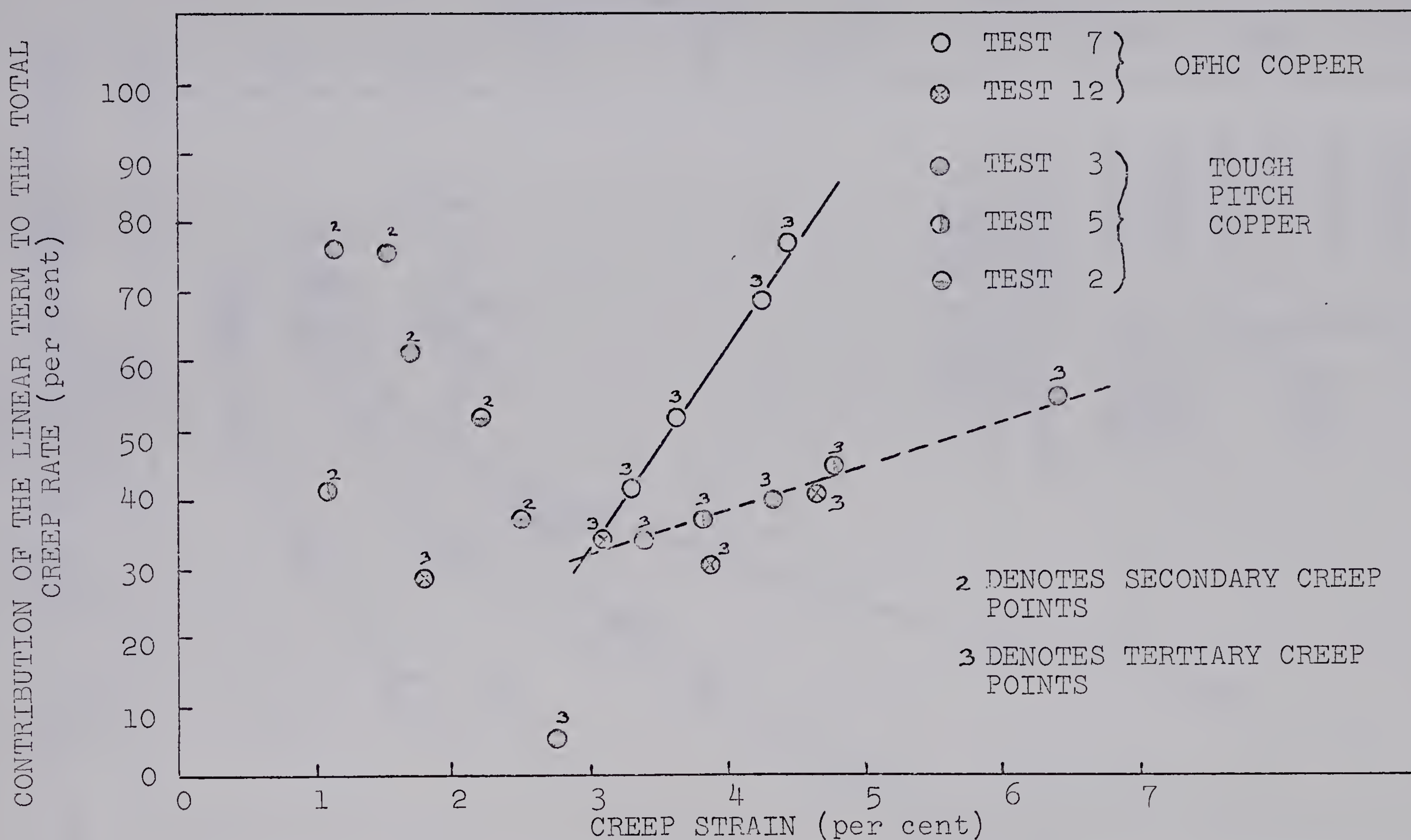

FIG. 30. CONTRIBUTION OF THE LINEAR TERM TO THE TOTAL CREEP RATE VERSUS THE CREEP STRAIN

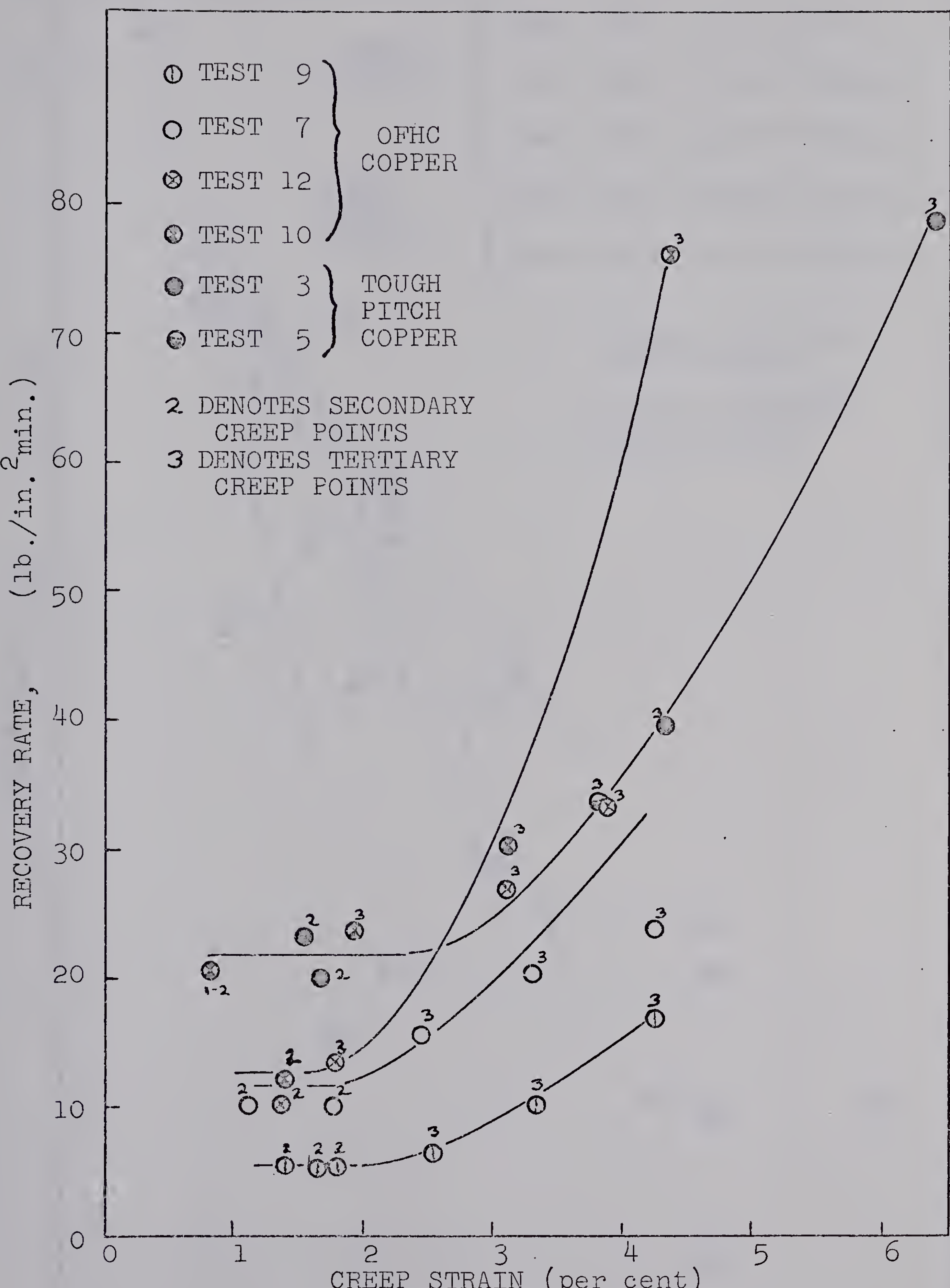

FIG. 31. THE INDUCTION TIME DATA PLOTTED ACCORDING TO EQUATION 25 OF THE TEXT

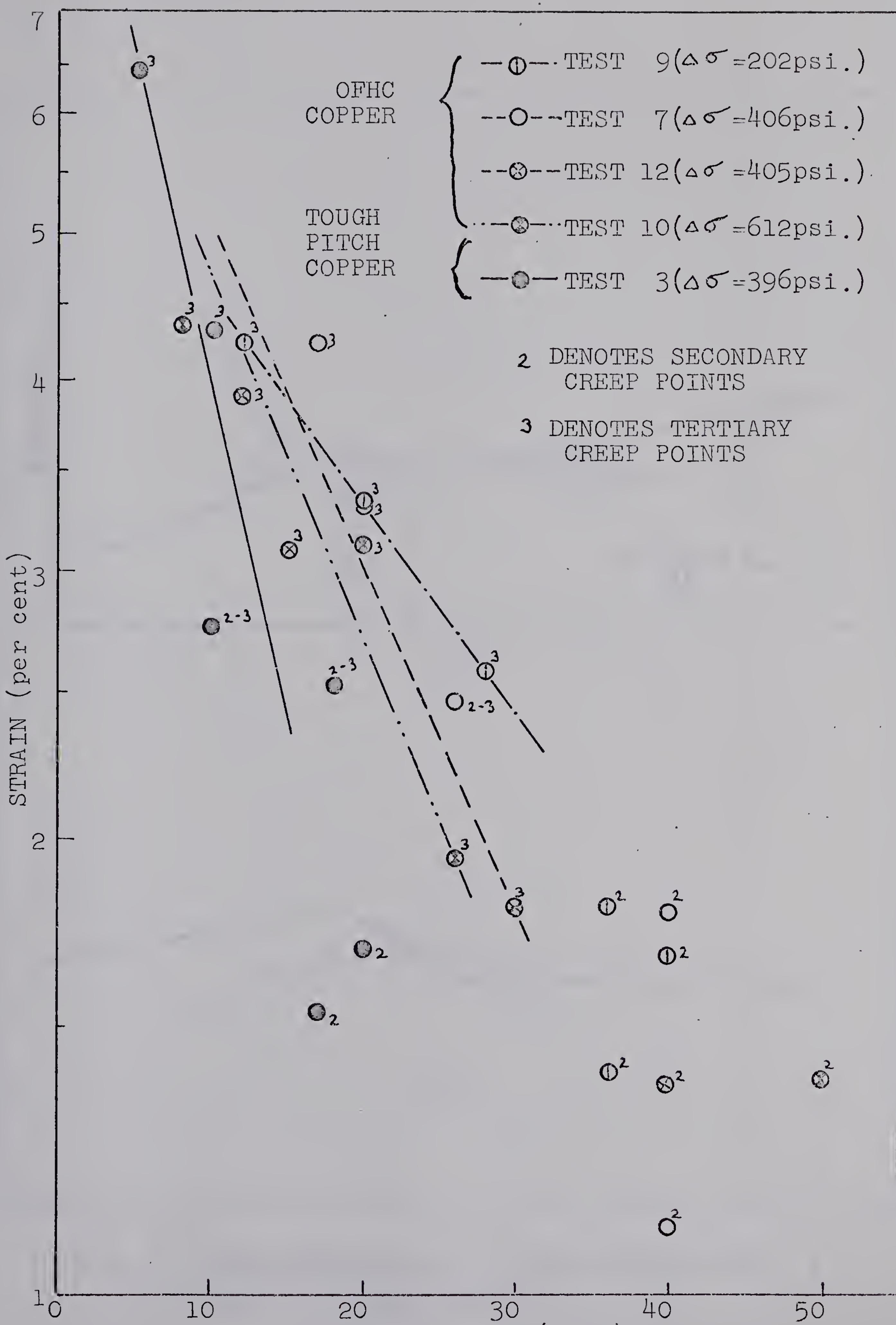

FIG. 32. A SEMI-LOGARITHMIC PLOT OF CREEP STRAIN VERSUS INDUCTION TIME

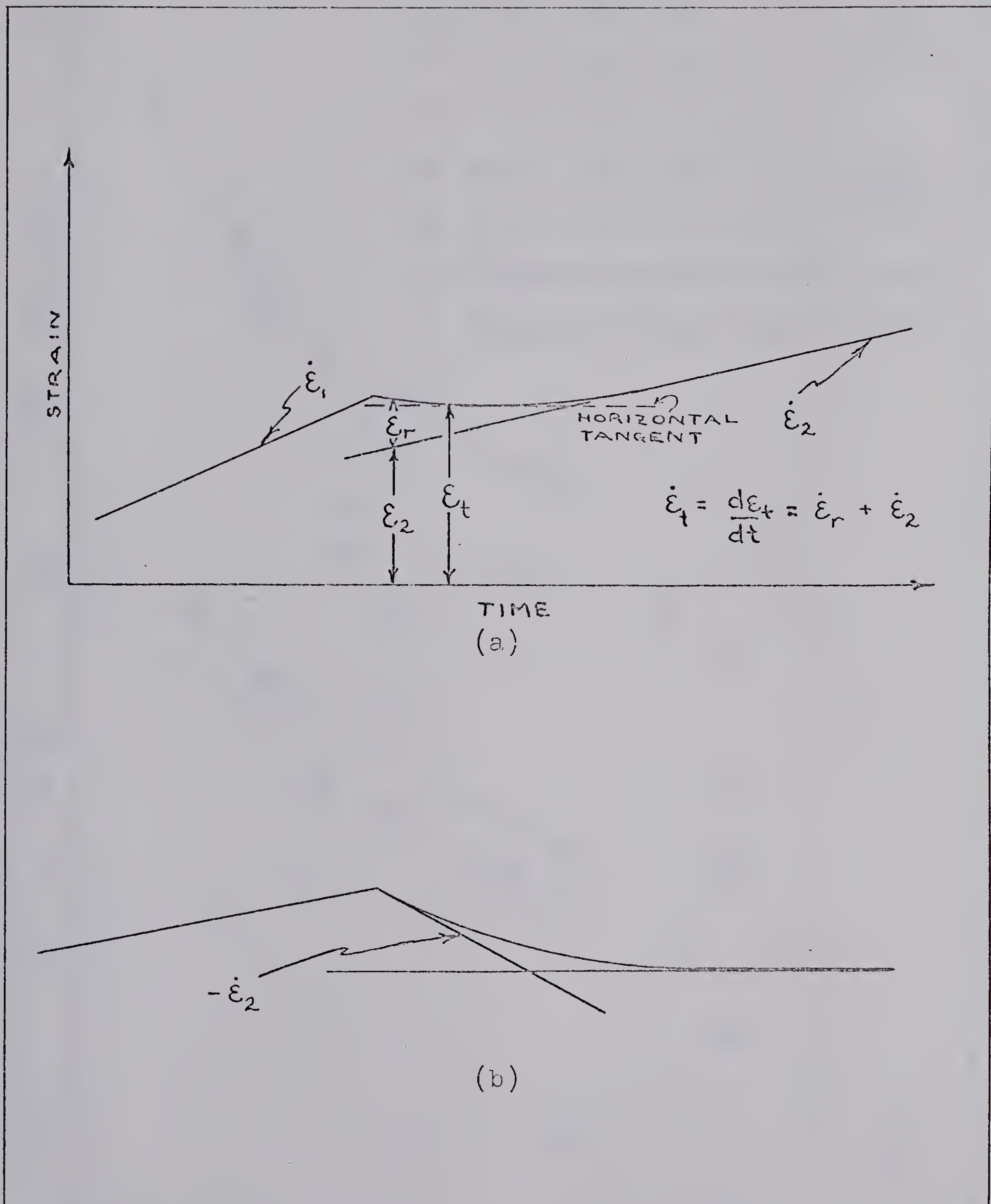

FIG. 33. THE DEFINITIONS OF RECOVERABLE STRAIN, ε_r , AND THE CREEP STRAIN, ε_2 .

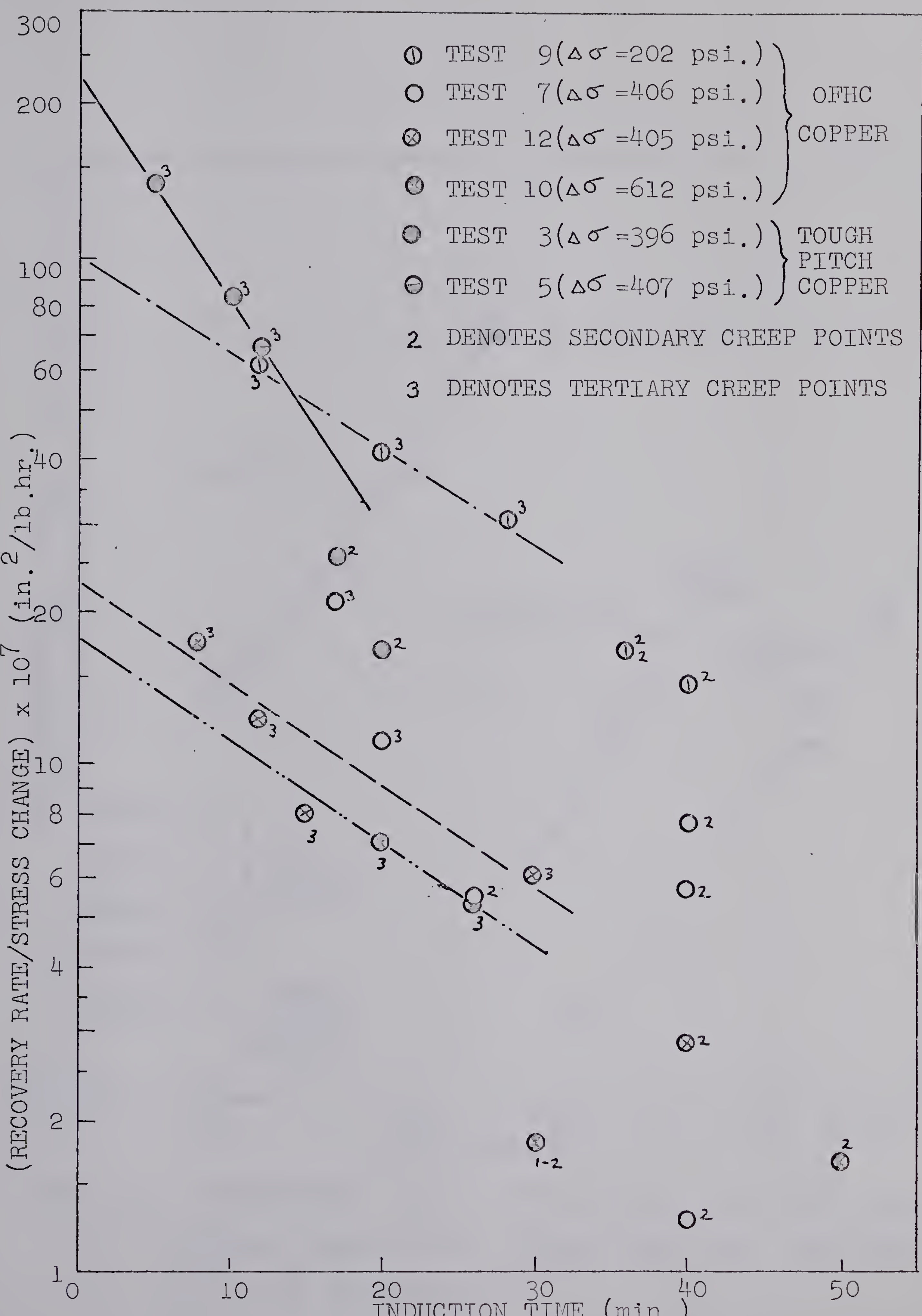

FIG. 34. A SEMI-LOGARITHMIC PLOT OF THE EXPERIMENTAL DATA ACCORDING TO EQUATION 36 OF THE TEXT

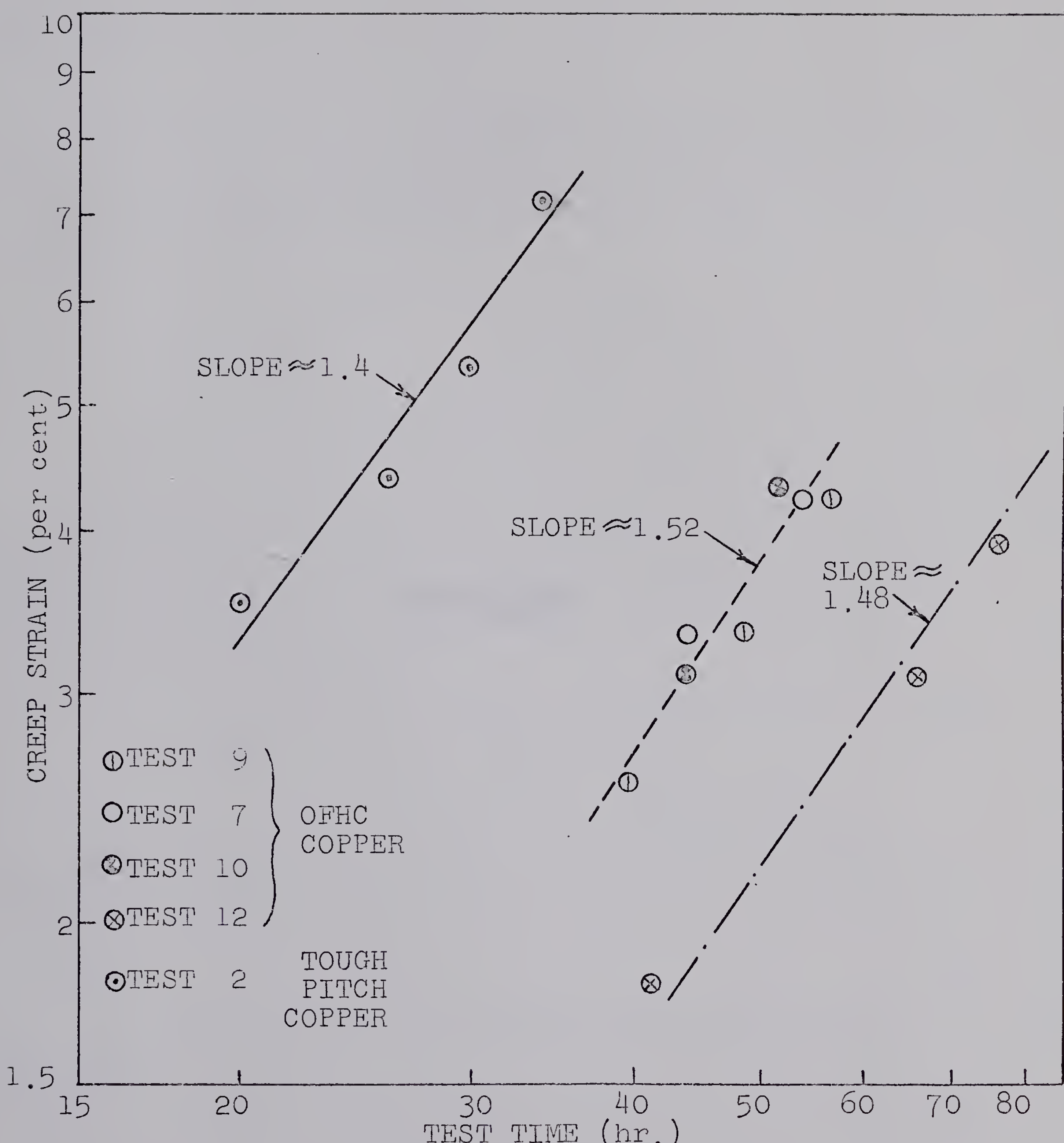

FIG. 35. A LOGARITHMIC PLOT OF TOTAL CREEP STRAIN FOR SOME TERTIARY CREEP POINTS VERSUS TEST TIME. THE DATA WAS TAKEN FROM TABLE 6.

APPENDICES

APPENDIX 1

CONSTANT STRESS CAM

A. DESIGN

The function of the constant stress cam is to change the load on the creep sample as the cross-sectional area of the sample changes during deformation. Then, for constant stress:

$$\sigma = P/A = P_o/A_o \qquad (A1)$$

where P, A, are the sample load and cross-sectional area, respectively;
the subscript "o" denotes initial conditions.

If the assumptions that the volume remains constant and the strain along the gauge length is uniform, are adopted, then an expression can be developed which can be used to design the cam graphically.

$$lA = l_oA_o = \text{constant} \qquad (A2)$$

where l is the sample length,
l_o is the initial gauge length.

Refer to Fig. A-1. The condition for mechanical equilibrium is that:

$$\Sigma M_A = 0 \qquad (A3)$$

where M_A are the moments about the pivot, A.

Therefore,

$$PR = Wx \qquad (A4)$$

or

$$P = Wx/R \qquad (A5)$$

Substitution of Equations A5 and A2 into Equation A1, plus some rearrangement, gives:

[illegible]

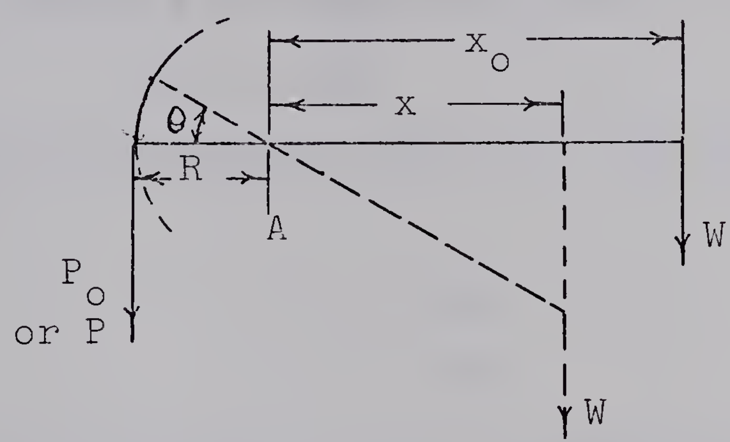

P_o is the sample reaction;
P is the reaction after rotation;
W is the weight by which the sample is loaded;
R is a constant radius, from the pivot, A, to the line of action of P, the sample reaction;
x is the moment arm which must be varied, as the sample elongates, to change P with changing sample area.

FIG. A-1. DEFINITION OF THE SYMBOLS USED IN APPENDIX 1-A.

$$xl = x_o l_o \tag{A6}$$

which is the geometrical condition for maintenance of constant stress.

As the sample length changes, the radius, R, rotates through an angle, θ. Thus, the change in sample length, l, can be expressed in terms of R and θ.

$$\Delta l = R\theta \tag{A7}$$

The sample length at any time after the beginning of the test would be:

$$\begin{aligned} l &= l_o + \Delta l \\ &= l_o + R\theta \end{aligned} \tag{A8}$$

Substitution of Equation A8 into Equation A6, with rearrangement, yields the equation used to design the cam graphically:

$$x/x_o = l_o/(l_o + R\theta) \tag{A9}$$

For the particular cam used in this program, values of l_o = 2 in., x_o = 20 in., and R = 2 in., were chosen. When substituted into Equation A9, this gives:

$$x/20 = 2/(2 + 2\theta) \tag{A10}$$

The cam shape is determined by choosing values for θ, substituting into Equation A10, solving for x, plotting θ and x, (as shown in Fig. A-2) and erection of a perpendicular to x and (x, θ). The cam shape is defined by the curve tangent to the perpendiculars.

Table A-1 gives the data used to design the cam employed for this program.

TABLE A-1

Rθ (in.-rad.)	θ (rad.)	θ (deg.)	x/l	x (in.)
0.2	0.1	$5^{\circ}43'$	0.91	18.2
0.4	0.2	$11^{\circ}27'$	0.834	16.7
0.6	0.3	$17^{\circ}11'$	0.77	15.4
0.8	0.4	$22^{\circ}55'$	0.715	14.3
1.0	0.5	$28^{\circ}38'$	0.667	13.3
1.2	0.6	$34^{\circ}22'$	0.626	12.5
1.4	0.7	$40^{\circ}06'$	0.588	11.7

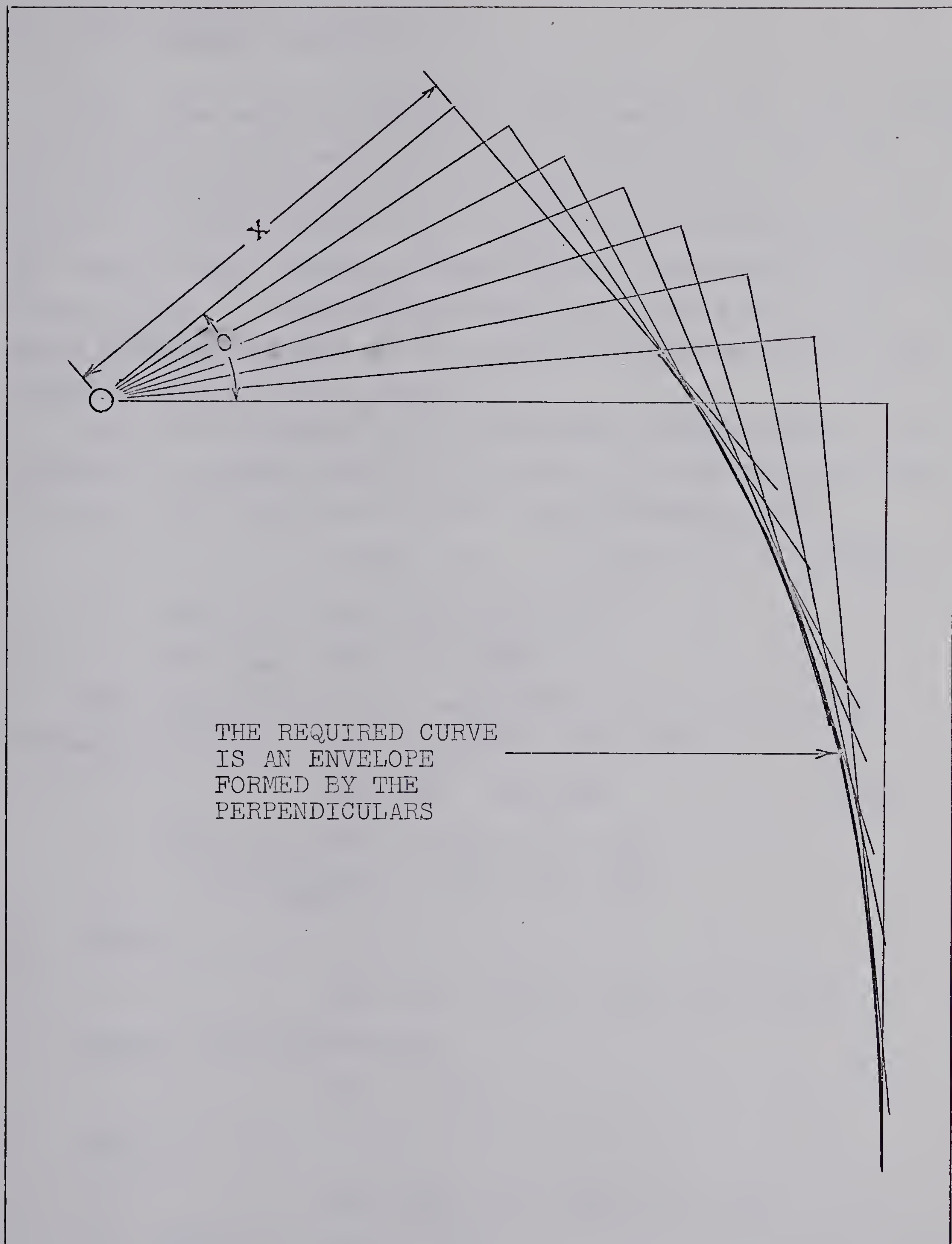

FIG. A-2. GRAPHICAL DETERMINATION OF THE CONSTANT STRESS CAM SHAPE. (SCALE: 1 in. = 4 in.)

B. CAM ASSEMBLY BALANCING

The load which is applied to the sample must arise from the weights on the weight pan only. This means that the cam assembly must balance at any angle of rotation, O. To prevent the cam assembly from contributing significantly to the sample load, thereby preventing the maintenance of constant stress, a counterbalance must be located on a line which passes through both the centre of gravity for the cam assembly and the pivot point, A.

This can be shown by the following consideration. By summing the moments about a, in Fig. A-3, then setting equal to zero, the condition of static equilibrium is met:

$$\Sigma M_A = 0 \tag{A11}$$

Let $M_{1A} = R\cos\,(\psi + \theta)w$
and $M_{2A} = r\cos\,(\phi + \theta)W_c$

For equilibrium to be maintained as the cam rotates through the angle θ, the following must hold:

$$dM_{1A}/d\theta = dM_{2A}/d\theta \tag{A12}$$

where $dM_{1A}/d\theta = R\sin\,(\psi + \theta)w$
and $dM_{2A}/d\theta = r\sin\,(\phi + \theta)W_c$

Hence,

$$R\sin\,(\psi + \theta)w = r\sin\,(\phi + \theta)W_c$$

Since, for equilibrium,

$$rW_c = Rw$$

then,

$$\sin\,(\phi + \theta) = \sin\,(\psi + \theta)$$

and $$\phi = \psi$$

Therefore, the cam centre of gravity and the counterbalance lie on the same line through the pivot point, A.

The point (r, ϕ) was taken to be the point of inter-

[illegible]

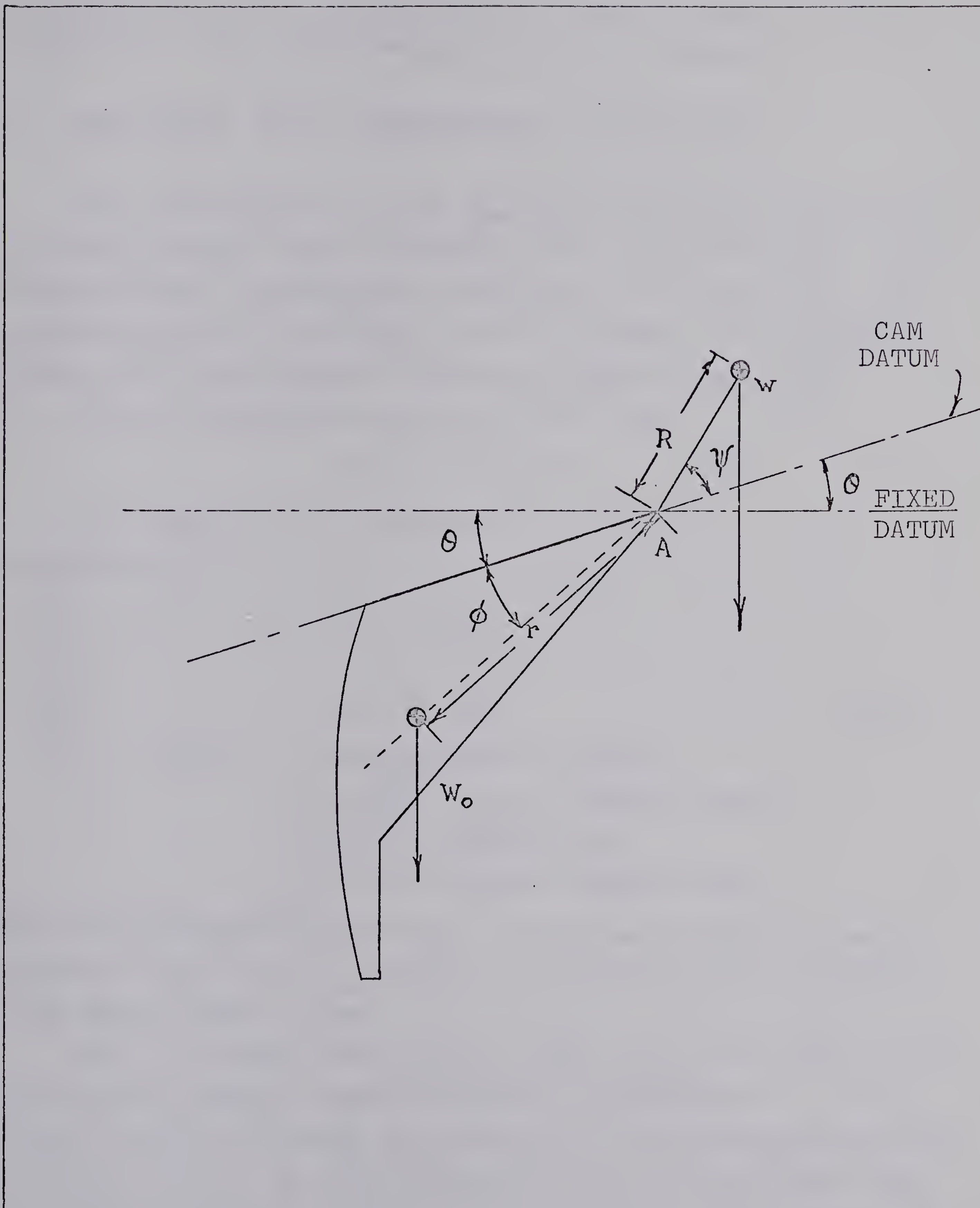

FIG. A-3. DEFINITION OF THE SYMBOLS USED IN APPENDIX 1-B.

section of two plumbed lines--each determined by suspending the finished cam assembly by a different corner. With ϕ determined, the counterbalance could be located.

C. EVALUATION OF CAM PERFORMANCE; CALIBRATION

The performance of the cam was evaluated by replacing the creep sample with a proving ring, which had been calibrated using a Houndsfield Tensometer, and measuring the load exerted by the weight pan and weights for different values of θ, and hence, different sample lengths, l.

Note, from Equations A1 and A2, that:

$$lP/\sigma = l_o P_o/\sigma \qquad \text{(A13)}$$

where σ is constant,

and therefore,

$$Pl = P_o l_o$$

or

$$l/l_o = P_o/P \qquad \text{(A14)}$$

where l is the sample length,
l_o is the initial sample length,
P is the sample load,
P_o is the initial sample load.

This relationship shows that, if constant stress is maintained, a plot of l/l_o versus P_o/P should give a straight line whose slope is one.

Fig. A-4 shows such a plot based upon the measurements of load and sample length outlined in paragraph 1. It is linear within the range of operation of the machine and has a slope of one. It was concluded from this exercise that the cam was able to change the load on the creep sample in a way which would keep stress constant, if the sample behaved according to the design assumptions.

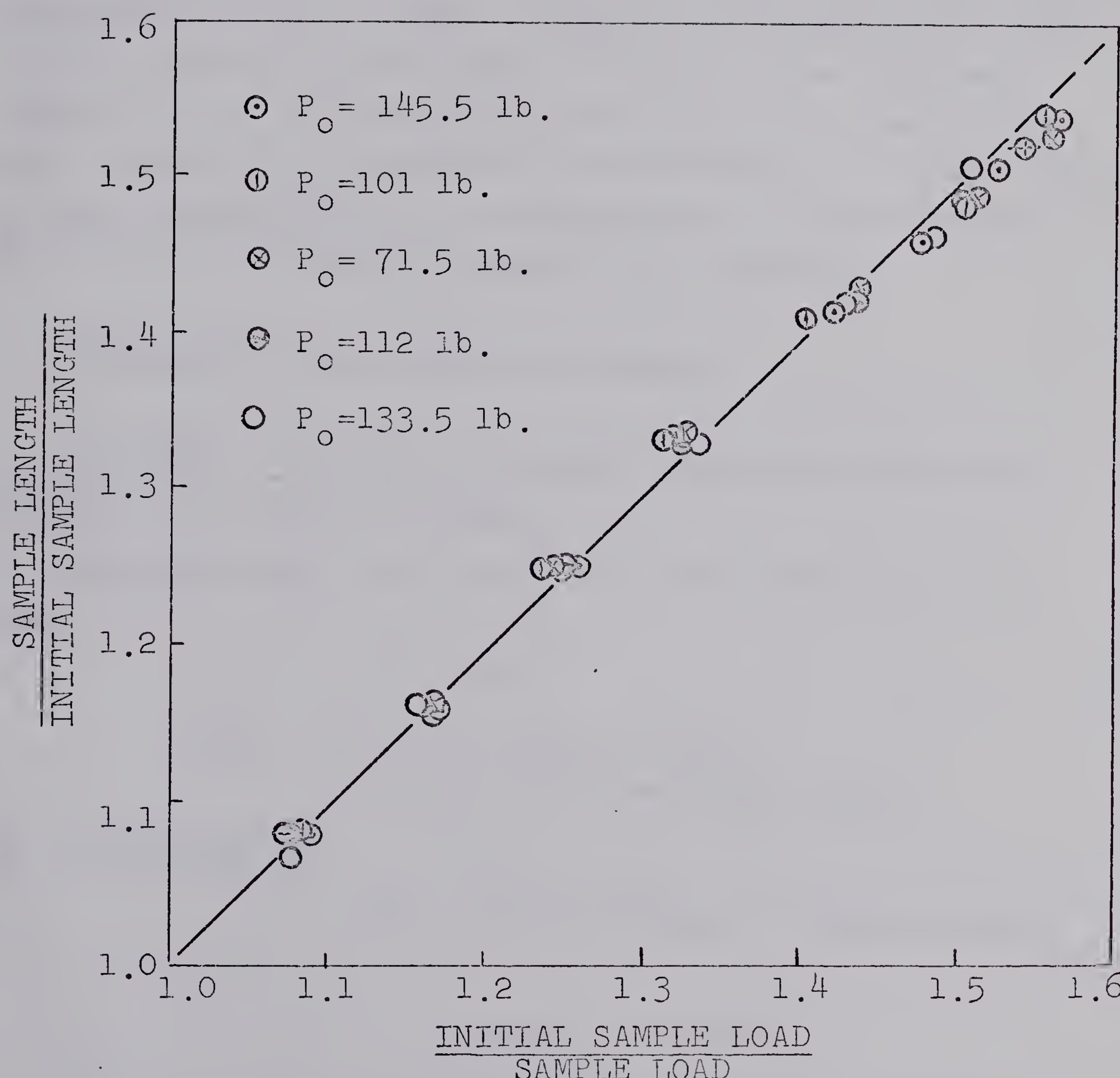

FIG. A-4. THE CAM EVALUATION DATA PLOTTED ACCORDING TO EQUATION A14. (APPENDIX 1-C)

APPENDIX 2

SOME METHODS OF ERROR ESTIMATION

Because this program was concerned more with the investigation of certain trends, and less with the establishment of exact values, a complete treatment of errors for all numbers was not done. However, some data was checked to get an idea of the magnitudes of some errors which could occur in such an investigation. Several cases of error estimation will be presented, for conciseness, in the form of a problem statement and a solution.

A. ESTIMATION OF THE ERROR IN STRESS

PROBLEM: To find an equation which describes the experimental error in stress.

SOLUTION: The differential of the expression for stress, σ,

$$\sigma = P/A$$

where P is the applied load,
A is the cross-sectional area,

can be written as:

$$d\sigma = (\partial\sigma/\partial P)dP + (\partial\sigma/\partial A)dA \tag{A15}$$

$$= dP/A - (P/A^2)dA$$

Upon substitution of the formula for the area of a circle,

$$A = \pi d^2/4$$

and $$dA = \pi(d/2)dd$$

the Equation A15 becomes:

$$d\sigma = (4/\pi d^2)dP - (8P/\pi d^3)dd \tag{A16}$$

[illegible]

[illegible]

[illegible]

[illegible]

[illegible]

[illegible]

[illegible]

[illegible]

[illegible]

[illegible]

An approximation to Equation A16 results when the exact differential is replaced by its approximation,

$$\Delta\sigma = (4/\pi d^2)\Delta P - (8P/\pi d^3)\Delta d \tag{A17}$$

This is the expression which was used to estimate the error in the stress, σ. The final form of the equation ensued upon substitution of the following values for the variables:

$$\Delta P = \pm 1 \text{ lb.},$$
$$d = 0.25 \text{ in.},$$
$$\Delta d = 0.5 \times 10^{-4} \text{in.}$$

The final form of Equation A17 is:

$$\sigma = \pm 20.4 \mp (8.16)10^{-3}P \tag{A18}$$

To calculate the error in stress, one needs only to substitute a value for P into Equation A18. For example, a sample load of 150 lb. would yield an error in stress of ± 18.2 psi. This is equivalent to a per cent relative error of:

$$\begin{aligned}(\Delta\sigma/\sigma)100 &= (\pm 18.2A/P)100 \\ &= (\pm 18.2)(0.0492)/150\ 100 \\ &= \pm 0.6 \text{ per cent}\end{aligned}$$

Notice that for a larger stress the error will be less than this, according to Equation A18. Errors of this magnitude are quite acceptable for the stress, especially when investigating trends.

B. GAUGE LENGTH CONFIDENCE LIMITS

PROBLEM: Twenty-two copper samples which were to have a gauge length of 2 in. were turned out on a lathe. To avoid the time-consuming operation of measuring the gauge length on each specimen, a sample of 7 specimens was chosen, and the gauge lengths recorded (each gauge length was meas-

ured 5 times and the average of these was used). For all the calculations which involved the sample gauge length in this investigation, it was assumed that the gauge length was, in fact, 2.000 in. Can one be 95 per cent confident that the gauge length of any given specimen will not differ significantly from the assumed value of 2.000 in.?

SOLUTION: Assuming a normal distribution for the gauge length population, the confidence limits are given by the equation:

$$l_o = \bar{l} \pm s t_\alpha N^{-1/2} \qquad \text{(A19)}$$

where l_o is the population mean,
$\bar{l}$ is the sample mean,
s is the standard error,
t_α is the value of the standardized variate for the Student's t distribution,
N is the number of items in the sample.

The standard error was calculated using:

$$s = \left\{\left[N \sum(l_i)^2 - (\sum l_i)^2\right]/N(N-1)\right\}^{1/2} \qquad \text{(A20)}$$

where Table A-2 gives the values used for the gauge length, l. Upon substitution of these numbers into Equation A20, a standard error of 2.76×10^{-2} results.

From tables of Student's t, it can be found that for 95 per cent confidence and 6 degrees of freedom, t_α takes the value 2.447.

The sample mean gauge length, $\bar{l}$, works out to be 2.008 in.

Substitution of these numbers into Equation A19 yields:

$$l_o = 2.008 \pm 0.026$$

These limits do include the population mean, l_o = 2.000 in. It was concluded, therefore, that one could be 95 per cent confident that the gauge length of any given specimen from the population would not differ significantly from the

TABLE A-2

l_i*	$(l_i)^2$
2.041	4.166
1.997	3.988
2.025	4.101
2.010	4.040
2.024	4.097
1.990	3.960
1.972	3.889
l_i = 14.059	$(l_i)^2$ = 28.241

$(\ l_i)^2 = 197.655$

* l_i is the measured gauge length of the sample. The units of measurement are inches.

assumed value of 2.000 in.

C. CONVERSION OF RECORDER CHART DIVISIONS TO ELONGATION

PROBLEM: The change in sample length was measured by an LVDT whose signal was recorded on a Heath recorder. How much elongation would 10 divisions on the recorder chart represent?

SOLUTION: A dial gauge, which could be read to 5×10^{-4} in., was attached to one of the extension arms of the creep machine. By rotation of the threaded crank on the lower extension arm, the cam assembly was positioned so that the recorder pen moved through a distance of 1/4 of the full scale. The amount of sample extension to which this was equivalent was read from the dial gauge and recorded. The cam was then positioned to 1/2 of the full scale, the difference in extension between the 1/4 scale and 1/2 scale values read from the dial gauge and recorded. This operation was repeated for 3/4 of full scale and full scale of the recorder chart. From each of these, the average elongation per 10 chart divisions was calculated by:

$$\frac{\text{Dial gauge reading for 25 divisions}}{\text{25 divisions/10 divisions}}$$

For each complete traverse of the recorder chart, a set of 4 numbers resulted, each of which expressed the amount of elongation per 10 chart divisions. These 4 numbers were averaged to give a mean value for that particular traverse. The recorder chart was traversed in this manner a total of 10 times. This gave 10 mean values for the amount of elongation per 10 chart divisions. These 10 values were treated statistically--as was the data in Appendix 2-B--to give the 99 per cent confidence limits for a normally distributed population. From this treatment, it was decided that one could be 99 per cent confident that a change in sample length producing a recorder

[illegible]

pen movement of 10 chart divisions would be equal to $(17.3 \pm 0.75)10^{-3}$ in.

D. ERROR FOR OTHER THAN 10 CHART DIVISIONS

PROBLEM: For a change in sample length of 17.3×10^{-3} in., the error is $\pm$ 0.75×10^{-3} in. What would the error be for something other than a change in length of 17.3×10^{-3} in.?

SOLUTION: Let L be the change in sample length,
n be the number of chart divisions,
f be the conversion factor for each division.

Therefore,

$$L = nf \tag{A21}$$

Also then,

$$dL = ndf + fdn$$

or, approximately,

$$\Delta L = n\,\Delta f + f\,\Delta n \tag{A22}$$

Equation A22 can be used to estimate the per cent relative error for a change in sample length equivalent to 1/100 of full scale, or 1 division. Using the following values of the variables:

$$n = 1 \text{ division},$$
$$\Delta f = \pm 0.075 \times 10^{-3} \text{ in.},$$
$$f = 17.3 \times 10^{-4} \text{ in.},$$
$$\Delta n = 1/3 \text{ division},$$

in Equation A22, results in $\Delta L = 6.25 \times 10^{-4}$ in. This yields a per cent relative error of:

$$(6.25)10^{-4}/(17.3)10^{-4}\ 100\%$$

$$= \pm 36 \text{ per cent.}$$

This is the order of magnitude which should be expected for

such a small change in length as this is near the limits of resolution of the length change measurement equipment. As greater length changes are measured, the per cent relative error will decrease to much lower values. For example, the per cent relative error is only $\pm$ 4.3 per cent for a change in sample length of 17.3×10^{-3} in.

E. ESTIMATION OF ERRORS IN STRAIN AND STRAIN RATE

PROBLEM: To develop expressions which will show the absolute error in the measurements of strain and strain rate.

SOLUTION: Consider the strain first. The strain was defined to be:

$$\varepsilon = \ln(l/l_o)$$

The approximation to the differential can be written as:

$$\Delta\varepsilon = (\Delta l/l) - (\Delta l_o/l_o) \qquad \text{(A23)}$$

where $\Delta\varepsilon$ is the error in strain,

Δl is the error in measurement of the sample length,

l is the sample length,

Δl_o is the error in the initial gauge length as determined under Appendix 2-B,

l_o is the initial gauge length.

Equation A23 becomes, after substitution for Δl_o and l_o:

$$\Delta\varepsilon = (\Delta l/l) \mp 0.013 \qquad \text{(A24)}$$

This expression can be used, then, to estimate the absolute error in the measurement of strain. Δl would have to be calculated for the particular elongation under consideration. The errors in sample measurement would be expressed by:

$$\Delta l = \Delta l_o + n\Delta L + L\Delta n$$

where Δl_o is the error in initial gauge length,

[illegible]

n is the number of chart divisions involved,

Δn is the error made in reading the number of chart divisions,

L is the change in sample length represented by n,

ΔL is the error in sample length, as determined from Appendix 2-D.

For a change in sample length of 17.3×10^{-3} in., the error in measurement of sample length was estimated to be $(0.776)10^{-3}$ in., using $\Delta l_o = 0.026$ in. and $(n \Delta L + L \Delta n) = (0.75)10^{-3}$ in. This, when substituted into Equation A24 and divided by the strain, to give the relative error, yielded 0.046; this is a relative error in per cent of 4.6. Again, for larger strains the per cent relative error would be smaller.

Consider the strain rate now. The strain rate is defined to be:

$$\dot{\varepsilon} = d\varepsilon/dt \approx \delta\varepsilon/\delta t$$

Again, the approximate error for the strain rate was derived by taking the complete differential, then substituting Δ in place of d. This resulted in an expression, such as:

$$\Delta\dot{\varepsilon} = \frac{\Delta(\delta\varepsilon)}{\delta t} - \frac{\delta\varepsilon\,\Delta(\delta t)}{(\delta t)^2} \qquad \text{(A25)}$$

where $\Delta\dot{\varepsilon}$ is the absolute error in strain rate,

$\Delta(\delta\varepsilon)$ is the error in the change of strain which occurred during the time δt,

$\Delta(\delta t)$ is the error in the measurement of time, δt,

$\delta\varepsilon$ is the change of strain occurring during the time δt.

The application of Equation A25 is more complex than any of the others which have been developed so far. Using

procedures similar to those already developed in earlier appendices, a value was computed for $\Delta(\delta\varepsilon)$ based on data from Test 12--for which there was a creep rate of $(3.74)10^{-4}$ in./in.hr. This value, along with the other numbers taken from a consideration of the data from Test 12, is listed as follows:

δt = 360 min.,

$\Delta(\delta t)$ = 6 min., assuming that the recorder speed of 0.5 in./hr. was more accurate than the chart could be read,

$\Delta(\delta\varepsilon) = 3.7 \times 10^{-4}$ in.,

$\delta\varepsilon = 2.24 \times 10^{-3}$ in.

A per cent relative error of $\pm$ 14.8 per cent was calculated for the creep rate of 3.74×10^{-4} in./in.hr. As the creep rate increased, the relative error would diminish.

The foregoing consideration of errors will help give an idea of the way in which estimates of the various kinds of error could be made, as well as provide an idea of the magnitudes of some errors which could occur. To establish more exact values for the parameters studied in this investigation, many more tests would have to be performed and their results treated statistically.